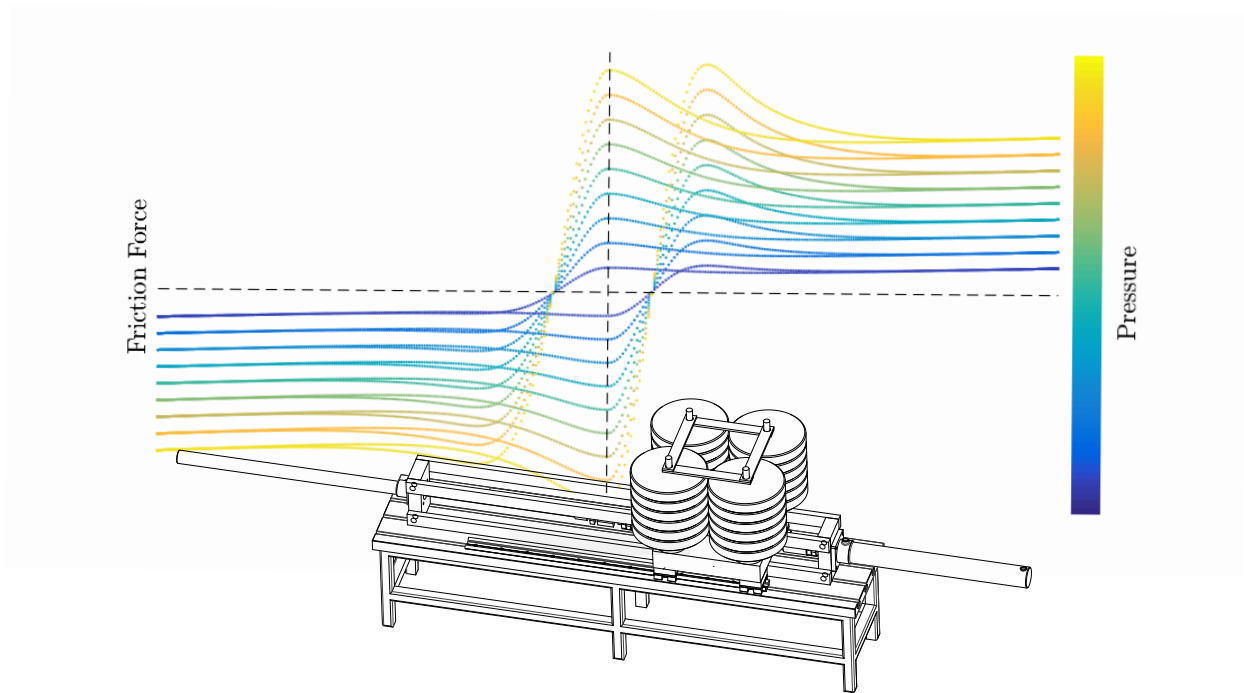
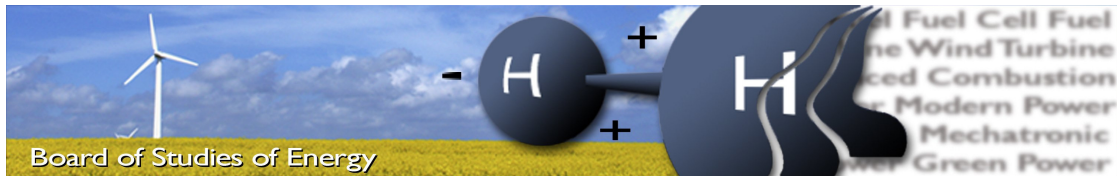


Characterisation of the Pressure Dependent Friction Behaviour in an Asymmetric Hydraulic Cylinder: An Empirical Approach



MSc IN MECHATRONIC CONTROL ENGINEERING
MASTER'S THESIS
GROUP MCE4-1029
DEPARTMENT OF ENERGY TECHNOLOGY
AALBORG UNIVERSITY
01.06.17



Title: Characterisation of the Pressure Dependent Friction Behaviour in an Asymmetric Hydraulic Cylinder: An Empirical Approach
Semester: MSc in Mechatronic Control Engineering: 4th Semester
Semester theme: Master's Thesis
Project period: 01.02.17 to 01.06.17
ECTS: 30
Supervisor: Henrik Clemmensen Pedersen
Project group: MCE4-1029

Niels Pedersen

Stefan Melvad Jørgensen

Copies: 4
 Pages, total: 151
 Appendices: 4
 Supplements: 2

Synopsis:

This thesis concerns an investigation of the pressure dependency in the friction force present in an asymmetric hydraulic cylinder. To characterise the pressure dependency, a test setup is designed and constructed where accurate measurements of the friction force and velocity is of great importance. A decentralised control strategy is designed to control the two pressures and velocity of the test cylinder ($\varnothing 50/35$).

With basis in the Modified LuGre model a velocity dependent friction model is proposed. This is partly validated by measurements. Furthermore an investigation of different methods to estimate the friction model parameters is made. A robust sequential method, where the steady state parameters are estimated from steady state measurements and the dynamic parameters are estimated using a Non-Linear Least Squares Method (NLSM), is proposed.

The pressure dependency of the friction model parameters are investigated for pressures from 20-200 bar. During these tests a position dependent friction was detected due to a lack of break in of the cylinder. A pressure dependency in F_c and F_s was indicated, yet further measurements should be conducted to further characterise the pressure dependency. Furthermore it is indicated that the friction force is behaving dynamically with pressure, though this is not further evaluated.

By accepting the request from the fellow student who uploads the study group's project report in Digital Exam System, you confirm that all group members have participated in the project work, and thereby all members are collectively liable for the contents of the report. Furthermore, all group members confirm that the report does not include plagiarism.

Preface

This thesis is written by group MCE4-1029. The thesis has been written during the spring of 2017 and is submitted as Master's Thesis in Mechatronic Control Engineering.

The thesis concerns dynamic modelling of the friction force acting in an asymmetric hydraulic cylinder. This thesis consists of two focus areas:

- Design and construction of a test facility for friction force measurements.
- Friction modelling and parameter estimation.

A part of the thesis concerns the design of the test facility. From the design of the test facility to the delivery of components, some time has been spend on analysing friction models and parameter estimation methods. This part is made without experimental data from the test facility but will be evaluated when measurements are available. Before submission date it was not possible to break in the cylinder due to time limitations. Furthermore the final measurements was only conducted once why consistency in the results can not be assured. Prior to the examination further break in will be conducted and new measurements will be made.

During the project the following software have been used:

- **LabVIEW** - For real time control and measurements.
- **Maple** - For algebraic manipulation of equations.
- **MATLAB** - For frequency analysis and data processing.
- **Simulink** - For simulation of dynamic systems.
- **Microsoft Visio** - For report illustrations.
- **LaTeX** - For report writing.

Readers Guide

To the report an appendix is attached which describes the design, modelling and control of the test facility together with some analyses of the experimental measurements. Furthermore a supplement is added with some further elaborations of the test facility design process.

In the beginning of the report a state of the art section is written where the state of the art in friction force characteristics and friction force modelling are elaborated. From this, a problem statement is formulated and the requirements for the test facility and the friction model are elaborated. Subsequently to that, investigations of friction models and parameter estimation methods is done. A friction model and parameter estimation method will be proposed and used to investigate the pressure dependencies in the friction force from measurements.

A nomenclature containing variables and their respective units used in the report is presented on page vii. The literature used in the report is presented in the bibliography on page 87.

Figures, tables and equations will be numbered as, [Chapter,Number].

Summary

The scope of this thesis is to accurately characterise and model the friction force in an asymmetric hydraulic cylinder. A state of the art investigation of friction force dependencies and models to describe these are conducted to investigate which friction dependencies are incorporated in existing friction models. The conclusion from this investigation is that the velocity dependency of friction is well described. Yet the characteristics of a temperature dependent friction and a pressure dependent friction have not attained much attention in previous works, and models to describe these dependencies accurately are not available.

This thesis concerns the characterisation and modelling of the pressure dependency in the friction force in an asymmetric hydraulic cylinder. The pressure dependency is investigated utilising an empirical approach by measuring the friction at different pressure combinations. To do this, a part of this thesis has concerned the design and construction of a test facility to accurately measure the friction force in the desired velocity and pressure range. Requirements for the test facility are formulated based on the state of the art investigation. These requirements regards an ability to individually control both pressures and the velocity of an asymmetric hydraulic cylinder and an ability to measure velocity and friction force accurately. To meet the requirements it is necessary to load the hydraulic cylinder, such it is possible to control each chamber pressure and the velocity individually, why different load topologies are investigated. The chosen topology to load the main cylinder is a hydraulic cylinder.

The mechanical design concerns, cylinder mounting, structural design, guidance etc. such the requirements are fulfilled. Furthermore a sensor setup is chosen such the friction force and velocity can be measured with the highest possible accuracy and without undesired characteristics, such as axial play and undesired friction forces.

A non-linear model of the system is made and a linear representation of this model is analysed utilising an RGA method to determine the most advantageous input / output combinations and to evaluate the couplings in the system. This is done in order to design a control structure such each chamber pressure and the velocity of the main cylinder can be controlled independently.

An analysis of existing velocity dependent friction models is made and a model which reduces the number of parameters by three compared to existing models is proposed. Different parameter estimation methods are evaluated by simulating measurement errors and comparing the estimation error. The chosen parameter estimation method is a sequential method where the steady state parameters are estimated from 15 steady state velocity steps in each direction. With knowledge of the steady state parameters the dynamic parameters are estimated using a non-linear least squares method (NLSM) which minimises the residual between the measured and modelled friction. This method is used to estimate the friction parameters for the proposed friction model for chamber pressures of 20-200 bar.

It is indicated from the results that the parameters F_S and F_C increases with pressure.

The pressure dependency is also investigated during transient pressures to see a potential dynamic pressure dependency. This analysis indicates that a dynamic relation is present, but this is not examined further.

Due to time limitations it has not been possible to break in the cylinder why a position dependency is seen in the friction force. Furthermore the final measurements were only conducted once why no consistency can be indicated. No further conclusions are made regarding the pressure dependency of the friction parameters. Subsequent to submission of this thesis new measurements will be conducted prior to the examination such consistent results may be presented.

Nomenclature

Symbol	Description	Unit
A	Area	$[m^2]$
F_f	Friction force	$[N]$
F_c	Coulomb Friction	$[N]$
F_s	Stribeck Friction	$[N]$
F_l	Load Force	$[N]$
h	Lubricant film thickness	$[-]$
H	Hose	$[-]$
k	Constant to determine v_b	$[-]$
k_τ	Relationship between τ_{hn} and τ_{hp}	$[-]$
k_q	Linearisation constant	$[m^3/s]$
k_{qp}	Linearisation constant	$[Pa \cdot s]$
L	Length	$[m]$
n	Stribeck exponent factor	$[-]$
p	Pressure	$[Pa]$
Q	Flow	$[m^3/s]$
x_p	Piston position	$[m]$
Re	Reynolds number	$[-]$
t	Time	$[s]$
T	Acceleration dependent friction term	$[s]$
v_s	Stribeck velocity	$[m/s]$
v_b	Lubricant film saturation velocity	$[m/s]$
V	Volume	$[m^3]$
z	Bristle deflection	$[m]$
β	Bulk modulus	$[Pa]$
β_F	Bulk modulus of fluid	$[Pa]$
β_A	Bulk modulus of air	$[Pa]$
ϵ_A	Volumetric ratio of free air in fluid	$[-]$
ϵ	Error	$[-]$
ζ	Damping ratio	$[-]$
λ	Friction factor	$[-]$
μ	Dynamic viscosity	$[\frac{kg}{s \cdot m}]$
μ	Mean	$[-]$
ρ	Density	$[kg/m^3]$
σ	Standard variance	$[-]$
σ_0	Bristle deflection friction coefficient	$[N/m]$
σ_1	Bristle damping friction coefficient	$[kg/s]$
σ_2	Viscous friction coefficient	$[kg/s]$
τ_{hp}	Lubricant film time constant for $h_{ss} > h$	$[s]$
τ_{hn}	Lubricant film time constant for $h_{ss} < h$	$[s]$
τ_{h0}	Lubricant film time constant for $\dot{x}_p = 0$	$[s]$
ω	Frequency	$[rad/s]$
ω_n	Natural Frequency	$[rad/s]$

General Subscripts

Symbol	Description
pm	Piston side main cylinder
rm	Rod side main cylinder
pl	Piston side load cylinder
rl	Rod side load cylinder
vp	Piston side valve on main side
vr	Rod side valve on main side
vl	Load valve
0	Linearisation point
s	Supply
T	Tank
exp	Expected
init	Initial

General Notation

Symbol	Description
x	x is a matrix or vector (Bold)
<i>x</i>	x is a variable (Italic)
\dot{x}	Time derivative of x (dot)
\ddot{x}	Double time derivative of x (double dot)
\hat{x}	Estimation of x (hat)
$ x $	Absolute value of x ()
\tilde{x}	Error of x (tilde)

Definitions

Coulomb Friction: A constant friction force in the opposite direction of the velocity.

Viscous Friction: A friction force proportional to the velocity.

Stribeck Friction: A friction force which decreases with velocity for lower velocities caused by partial lubrication.

Steady State Friction: The friction force at constant velocity.

Break Away Force: The force required to overcome the static friction force.

Dahl Effect: The dynamic friction effects for applied forces less than the break away force where the friction behaves as a stress / strain relation and is thus not a function of the velocity but displacement.

Fluid Lubrication Regime: The regime where the surfaces are fully lubricated i.e. where the friction force increases linearly with velocity.

Partial Lubrication: The regime where the surfaces are not fully lubricated.

Negative Resistance Regime: The regime where the friction force decreases with velocity caused by partial lubrication.

Contents

1	Introduction	1
2	State of The Art	3
2.1	Friction Dependencies	3
2.2	Friction Models	8
3	Problem Statement	15
3.1	Test Facility Requirements	15
3.2	Friction Model Requirements	18
I	Friction Modelling	19
4	Introduction	21
5	Velocity Dependent Friction Model	23
5.1	Steady State Friction Model	23
5.2	Dynamic Friction Model	31
6	Parameter Estimation	37
6.1	Estimation of Steady State Parameters	37
6.2	Estimation of Dynamic Parameters	40
6.3	Complete Parameter Estimation	46
6.4	Comparison of Parameter Estimation Methods	49
6.5	Parameter Estimation Evaluation	52
7	Validation of Proposed Friction Model	59
7.1	Steady State Friction Model Validation	60
7.2	Complete Friction Model Validation	63
8	Validation of Parameter Estimation Methods	67
9	Pressure Dependency in the Friction Force	71
9.1	Static Pressure Dependency	71
9.2	Dynamic Pressure Dependency	74
II	Closure	77
10	Discussion	79
10.1	Friction Modelling and Parameter Estimation	79
10.2	System Design	80
10.3	Experimental Measurements	82
11	Conclusion	85
	Bibliography	86

III Appendix 89

Appendix A System Design	91
A.1 Mechanical Setup	92
A.1.1 Hydraulic Cylinders	93
A.1.2 Structural Design	95
A.1.3 Strut Dimensioning	95
A.1.4 Slider System	97
A.1.5 Couplings	100
A.1.6 Summary	101
A.2 Hydraulic Setup	101
A.2.1 Valves	102
A.2.2 Accumulator Dimensioning	104
A.2.3 Hoses	105
A.3 Sensor Setup	106
A.3.1 Position/Velocity/Acceleration Measurement	106
A.3.2 Force Measurement	107
A.3.3 Pressure Transducer	107
A.3.4 Temperature Sensor	108
A.3.5 Summary	108

Appendix B System Modelling and Analysis	109
B.1 System Model	109
B.1.1 Mechanical Model	110
B.1.2 Valves	110
B.1.3 Pressure Dynamics	111
B.1.4 Model Validation	111
B.2 Analysis and Control	112
B.2.1 Linear Model	113
B.2.2 Analysis of Linear Model	116
B.2.3 Control Design	118

Appendix C Appendix for Part I	125
C.1 Method to Place Sampling Points	125

Appendix D Experimental Measurements	127
D.1 Break in	127
D.2 Evaluation of Velocity Step Duration for Steady State Measurements	128
D.3 Steady State Friction Sampling Instance	129
D.4 Position Dependency	132

IV Supplement 135

Supplement E System Topology	137
E.1 Variable Mass as Load	137
E.2 Dynamic Load	141
E.3 Further Analysis of Hydraulic Load Solution	144

Supplement F Further Design Considerations	149
F.1 Friction Joints and Pre tensioning	149
F.2 Electrical Network	150
F.3 Model Parameters	151

1 | Introduction

Friction is a phenomenon which is seen in all mechanical systems. A lot of work have been done in modelling the friction force which is seen to be highly non-linear and behaving dynamically (Armstrong-Helouvry, 1991). In general the friction force for constant velocities are well described and consists of Coulomb friction: a constant friction force in the opposite direction as the motion, viscous friction: a friction force proportional to the velocity and Stribeck effect: a friction force which decreases with velocity for lower velocities.

The steady state friction can be modelled with simple 4 or 5 parameter models (Armstrong-Helouvry, 1991). Even though a steady state model is adequate in most cases, it is desired to utilise more accurate models for some purposes. The dynamics of the friction force is shown in (Courtney-Pratt and Eisner, 1957) where it is seen that the friction force in the pre-sliding regime, before the break away force is met, is evolving with position and not velocity. This was first modelled by P.R Dahl which describes the pre-sliding friction as stress/strain behavior (Dahl, 1969). The dynamics of the friction force has since been reformulated several times (de Wit et al., 1995), (Swevers et al., 2000), (Lampaert et al., 2003), (Al-Bender et al., 2005), (Lampaert et al., 2002), (Dupont et al., 2014), (Merola et al., 2015) among others. These models are seen to accurately describe the friction force, both during steady state and transient response. Though in (Yanada and Sekikawa, 2008) it is seen that the existing models are inadequate in describing the friction force in hydraulic cylinders. The Modified LuGre Model (Yanada and Sekikawa, 2008) which is an extension to the LuGre model (de Wit et al., 1995) shows that it is possible to describe the friction force in a hydraulic cylinder accurately by incorporating a dynamic lubricant film thickness which is described by (Hess and Soom, 1990).

There are three major areas of utility for accurate friction models of hydraulic cylinders:

- **Accurate modelling of systems:** To model and analyse systems with friction, an accurate friction model can improve the accuracy of the system model.
- **Friction compensated control:** An accurate friction model can be utilised to enhance the performance of control systems by compensating for the friction force. This is especially seen to be useful for high performance systems which should accurately control motion around zero velocity (Jianyong Yao, 2015).
- **System Diagnosis:** The friction force in a hydraulic cylinder is assumed to be dependent on the condition of the sealings in the cylinder. If it is possible to detect changes in the friction force it might be possible to detect incipient faults or wear in the cylinder.

This thesis will concern the accurate modelling of the friction force in hydraulic cylinders and the accuracy of the parameter estimation will be investigated.

This thesis will be initiated with a state of the art investigation of the friction force dependencies seen in hydraulic cylinders and the existing friction models to describe these. From this investigation it is found that the velocity dependent friction force in hydraulic cylinders can be accurately described by dynamic friction models (Yanada and Sekikawa, 2008), (Tran et al., 2011). Though other dependencies in the friction force is seen:

- **Pressure Dependency:** The friction force in hydraulic cylinders is seen to be dependent on the pressure levels in the cylinder. The pressures in the cylinder chambers affect the sealings which is one of the contact surfaces causing the friction. An attempt to model the pressure dependency has been made in (Tran et al., 2011), yet it

is indicated from the state of the art investigation that this model does not describe the complete pressure dependency in the friction.

- **Viscosity dependency:** It is seen that the friction force is dependent on the viscosity of the fluid in hydraulic cylinders. Since the viscosity of the fluid changes with temperature this might cause the friction to change over time.

This thesis will concern the accurate friction force modelling of the pressure dependent friction force since it is indicated from the state of the art investigation that pressure dependency have a large influence in the friction force, yet only inconclusive work has been done in the area of this.

The thesis is a two part thesis: One part concerns the design and control of a test facility where the friction force can be measured accurately in every desirable operating point. The other part concerns the friction modelling and is initiated by an analysis of the existing models describing the velocity dependent friction. From these a modified model will be proposed. This is followed by an analysis of the parameter estimation, where different methods will be tested and the most accurate methods will be utilised. The parameters for the proposed velocity dependent friction model will be estimated at different pressure combinations to investigate how they change with pressure. Subsequently the pressure dependency will be incorporated in this friction model.

The following steps will be done to describe the pressure dependency in hydraulic cylinders:

1. Design of test facility
 - (a) Topology choice which fulfils the requirements
 - (b) Specific topology choice for structural design and sensor configuration.
 - (c) Structural Design
 - (d) Non-linear dynamic modelling of the system
 - (e) Control design for individual control of each chamber pressure in the main cylinder and the velocity of the system.
2. Friction modelling
 - (a) Analysis of existing friction models used to propose a simple and accurate model together with a consistent parameter estimation.
 - (b) Evaluation of different parameter estimation methods.
 - (c) Mapping of the pressure dependency in each model parameter.

The thesis will be initiated in the next chapter with a state of the art investigation of the friction force in hydraulic cylinders and the modelling of this.

2 | State of The Art

In this chapter a state of the art investigation is made regarding friction force dependencies and friction force modelling of hydraulic cylinders. Furthermore it is desired to investigate which friction force dependencies are characterised and modelled by the state of the art models. From the state of the art knowledge it is possible to indicate inconclusive or lacking parts of the current models.

In the next section the friction dependencies will be described. Subsequently it is investigated which models describe the friction in hydraulic cylinders and it is investigated how the model parameters are determined.

2.1 Friction Dependencies

It is well known that the friction depend on the velocity, though in hydraulic cylinders the friction is also known to depend on other factors such as pressure, temperature and type of oil.

2.1.1 Velocity Dependency

The velocity dependency is well described during steady state operation (Armstrong-Helouvry, 1991), though the friction is seen to vary dynamical with the velocity.

Steady State Friction Force

The steady state friction force consists in general of three different components, Coulomb friction, viscous friction and Stribeck friction (Armstrong-Helouvry, 1991). In Figure 2.1 the different friction components are seen. Coulomb friction is a constant friction force acting in the opposite way of the motion. Viscous friction is a friction force proportional to the velocity. Stribeck friction is a negative viscous friction which have an exponential decay with velocity. The Stribeck effect results in a decrease of friction force at increasing low velocities before entering the fluid lubrication regime, where the friction force is proportional to the velocity. This exponential decrease in friction is due to a partial lubrication, which means that only part of the surface is lubricated. The decrease is seen until a full lubrication of the surface is obtained.

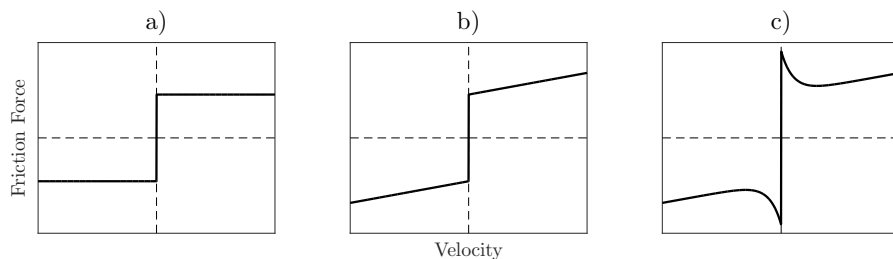


Figure 2.1: Steady state friction force: a) Coulomb, b) Coulomb+Viscous, c) Coulomb+Viscous+Stribeck

Dynamic Friction Force

Two phenomena causes the friction force to change dynamical, the Dahl effect and the dynamic lubricant film thickness.

In (Dahl, 1969), the Dahl effect is described. The Dahl effect describes how friction in the pre-sliding regime acts as stress/strain relation between the surfaces. This means that in the pre-sliding regime, before the break away force is met, the friction force is dependent on the displacement and not the velocity (Armstrong-Helouvry, 1991).

Another reason why the friction force is changing dynamically is the fact that the friction force is dependent on the lubricant film thickness between the surfaces (Hess and Soom, 1990), (Sugimura and Spikes, 1997). In the steady state negative resistance regime described by the Stribeck friction, the effect of the boundary lubrication film thickness is incorporated without a separate state for the lubricant film thickness. Though during dynamic response, the lubricant film thickness is seen to lag the velocity which makes it necessary to describe the thickness by incorporating a new state in the friction model, this is described in Section 2.2. The lubricant film is furthermore seen to have different dynamics for rising and falling thickness (Hess and Soom, 1990).

In Figure 2.2 the difference between the measured dynamic friction force and the steady state friction force during a sine wave for a hydraulic cylinder is seen. In (Yanada and Sekikawa, 2008) and (Tran et al., 2011), the implementation of a dynamic lubricant film thickness in friction models for hydraulic cylinders has shown to improve the accuracy of the models. This is seen in Figure 2.3 where the friction force in Figure 2.2 is modelled with the LuGre model with and without implemented dynamic lubricant film thickness. In Figure 2.2 the friction in the first quadrant is much higher in one curve since this is the friction measured after stand still where the film thickness is very low.

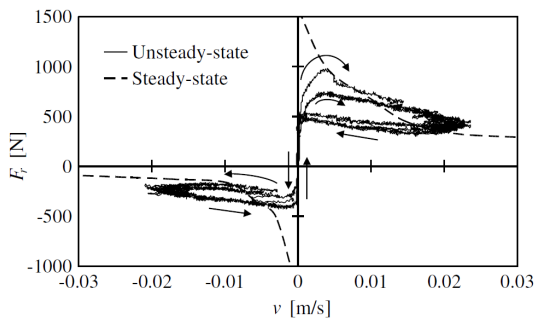


Figure 2.2: Measured friction force in a $\text{Ø}32/18$ cylinder during a sine wave of 0.5Hz and the corresponding steady state friction model (Yanada and Sekikawa, 2008).

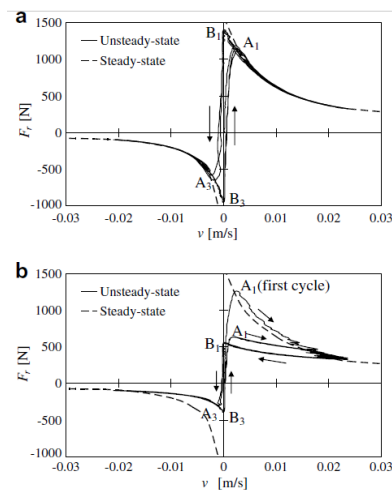


Figure 2.3: Modelled friction force corresponding to the measurements shown Figure 2.2. (a): LuGre model, (b): LuGre with incorporated dynamic lubricant film (Yanada and Sekikawa, 2008).

2.1.2 Pressure Dependency

Former papers and projects have investigated the pressure dependency in the friction force in hydraulic cylinders. The results from this work is described below. In this section it is

2.1. Friction Dependencies

investigated which relations between pressure and friction force is made in former work. In former work done by the authors (Pedersen and Jørgensen, 2016), the friction force in two asymmetric cylinders mounted rod to rod was investigated. The pressure dependency was investigated at steady state as function of the sum of pressures in the system. The pressure levels were varied by changing the supply pressure up to 120 bar. The pressure dependency in (Pedersen and Jørgensen, 2016) is seen in Figure 2.4. During the measurements it was not possible to obtain a constant low supply pressure why complete steady state conditions was not obtained. Yet it was indicated that the friction force increased with pressure.

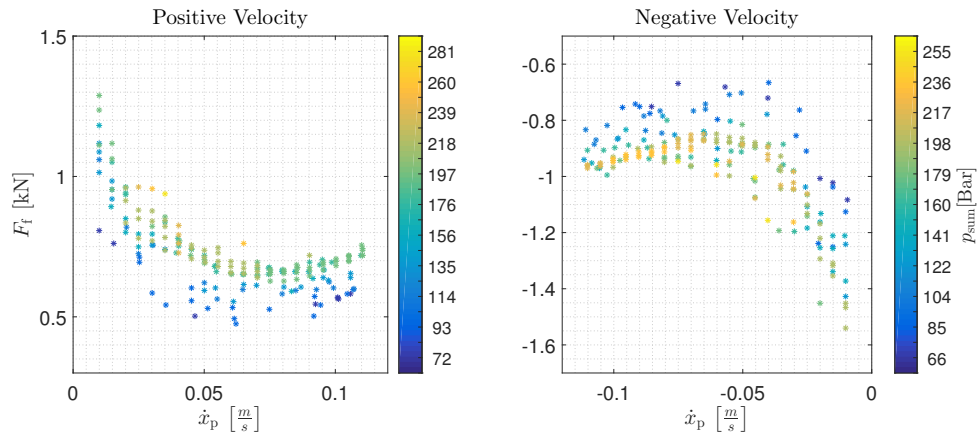


Figure 2.4: Pressure dependent friction as function of the sum of pressure (Pedersen and Jørgensen, 2016).

In (Parker, 2010), which is a product sheet from a seal manufacturer, it is seen that the pressure dependent friction saturates at certain pressure levels. Above 200 bar the pressure dependency is constant for all seals. The pressure dependency is measured at 0.1 m/s and is investigated from 0-200 bar. The friction force as function of pressure is seen in Figure 2.5 for different seals.

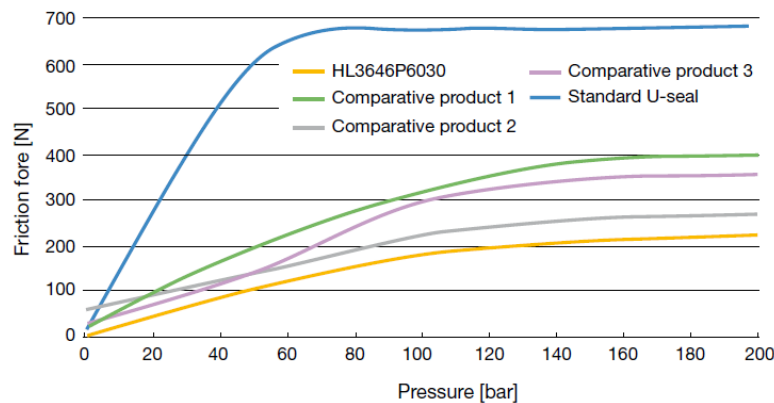


Figure 2.5: Pressure dependent friction seen for different seal types, measured at 0.1 m/s (Parker, 2010).

In (Cho et al., 2015) the friction in a multi chamber cylinder is tested at different loads. The friction is seen to be dependent on the load force. The friction force is seen to change up to a factor of 3 for different loads(100, 200, 400 kg). The pressures in the system is varying in a range of 0-40 bar. Though it should be noted that at very low pressures, other factors

might have an impact on the friction force such as the amount of air in the fluid. Figure 2.6 shows the steady state friction. It is seen that not only the friction levels changes with load but the curve changes as well.

In (Bullock, 2010), the dynamic friction during a sine wave with an amplitude of 12.5 mm/s and a frequency of 0.02 Hz is measured at different pressures from 10-80 bar. The friction force level is seen to change in the whole range of pressure, and the friction curve is seen to change with pressure as well.

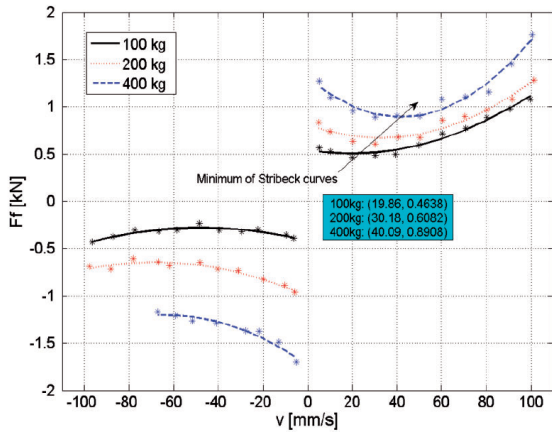


Figure 2.6: Load dependent friction seen in (Cho et al., 2015).

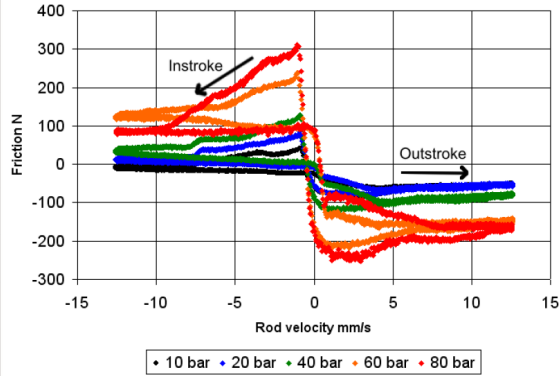


Figure 2.7: Pressure dependent friction during a sine wave seen in (Bullock, 2010).

In (Yanada et al., 2010) parameters for the Modified LuGre Model, described in Section 2.2, is identified at three different supply pressures. Most of the parameters, both steady state (F_s , F_c , v_s , n , σ_2 , v_b) and dynamic parameters (τ_{hp} , τ_{hm} , τ_{h0} , σ_0 , σ_1), are seen to change with pressure. The steady state and dynamic parameters identified are seen in Figure 2.8 and 2.9 respectively.

Parameters		F_s [N]	F_c [N]	v_s [m/s]	n	σ_2 [Ns/m]	v_b [m/s]
$p_s=3$ MPa	$v>0$	1.14×10^3	100	8.3×10^{-3}	0.84	196	0.03
	$v<0$	-744	-74	-6.3×10^{-3}	0.78	253	-0.03
$p_s=5$ MPa	$v>0$	1.56×10^3	200	1.65×10^{-2}	0.93	97	0.03
	$v<0$	-780	-48	-1.19×10^{-2}	1.53	585	-0.03
$p_s=7$ MPa	$v>0$	2.10×10^3	252	1.31×10^{-2}	1.10	1	0.025
	$v<0$	-1.13×10^3	-1.0	-1.15×10^{-2}	1.36	793	-0.025

Figure 2.8: Steady state friction parameters for different supply pressures (Yanada et al., 2010).

p_s [MPa]	τ_{hp} [s]	τ_{hm} [s]	τ_{h0} [s]	σ_0 [N/m]	σ_1 [Ns/m]
3	0.13	1.1	8.1	10^8	0.1
5	0.28	1.8	17		
7	0.32	2.4	43		

Figure 2.9: Dynamic friction parameters for different supply pressures (Yanada et al., 2010).

In (Tran et al., 2011) the steady state friction parameters, F_s and F_c in the New Modified

2.1. Friction Dependencies

LuGre model, are seen to vary with loads from 100-1200 N, which results in pressure levels varying from 10-60 bar. In Figure 2.10 and 2.11 the steady state friction parameters are seen for extending and retracting stroke respectively. It is seen that the two friction parameters changes with pressure, this relation is described in Section 2.2.3

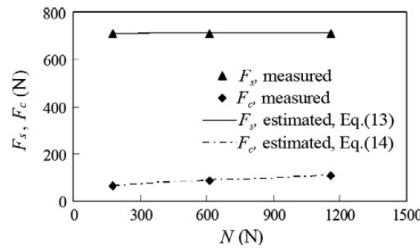


Figure 2.10: Steady state friction parameters, F_s and F_c for different loads for extending stroke (Tran et al., 2011).

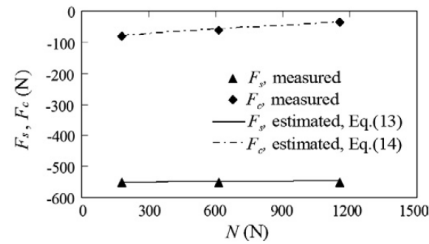


Figure 2.11: Steady state friction parameters, F_s and F_c for different loads for retracting stroke (Tran et al., 2011).

2.1.3 Viscosity Dependency

In (Hideki Yanada, 2010) the viscosity dependency of friction is investigated empirically by evaluating changes of friction parameters for the Modified LuGre Model for different viscosities. As seen in Figure 2.12, the viscosity is dependent on the oil temperature, why it might change during operation.

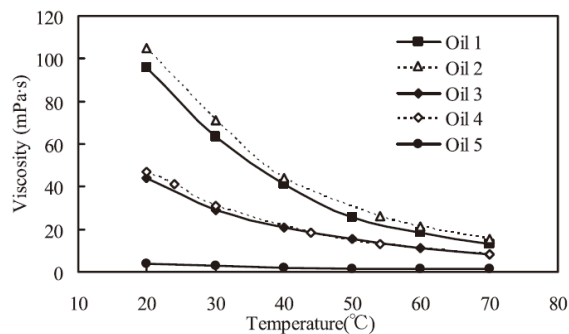


Figure 2.12: Viscosity as function of the oil temperature for different oils (Hideki Yanada, 2010).

In (Hideki Yanada, 2010) different oils are tested at different temperatures and both steady state and dynamic friction parameters are seen to change with viscosity. In Figure 2.13 the steady state parameters for a certain oil is seen at different viscosities. This is investigated by changing the temperature. It is seen that most of the parameters changes with viscosity. In Figure 2.14 the time constants for the lubricant film dynamics is seen to change with viscosity as well.

Parameters	F_s [N]	F_c [N]	v_s [m/s]	n	σ_2 [Ns/m]	v_b [m/s]	
83 mPa·s (24 °C)	$v>0$	1500	180	9.8×10^{-3}	0.95	105	3.5×10^{-2}
	$v<0$	-420	0	-1.0×10^{-2}	0.71	150	-3.5×10^{-2}
35 mPa·s (44 °C)	$v>0$	1623	165	1.0×10^{-2}	0.92	100	3.5×10^{-2}
	$v<0$	-698	-22	-1.0×10^{-2}	0.70	152	-3.5×10^{-2}
25 mPa·s (54 °C)	$v>0$	1694	140	1.0×10^{-2}	0.91	110	3.5×10^{-2}
	$v<0$	-878	-48	-1.2×10^{-2}	0.72	145	-3.5×10^{-2}

Figure 2.13: Table showing parameter changes for oil 1, at different viscosities (Hideki Yanada, 2010).

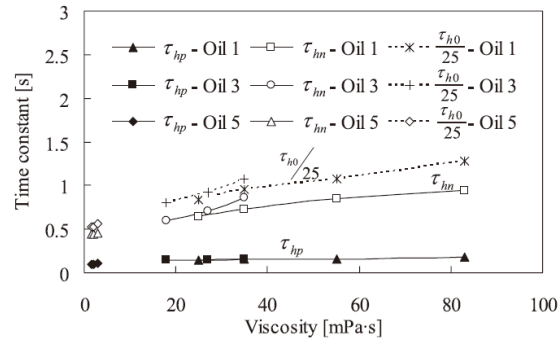


Figure 2.14: Lubricant film time constants as function of viscosity (Hideki Yanada, 2010).

2.1.4 Summary

The friction force is dependent not only on the velocity but also on time since it varies dynamical with the velocity. This is caused the Dahl effect and by dynamics in the lubricant film thickness between the surfaces.

In previous work the pressure dependency in the friction force is seen to have a significant contribution. It is indicated that both the steady state and the dynamic friction parameters are pressure dependent. Yet no conclusive work have been made. In (Parker, 2010) the steady state friction is seen for different seals in the range 0-200 bar, where the pressure dependency saturates at a certain pressure level, approximately 180 bar.

The viscosity is seen to have an impact on the friction force, both during steady state and dynamic operation. Since the viscosity changes with temperature, the friction force is dependent on the oil temperature.

2.2 Friction Models

Friction models have been used extensively to analyse and control systems. The first friction models used was a velocity dependent steady state friction models. Though the friction was seen to behave dynamical why dynamic friction models was developed (Armstrong-Helouvy, 1991). It has been shown that the friction in hydraulic cylinders is not only changing with velocity and time, but also with pressure and viscosity. In this section it will be investigated how the friction force is modelled for hydraulic cylinders in previous work. The existing friction models for hydraulic cylinders is based on the dynamical friction model proposed by P.R.Dahl (Dahl, 1975). This model does not incorporate the Stribeck effect, but it was modified to incorporate this in the LuGre model (de Wit et al., 1995). In the next subsection the LuGre model is elaborated and subsequently modifications to the LuGre model is described to model the friction in hydraulic cylinders. Subsequently to the friction model investigation, a review of the parameter estimation methods of the friction models will be done.

2.2.1 LuGre Model

In (de Wit et al., 1995) the friction force was modelled, based on the average behaviour of bristles, illustrated in Figure 2.15 where one surface has rigid bristles and the other has elastic bristles with damping. The friction force, F_f , is then modelled using the average bristle behaviour as:

$$F_f = \sigma_0 z + \sigma_1 \frac{dz}{dt} + \sigma_2 \dot{x}_p \quad (2.1)$$

Where z is the bristle deflection, σ_0 , σ_1 and σ_2 respectively are the bristle stiffness, the bristle damping and the viscous friction parameter. The bristle deflection is described by:

$$\frac{dz}{dt} = \dot{x}_p - \frac{|\dot{x}_p|}{g_s(\dot{x}_p)} z \quad (2.2)$$

Where $\sigma_0 g_s$ is equal to the Coulomb and Stribeck friction as:

$$\sigma_0 g_s = F_c + [F_s - F_c] e^{-\left(\frac{\dot{x}_p}{v_s}\right)^2} \quad (2.3)$$

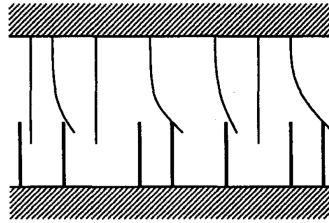


Figure 2.15: Bristle model proposed in (de Wit et al., 1995).

Since the LuGre model was formulated, it has been found that the LuGre model is inadequate in describing the friction force in the pre-sliding domain, since the LuGre model describes the pre-sliding domain without non-local memory in the hysteresis loop. A wide range of works have, since the LuGre model, used different methods to describe the pre-sliding domain accurately in dynamic friction models (Lampaert et al., 2003), (Al-Bender et al., 2005), (Lampaert et al., 2002), (Lampaert et al., 2014), (Dupont et al., 2014), (Merola et al., 2015).

Different efforts have been done to describe the friction in hydraulic cylinders. In the next section it is described how the LuGre model was modified to incorporate the dynamic lubricant film thickness.

2.2.2 Modified LuGre Model

In (Yanada and Sekikawa, 2008) the LuGre model was modified into the Modified LuGre model, since the LuGre model was seen to be inadequate in modelling the friction in hydraulic cylinders. This was caused by the fact that the lubricant film thickness was changing dynamically. This was solved by incorporating a dynamic changing lubricant film thickness, h . This is incorporated in the steady state friction model as:

$$g_s(\dot{x}_p, h) = F_c + [(1-h)F_s - F_c] e^{-\left(\frac{\dot{x}_p}{v_s}\right)^n} \quad (2.4)$$

The lubricant film thickness is lagging the velocity with first order dynamics as:

$$\frac{dh}{dt} = \frac{1}{\tau_h} (h_{ss} - h) \quad (2.5)$$

It is shown in (Hess and Soom, 1990) and (Sugimura and Spikes, 1997) that the dynamics of the lubricant film thickness, described by the time constant, τ_h , is different for increasing thickness, decreasing thickness and dwell time such:

$$\tau_h = \begin{cases} \tau_{hp} & \text{for } \dot{x}_p \neq 0, h \leq h_{ss} \\ \tau_{hn} & \text{for } \dot{x}_p \neq 0, h > h_{ss} \\ \tau_{h0} & \text{for } \dot{x}_p = 0 \end{cases} \quad (2.6)$$

The steady state lubricant film thickness h_{ss} is proportional to the velocity to the power of 2/3 with the gain K_f which is shown experimentally in (Sugimura and Spikes, 1997). The lubricant film thickness, h , is modelled to saturate at a certain velocity v_b , where the fluid lubrication regime begins, why the steady state thickness is described as:

$$h_{ss} = \begin{cases} K_f |\dot{x}_p|^{\frac{2}{3}} & \text{for } |\dot{x}_p| \leq |v_b| \\ K_f |v_b|^{\frac{2}{3}} & \text{for } |\dot{x}_p| > |v_b| \end{cases} \quad (2.7)$$

Where K_f is calculated as:

$$K_f = \left(1 - \frac{F_c}{F_s}\right) |v_b|^{-\frac{2}{3}} \quad (2.8)$$

This relationship is obtained by evaluating the steady state friction force, g_s , in the point where the fluid film saturates such $h = h_{max}$. In this point the Stribeck effect is negligible and can be assumed to be zero such:

$$F_f = F_c + \underbrace{[(1 - h_{max})F_s - F_c]}_{=0} e^{-\left(\frac{\dot{x}_p}{v_s}\right)^n} + \sigma_2 \dot{x}_p \Rightarrow 0 = [(1 - h_{max})F_s - F_c] \quad (2.9)$$

Substituting h_{max} with the known relationship in Equation (2.7) for $|\dot{x}_p| > |v_b|$ and isolating this for K_f yields:

$$0 = [(1 - h_{max})F_s - F_c] \quad \text{where } h_{max} = K_f |v_b|^{\frac{2}{3}} \implies K_f = \left(1 - \frac{F_c}{F_s}\right) |v_b|^{-\frac{2}{3}} \quad (2.10)$$

In the Modified LuGre model the bristle deflection is described as:

$$\frac{dz}{dt} = \dot{x}_p - \frac{\sigma_0 z}{g_s(\dot{x}_p, h)} \dot{x}_p \quad (2.11)$$

In the next subsection it is described how the Modified LuGre model was modified further to describe the friction in hydraulic cylinders.

2.2.3 New Modified LuGre Model

In (Tran et al., 2011) the Modified LuGre model was extended into the New Modified LuGre model. This model incorporates pressure dependency for the parameters F_s and F_c which was incorporated linearly as function of the load, N , as:

$$F_s = F_{s0} + C1 \left(\frac{N}{N_0} - 1\right) \quad F_c = F_{c0} + C2 \left(\frac{N}{N_0} - 1\right) \quad (2.12)$$

The pressure dependency was seen to change linearly in the range of 0-40 bar. Furthermore the New Modified LuGre model incorporates a friction proportional to the acceleration since it was seen that the residual between the modelled and measured friction force was proportional to the acceleration why the friction force is described as:

$$F_f = \sigma_0 z + \sigma_1 \frac{dz}{dt} + \sigma_2 \left(\dot{x}_p + T \frac{d\dot{x}_p}{dt} \right) \quad (2.13)$$

The authors of this thesis have in previous work used and further modified the New Modified LuGre model. This is described in the next subsection.

2.2.4 Former Work By the Authors

In (Pedersen and Jørgensen, 2016) modifications to the New Modified LuGre model was made to describe the friction in two cylinders mounted rod to rod. The modifications regarded:

- Neglecting of the bristle damping term, σ_1 , since the contribution from this term was negligible.
- Reformulation of the pressure dependency of friction, such F_s and F_c was a function of the sum of pressures.
- Reformulation of the acceleration dependent friction since it was seen that the incorporation of the acceleration term in the New Modified LuGre model resulted in discontinuities in the friction force model.
- Incorporation of a friction force term proportional to the change in the lubricant film thickness since this was seen to improve the model accuracy.

These modifications of the friction model proved to improve the accuracy of the friction model for the specific type of test system used.

2.2.5 Parameter Estimation

The parameter estimation is an essential part of friction modelling. In this section it will be described how the parameters for the models described in (Yanada and Sekikawa, 2008), (Tran et al., 2011) and (Pedersen and Jørgensen, 2016) are estimated.

Steady State Parameters

In (Yanada and Sekikawa, 2008), (Tran et al., 2011) and (Pedersen and Jørgensen, 2016) the steady state parameters are found by measuring the friction force levels during steady state at different velocities. Then using a Non-linear Least Squares Method (NLSM) to estimate the parameters.

In (Yanada and Sekikawa, 2008) and (Tran et al., 2011) the parameter v_b was chosen manually, though in (Pedersen and Jørgensen, 2016) it was included in the optimisation of the steady state parameters as an independent parameter.

In (Pedersen and Jørgensen, 2016) a study of the parameter estimation was performed under ideal conditions in simulations. This study showed that the model might be ill defined since the parameters v_s and n differed greatly from the simulated, or this could be caused by a lack of sample points at lower velocities. Furthermore it was seen that the estimation of v_b was wrong for negative velocities, resulting in a wrong dynamic friction force.

Lubricant Film Dynamics

During a small step in the velocity, not starting from zero, it has proved possible to isolate the lubricant film thickness, thus estimating the dynamics of the lubricant film thickness with velocity as input.

In (Yanada and Sekikawa, 2008) and (Tran et al., 2011) the dynamics was found by neglecting the dynamics of the velocity input. In (Pedersen and Jørgensen, 2016) an ARMAX algorithm was utilised to estimate the dynamics of the lubricant film thickness with the velocity as input. This method proved to be accurate.

Bristle Parameters

In (Yanada and Sekikawa, 2008) and (Tran et al., 2011) the bristle stiffness, σ_0 , was found by manually fitting the model to measurements. The bristle damping, σ_1 , was found as the square root of the stiffness in (Yanada and Sekikawa, 2008) and manually chosen in (Tran et al., 2011).

In (Pedersen and Jørgensen, 2016) the bristle stiffness was found by minimising the mean squared error between the friction model and the friction measurements. Due to a measurement error in the velocity due to axial play of the velocity sensor, the friction force was leading the velocity during change in direction, why a large error was seen. This large error might have resulted in a wrong estimation of the bristle stiffness. σ_0 was disregarded in (Pedersen and Jørgensen, 2016) due to a small contribution to the friction force.

Acceleration Dependent Friction

In (Tran et al., 2011) the acceleration dependent friction parameter, T , was found by plotting the residual of the modelled and measured friction against the acceleration, this is seen in Figure 2.16.

In (Pedersen and Jørgensen, 2016), T , was found directly from measurements under conditions where it could be isolated. The acceleration dependent friction showed to have a negative contribution to the friction model accuracy using this method, this is seen in figure 2.17.

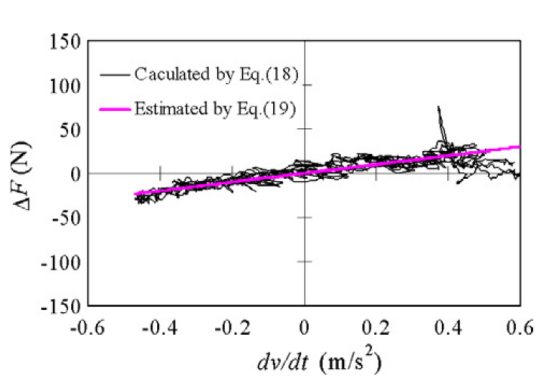


Figure 2.16: Measured and estimated acceleration dependency from (Tran et al., 2011).

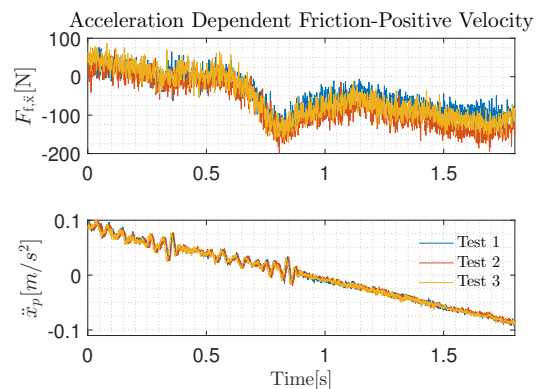


Figure 2.17: Measured acceleration dependency from (Pedersen and Jørgensen, 2016).

2.2.6 Summary

Different dynamic friction models have been reviewed. The most recent and accurate friction model for hydraulic cylinders is the New Modified LuGre model (Tran et al., 2011) which describes the friction force well during a sine wave of 0.5 Hz with an amplitude of 0.15 m/s. The pressure dependency, proportional to the load, is incorporated in the parameters F_s and F_c . This is examined in the range 0-40 bar and has shown good compliance with the measurements. In (Pedersen and Jørgensen, 2016) further modifications to the New Modified LuGre model was made. These modifications regards, bristle damping, pressure dependency, acceleration dependency and incorporation of a friction force term proportional to the change in the fluid film, though measurement errors was experienced why no conclusions were drawn.

The parameter estimation for the friction models is essential for correct modelling. The estimation method for the steady state parameters has shown to be inconsistent in the estimation of v_s and n , this maybe due to an ill defined friction model or a lack of sampling points at lower velocities. The mentioned parameter estimation methods for most of the dynamical parameters showed good results, though problems have been described in estimating the acceleration dependent term, T .

3 | Problem Statement

From the state of the art it is indicated that the current friction models can model the velocity dependent friction well. Though only inconclusive work is made in the field of pressure dependent friction modelling. The New Modified LuGre model describes a linear pressure dependency in the range 0-40 bar in two of the steady state parameters. Though in (Yanada et al., 2010) it is found that almost all of the friction parameters, both steady state and dynamic friction parameters changes with pressure, yet no conclusive work is presented since the tests are only made for few pressure combinations in a low range of pressures. It is seen in (Parker, 2010) that the steady state friction is not linear dependent on the pressure, but saturates at some point.

Besides the velocity and pressure dependencies, the friction force also changes with viscosity which changes with temperature. This thesis will not concern viscosity dependent friction since a constant oil temperature is assumed.

This thesis will concern the pressure dependency in an asymmetric hydraulic cylinder since this is used in a wide variety of applications and is an area which is not investigated thoroughly.

It is desired to investigate the pressure dependency in each chamber separately and the findings will be incorporated in an improved friction model. The following problem statement is formulated:

”How can the pressure dependent friction force characteristics in an asymmetric hydraulic cylinder be incorporated in a dynamic friction model to describe the friction force accurately? And how can the parameters be estimated in a simple, accurate and consistent way?”

To answer the problem statement it is desired to design and construct a test facility in which the friction force can be measured in a desired operating range with high accuracy. The design and control of this system is elaborated in Appendix A. Furthermore it is desired to propose an accurate dynamic friction model which can describe the velocity dependencies well, with the least number of parameters, since it is assumed that a low number of parameters ensure more consistent parameter estimations. A robust and accurate parameter estimation algorithm for this dynamic friction model will also be proposed. This velocity dependent dynamic friction model and parameter estimation method will be utilised to investigate how the friction model parameters changes in the desired range of chamber pressure.

The state of the art in friction dependencies, friction models and estimation methods are used to formulate which requirements the test facility should accommodate. This is elaborated in the next section. Subsequently to that, the requirements for the desired friction model and parameter estimation is described.

3.1 Test Facility Requirements

It is desired to construct a test facility such the friction force in an asymmetric hydraulic cylinder can be characterised accurately. For practical reasons the test bench should be dimensioned to withstand cylinders up to Ø80 since this is a size utilised in many applications. Furthermore a constant oil temperature should be assured due to the neglect of the friction force dependency of the viscosity.

3.1.1 Operating Range for Test Facility

The requirements to the operating range is formulated for the piston velocity, dynamic response and pressure.

Velocity Range Requirement

In this subsection the required velocity range for the test setup is defined. The test bench should be able to reach velocities such the velocity dependent friction parameters, related to known friction models (Yanada and Sekikawa, 2008), (Tran et al., 2011) and (Yanada et al., 2010), can be fully defined. Therefore the test system should be able to operate at velocities well into the fluid lubrication regime i.e. where the steady state friction increases linearly with velocity, such the slope can be well determined. In Table 4.1 previous found parameter sets for different hydraulic cylinders are shown. From this table it is seen that v_b , which is the velocity at which the friction force enters the fluid lubrication regime, is varying between 0.03 and 0.15 m/s. It is chosen that the hydraulic system should be able to reach velocities of approximately $0.25 \frac{m}{s}$ to assure that the fluid lubrication regime is well described in all cases.

It should be noted that the eight examples for v_b in Table 4.1 is for different sizes of hydraulic cylinders and different seals. Yet 0.25 m/s is well above the highest value of $v_b=0.15$, and it is assumed that this is adequate to determine the viscous friction. It is furthermore assessed that 0.25 m/s is a reasonable requirement for the test bench to be designed. At low velocities, in the negative resistance regime, the friction force changes rapidly described by the two "shaping parameters" n and v_s . In (Pedersen and Jørgensen, 2016) a problem of determining these two parameters consistently was observed, which might be due to a lack of friction measurements at small velocities below 0.01 m/s. Therefore it is required that the system can be controlled to obtain steady state velocities down to 0.001 m/s to fully characterise the friction force in the negative resistance regime.

Dynamic Performance Requirement

Due to limitations of the test bench, in the previous work done by the authors (Pedersen and Jørgensen, 2016), it was only possible to reach small accelerations of 0.124 m/s^2 during a sine trajectory. At these small accelerations the effects of the lubricant film dynamics does not have a great impact on the friction force. Therefore it is required that higher accelerations is obtainable to emphasise the effect of the lubricant film dynamics. Furthermore the friction model can be validated in a large operating range. If the dynamics of the friction force is much faster than the system response it might be difficult to estimate the dynamic parameters. In previous papers examining friction models including lubricant film dynamics, (Yanada and Sekikawa, 2008), (Tran et al., 2011), the friction force is measured at frequencies up to 2 Hz and compared to simulations. Based on the observations in these works, it is assumed sufficient to require that the system should be able to track sine waves with a frequency of 1 Hz in the whole velocity range, since the dynamic effects of the friction force is well seen during this response. With a maximum velocity of 0.25 m/s this results in a maximum acceleration of 1.57 m/s^2 .

Pressure Range Requirement

In Section 2.1.2 the state of art research in pressure dependent friction is seen. As seen, several investigations are made on the pressure dependency in the friction force in hydraulic cylinders. Yet so far no conclusive work is done in the field of pressure dependent friction. Different variables influence the friction parameters such as load force and supply pressure. These factors influence the chamber pressures causing the friction force to change. To investigate the pressure dependency in the friction force it is desired to control the two chamber pressures individually, to model the friction as function of the two pressures. From a model which is dependent on the chamber pressures it is possible to reformulate this to be dependent on e.g. the load force. With a friction model dependent on the pressures it is possible to describe the friction in a general way applicable for all systems with an asymmetric hydraulic cylinder.

In Section 2.1.2 it is seen that the friction force is changing with pressures up to around 180 bar. It is thus desired to investigate the pressures up to 200 bar, and to control each chamber pressure separately, such the full change in pressure dependent friction parameters can be characterised. If this range shows to be insufficient it might result in a model which is inaccurate for pressures above 200 bar.

It is desired to maintain pressure levels within ± 5 bar during steady state and ± 10 bar during transient behaviour. It is assumed that these requirements are adequate to characterise the pressure dependency, since the range of pressures are much higher (20-200 bar). It is desired to investigate if the friction force changes dynamical with pressures why it is desired to control the pressures dynamical as well.

3.1.2 Accuracy Requirements

In hydraulic cylinders the frictional forces are typically very small compared to the remaining forces acting in the cylinder. In the eight examples in 4.1 the maximum F_s found from previous work is 2100N and a cylinder of $\varnothing:32/18$ mm, at a load pressure of 200 bar is able to press with 16kN. In this thesis it is desired to measure the friction force with an accuracy much lower than the actual friction force level, so the results can be used to model the friction force with adequate accuracy. In Table 4.1 different friction forces measured in previous works are listed. The friction force levels differ greatly, and it is not possible to approximate a friction force level for the main cylinder.

It is though assumed that the friction force compared to the other forces acting on the cylinder is very small, thus requiring high precision sensors to obtain an exact friction force measurement.

3.1.3 Summary of Requirements

Velocity	It is desired to measure the friction force at velocities from 0.001-0.25 m/s. Furthermore the closed loop system should be able to track sine trajectories of 1 Hz, such the friction force dynamics can be well characterised.
Pressures	It is desired to estimate the friction force at pressures up to 200 bar, and it is desired to be able to control each chamber pressure individually to decouple the dependencies. It is desired to control the pressure within ± 5 bar during steady state and ± 10 bar during transient behavior.

Control	It is desired to decouple the frictional dependencies from the velocity and from each chamber pressure thus requiring separate control of each chamber pressure and the velocity.
Accuracy	An effort should be done in finding the most accurate solution to obtain friction force measurements and the test facility should support measurements which is not influenced by undesired characteristics e.g. axial play or characteristics of other components.
Viscosity	It is desired to neglect frictional changes due to viscosity. To obtain this it is necessary to maintain a constant oil temperature.
Test Object	It is desired to construct a flexible test bench which is dimensioned to test cylinders up to $\varnothing 80$. Yet this project will not necessarily concern a $\varnothing 80$ cylinder. A long stroke is desired for easy parametrisation of the friction models.

3.2 Friction Model Requirements

To investigate the pressure dependencies of friction, it is desired to have a velocity dependent friction model and parameter estimation method to describe the friction force accurately and consistently.

3.2.1 Friction Model

It is desired that the model can describe the friction force well in the velocity range during steady state and transient response. This way it is possible to determine model parameters in the entire pressure range to investigate how they change with pressure.

A study of the friction models described in the state of the art section should be made and the possibilities of improving these models should be investigated to utilise the most accurate and robust steady state model. By a robust steady state model, it is meant that small deviations between the model structure and the measured friction force should not result in highly varying estimated steady state parameters. Both the steady state model and the dynamic model should be analysed such parameters with little influence can be disregarded to obtain a simpler model structure with the least independent variables. It is assumed that this will make the parameter estimation simpler and more robust.

3.2.2 Parameter Estimation

It is desired to utilise a parameter estimation method which results in the lowest residual between the modelled and measured friction force. Since the parameters for the friction model should be determined repeatedly, at different pressure combinations, it is desired to develop a parameter estimation algorithm which can find the friction parameters consistently, at all time. By this the pressure dependency of each friction model parameter can be characterised and implemented in a new proposed friction model.

Standardised estimation methods are desired to determine all parameters such analyses can be made of different parameter estimation techniques and the most accurate, simple and consistent method is utilised to estimate the parameters as function of the pressures.

Part I

Friction Modelling

4	Introduction	21
5	Velocity Dependent Friction Model	23
5.1	Steady State Friction Model	23
5.1.1	Implementation of Changing Lubricant Film	24
5.1.2	Fit of Steady State Friction Models	26
5.1.3	Sensitivity Analysis of Steady State Models	28
5.1.4	Summary	31
5.2	Dynamic Friction Model	31
5.2.1	Neglecton of Bristle Damping - σ_1	32
5.2.2	Neglecton of Acceleration Dependent Friction - T	32
5.2.3	Reformulation of Lubricant Film Time Constant - τ_{hp}	33
5.2.4	Impact of Dynamic Model Assumptions	35
5.2.5	Summary	36
6	Parameter Estimation	37
6.1	Estimation of Steady State Parameters	37
6.1.1	Parameter Estimation from Steady State Conditions	37
6.1.2	Steady State Parameter Estimation from Sine Trajectory	38
6.1.3	Summary	40
6.2	Estimation of Dynamic Parameters	40
6.2.1	Separate Estimation of Dynamic Parameters	41
6.2.2	Optimisation Based Estimation of Dynamic Parameters	44
6.3	Complete Parameter Estimation	46
6.4	Comparison of Parameter Estimation Methods	49
6.4.1	Impact of Pressure Dependent Friction in the Estimation	50
6.5	Parameter Estimation Evaluation	52
6.5.1	Convergence of the Parameter Estimation	52
6.5.2	Sub Conclusion	53
6.5.3	Complete Estimation Utilising Sequential Method	54
7	Validation of Proposed Friction Model	59
7.1	Steady State Friction Model Validation	60
7.1.1	Evaluation at Different Pressure Combinations	61
7.2	Complete Friction Model Validation	63
7.2.1	Evaluation at Different Pressure Combinations	64
8	Validation of Parameter Estimation Methods	67
9	Pressure Dependency in the Friction Force	71
9.1	Static Pressure Dependency	71
9.2	Dynamic Pressure Dependency	74

4 | Introduction

This part of the thesis concerns the modelling of the friction force in hydraulic cylinders. The overall goal of this part is to propose a friction model which describes the friction force accurately in the whole velocity range, both steady state and dynamical. It is desired to incorporate accurate pressure dependency in the friction model. For this purpose it is desired to have a robust, as simple as possible, model with the least amount of parameters for easy parametrisation, without compromising the accuracy of the model. By this the pressure dependency can be modelled by characterising the change in the velocity dependent parameters at different pressure combinations.

The first chapter will concern the velocity dependent friction modelling. This chapter will include an analysis of different steady state models, a discussion of the dynamic parameters and which might be neglected. From the first chapter a model will be proposed which can describe the velocity dependent friction force accurately. In the second chapter different parameter estimation methods will be proposed and their ability to determine the parameters for the proposed model will be compared on simplicity, accuracy and sensitivity.

For the purpose of proposing a friction model and friction model parameter estimation method able to determine the friction parameters consistently and robustly, friction measurements for a hydraulic cylinder is necessary. Since the test setup is not constructed at this stage of the project, the following analyses are based on previous found friction model parameters for the Modified LuGre model seen in Table 4.1 and 4.2 found in: #1, #2, #3, #4 (Tran et al., 2011) for cylinders with different sealing types, #5 (Yanada and Sekikawa, 2008) and #6, #7, #8 (Yanada et al., 2010) found for the same cylinder at three different supply pressures. It is assumed that these parameters can represent actual friction measurements in hydraulic cylinders. Since no measurement data is available, simulation data utilising the previous found parameters will be used to simulate "measurements". A set of parameters which is assumed to be in the range of the friction force in the main cylinder, 50x35, is chosen to represent the "measurements", these are marked as "Expected Parameters" in the tables. The values F_s , F_c and σ_2 are chosen relatively high compared to the parameters seen in the table since a larger cylinder is assumed to have a higher friction force level, while the dynamic and shaping parameters are chosen in the same range as the cylinders in the table. When the expected parameters are utilised in simulation the resulting friction force will be referred to as "expected measurement".

When measurements are available, the proposed friction model and parameter estimation will be validated.

The velocity dependent model and parameter estimation method will be utilised to investigate the pressure dependency in each parameter, by estimating the parameters in a wide range of pressure combinations. Furthermore it will be investigated if the friction force is dynamically connected to the chamber pressures.

Source	Size[mm]		F_s	F_c	v_s	v_b	n	σ_2
#1	32/18	$v > 0$	710	65	0.02	0.06	0.5	150
		$v < 0$	-550	-80	-0.02	-0.05	0.5	280
#2	32/18	$v > 0$	1100	360	0.06	0.13	0.8	80
		$v < 0$	-1112	-440	-0.08	-0.13	0.5	100
#3	32/18	$v > 0$	1450	240	0.08	0.15	0.8	20
		$v < 0$	-1400	-320	-0.08	-0.15	0.8	25
#4	20/12	$v > 0$	160	50	0.02	0.04	0.7	150
		$v < 0$	-140	-35	-0.02	-0.04	0.8	180
#5	32/18	$v > 0$	1575	239	0.0213	0.03	0.783	66.2
		$v < 0$	-1283	-61.7	-0.00477	-0.030	0.612	264
#6	32/18	$v > 0$	1140	100	8.3e-3	0.03	0.84	196
		$v < 0$	-744	-74	-6.3e-3	-0.03	0.78	253
#7	32/18	$v > 0$	1560	200	1.65e-2	0.03	0.93	97
		$v < 0$	-780	-48	-1.19e-2	-0.03	1.53	585
#8	32/18	$v > 0$	2100	252	1.31e-2	0.025	1.10	1
		$v < 0$	-1130	-1	-1.15e-2	-0.025	1.36	793
$v > 0$		Max	2100	360	0.08	0.15	1.10	196
		Min	160	50	0.0083	0.025	0.5	1
$v < 0$		Max	-140	-1	-0.00477	-0.025	0.5	25
		Min	-1400	-440	-0.08	-0.15	1.53	793
Expected Parameters		$v > 0$	2000	200	0.01	0.1	1.2	300
		$v < 0$	-2500	-600	-0.01	-0.05	1.2	500

Table 4.1: Eight different steady state parameter sets for the Modified LuGre model found in previous work. The "Expected Parameters" category are the parameters chosen to represent the friction force in the main cylinder in the analyses in the next chapters.

Source	Size[mm]	τ_{hp}	τ_{hn}	τ_{h0}	σ_0	σ_1
#1	32/18	0.25	1	40	2.0e7	0.1
#2	32/18	0.12	0.3	40	1.5e7	0.1
#3	32/18	0.05	0.2	40	1.5e7	0.1
#4	20/12	0.05	0.3	40	1.0e7	0.1
#5	32/18	0.033	2.0	10.0	1.0e8	1e4
#6	32/18	0.13	1.1	8.1	1.0e8	0.1
#7	32/18	0.28	1.8	17	1.0e8	0.1
#8	32/18	0.32	2.4	43	1.0e8	0.1
Max/Min		0.32 / 0.033	2.4 / 0.2	43 / 8.1	1e8 / 1.0e7	1e4 / 0.1
Expected Parameters		0.3	0.3	30	1.0e7	5000

Table 4.2: Eight different dynamical parameter sets for the Modified LuGre model found in previous work. The "Expected Parameters" category are the parameters chosen to represent the friction force in the main cylinder in the analyses in the next chapters.

5 | Velocity Dependent Friction Model

This chapter will concern the modelling of the velocity dependent friction force, both steady state and dynamical. It is desired to utilise a simple and accurate model which is not sensitive to potential measurement errors or non modelled friction characteristics. By defining a model with the least amount of independent parameters it is assumed that the parameter estimation will be more consistent. It is assumed that more parameters will increase the possibility of the parameters compensating for each other since the sensitivity of the friction force from the different parameters might interfere.

The chapter consists of the following sections:

- **Steady State Friction Model:** Different steady state models are reviewed.
 - **Incorporation of dynamic lubricant film:** The models are modified to incorporate changing lubricant film thickness where a scheme for determining the saturation velocity, v_b , as function of the steady state parameters is developed.
 - **Fit of steady state models:** The models are fitted to earlier found steady state friction characteristics to compare the accuracy of the models.
 - **Sensitivity:** The sensitivity of the individual friction model parameters are investigated by utilising sensitivity equations. Furthermore the sensitivity of the parameter changes due to potential measurement errors are evaluated.
- **Dynamic Friction Model**
 - **Neglecton of Bristle Damping:** The bristle damping term is neglected since the contribution from this is small.
 - **Neglection of Acceleration Dependent friction:** The acceleration dependent friction is neglected since this is assumed to be an ill defined pressure dependency.
 - **Reformulation of The Lubricant Film Dynamics:** The dynamics of the lubricant film is governed by τ_{hp} for increasing thickness. The impact from the dynamics of the lubricant film during thickening of the film is seen to be negligible, why this parameter is reformulated.

Based on these analysis a steady state model is chosen to describe the steady state friction behaviour and a dynamical friction model is proposed to describe the dynamics of the friction in hydraulic cylinders. Since measurements are not available at this time of the project, measurements will be simulated with the proposed model, this is done in the lack of better options. Throughout this chapter the analyses are made with basis in the simulated measurements made with the expected parameters from Table 4.1 and 4.2 if nothing else is stated.

A practical validation of the friction model is conducted in Chapter 7

5.1 Steady State Friction Model

In this section different methods to model the steady state friction are described. The steady state friction consists of Coulomb friction, F_c , which have the same sign as the velocity. It also consists of viscous friction which is modelled as: $\dot{x}\sigma_2$. Where σ_2 is the viscous friction coefficient. The steady state friction force also contains Stribeck friction which is a negative viscous friction at low velocities. Since the Stribeck friction region has been described by

different models in the past, these models will be described and analysed in the following. The Stribeck friction characteristics was first modelled by the Tustin model as shown in Equation 5.1 (Armstrong-Helouvry, 1991): Where F_s is the Stribeck friction parameter and v_s is a parameter used to shape the Stribeck curve. Though the first Stribeck model was the Tustin model, several models have since the Tustin model described the Stribeck curve. In (Armstrong-Helouvry, 1991) different Stribeck models are described. These are the Tustin model, Gaussian model and the Lorentzian model which are defined:

$$\underbrace{(F_s - F_c)e^{-(\dot{x}/v_s)}}_{\text{Tustin}} \quad \underbrace{(F_s - F_c)e^{-(\dot{x}/v_s)^2}}_{\text{Gaussian}} \quad \underbrace{(F_s - F_c)\frac{1}{1 + (\dot{x}/v_s)^2}}_{\text{Lorentzian}} \quad (5.1)$$

In (Yanada and Sekikawa, 2008) the steady state friction was modeled as the Gaussian model, though the exponent was made as a variable, n , to increase the accuracy of the model as:

$$(F_s - F_c)e^{-(\dot{x}/v_s)^n} \quad (5.2)$$

This friction model will be referred to as the Modified Gaussian (MG).

It is in some cases seen that the Lorentzian model fits experimental data better than the other models (Armstrong-Helouvry, 1991). To investigate if the Lorentzian model can be modified for a better fit, it is decided to construct a Modified Lorentzian model (ML) with a variable exponent which is described as:

$$(F_s - F_c)\frac{1}{1 + (\dot{x}/v_s)^n} \quad (5.3)$$

An example of the 5 steady state models are seen in Figure 5.2.

5.1.1 Implementation of Changing Lubricant Film

In this subsection the implementation of a changing lubricant film thickness is described. The lubricant film thickness saturation velocity, v_b , is discussed and a method to determine v_b will be proposed.

The method to place v_b in this section is one method to do it, such v_b is placed at the correct velocity as a dependent variable as function of v_s and n , yet other methods may also work. The method proposed in this section to determine v_b is validated in Section 7.1.

This method to define v_b as function of v_s and n may improve the robustness of the estimation of the remaining parameters, since v_b are coupled to these.

To incorporate the changing lubricant film thickness in the friction models, the thickness, h , is multiplied on the Stribeck friction parameter as (Yanada and Sekikawa, 2008): $g_s = F_c + ((1 - h)F_s - F_c) \cdot \text{Stribeck}$, where "Stribeck" is the functions describing the Stribeck curve, elaborated in the previous section. The lubricant film thickness, h , is calculated as:

$$h = \begin{cases} K_f |\dot{x}_p|^{\frac{2}{3}} & \text{for } |\dot{x}_p| \leq |v_b| \\ K_f |v_b|^{\frac{2}{3}} & \text{for } |\dot{x}_p| > |v_b| \end{cases} \quad (5.4)$$

Where K_f is calculated as:

$$K_f = \left(1 - \frac{F_c}{F_s}\right) |v_b|^{-\frac{2}{3}} \quad (5.5)$$

An elaboration of this is seen in Section 2.2.2. v_b is defined as the velocity at which the lubricant film thickness saturates (Yanada and Sekikawa, 2008), (Tran et al., 2011), (Yanada et al., 2010). The determination of the parameter, v_b , has been conducted in different ways in previous work. In (Yanada and Sekikawa, 2008) and (Yanada et al., 2010), v_b is determined as the velocity at which the measured steady state friction is (almost) minimum. In (Tran et al., 2011), v_b is determined as 1.5 times the velocity at which the steady state friction is minimum. In (Pedersen and Jørgensen, 2016), v_b was used as an independent parameter in the parameter estimation of the steady state friction using a NLSM. The results in (Pedersen and Jørgensen, 2016) indicated that a higher value of v_b , for negative velocities, would result in a better dynamic friction model than when v_b was estimated to be at the point where the steady state friction is minimum, as was the case when having v_b as an independent parameter in the NLSM. It was indicated that v_b should be placed at the velocity where the steady state friction curve is almost linear proportional to velocity, e.i. where the decreasing Stribeck term is small. This was also the result obtained from (Tran et al., 2011) where v_b was determined as 1.5 times the velocity where the steady state friction is minimum.

In this project it is preferred that the parameter estimation can be done without manually choosing parameters. Furthermore it is desired to propose a robust and consistent parameter estimation. Since it was seen in (Pedersen and Jørgensen, 2016) that the NLSM placed v_b at a "wrong" value, it is preferred that v_b can be calculated based on the other steady state parameters, such v_b is at the velocity where the steady state friction enters the fluid lubrication regime. This way a consistent estimation of v_b is made.

Even though the placement of v_b , with this method, should be evaluated at practical measurements, it is consistently placed to ensure a robust parameter estimation of the remaining parameters.

Two methods are considered: one where v_b is placed where the derivative of the Stribeck curve is (almost) zero and one where v_b is placed where the value of the Stribeck curve is (almost) zero.

By choosing v_b at the velocity where the Stribeck friction is (almost) zero, the method complies with the assumption that the Stribeck friction force should almost be zero at v_b . The proposed method to determine v_b is based on the equations describing the Stribeck curve, respectively Tustin, Gaussian, Modified Gaussian (MG), Lorentzian and Modified Lorentzian (ML).

The method is shown for the MG model, which then holds true for the Tustin and Gaussian model since the models are described by the same structure. The velocity where $\dot{x}_p = v_b$ is chosen such the Stribeck friction attains a certain percentage of its maximum value. This can be obtained by using the following relationship:

$$(F_s - F_c) e^{-\left(\frac{\dot{x}_p}{v_b}\right)^n} \Bigg|_{\dot{x}_p=v_b} = (F_s - F_c) k \Rightarrow \dot{x}_p = e^{\left(\frac{\ln(-\ln(k))}{n}\right)} v_b = v_b \quad (5.6)$$

Where k is a parameter which defines the percentage the Stribeck friction should have decreased at v_b . It is found that for different values of the parameter, n , the value of k should change accordingly for v_b to be at the velocity where the steady state friction starts to be approximately linear proportional to the velocity. This relationship is found ad hoc. Utilising a definition of k as function of n , results in a value of v_b in the correct region. This definition of v_b with $k = \frac{0.002}{n^{4.5}}$, which is chosen ad hoc, results in a value of v_b placed as shown in Figure 5.1 where the steady state parameters are 5 sets of random generated parameters within the parameter values from Table 4.1. The saturation velocity v_b is placed

at different velocities since the curvature of the five steady state curves is different to each other, yet v_b is approximately placed at the correct velocity where the fluid film lubrication regime starts. This method to determine v_b is seen to be accurate for values of $n=0.5-2$ which is within the earlier found parameters shown in Table 4.1. The method will be evaluated when practical measurements are obtained.

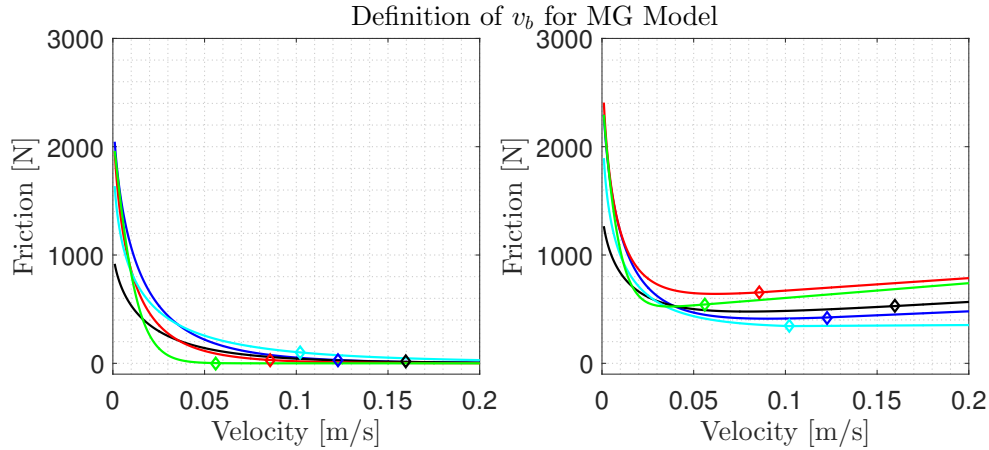


Figure 5.1: This figure is showing where the lubricant film thickness saturation velocity is placed for random chosen friction model parameters.

The same method is used to describe a general definition of k for the Lorentzian model and Modified Lorentzian model. The value used for k for each Stribeck model together with the equation for v_b is shown in Table 5.1. These definitions of v_b will be utilised in the following analyses.

	Stribeck Model	v_b	k
Tustin	$((1-h)F_s - F_c)e^{(-\dot{x}/v_s)}$	$-\ln(k)v_s$	0.002
Gaussian	$((1-h)F_s - F_c)e^{(-\dot{x}/v_s)^2}$	$\sqrt{-\ln(k)}v_s$	$\frac{0.002}{24.5}$
Lorentzian	$((1-h)F_s - F_c)\frac{1}{1+(\frac{\dot{x}}{v_s})^2}$	$e^{\frac{\ln(-\frac{k-1}{k})}{2}}v_s$	$\frac{0.06}{2^2}$
M-Gaussian	$((1-h)F_s - F_c)e^{(-\dot{x}/v_s)^n}$	$e^{\frac{\ln(-\ln(k))}{n}}v_s$	$\frac{0.002}{n^{4.5}}$
M-Lorentzian	$((1-h)F_s - F_c)\frac{1}{1+(\frac{\dot{x}}{v_s})^n}$	$e^{\frac{\ln(-\frac{k-1}{k})}{n}}v_s$	$\frac{0.06}{n^2}$

Table 5.1: In this table the equation of the five different methods to describe the steady state friction are shown with an expression for v_b .

5.1.2 Fit of Steady State Friction Models

In this subsection a comparison of the five different representations of the Stribeck friction will be evaluated by investigating how accurate the different models fit previous measured friction data. The five models will be fitted to the eight steady state friction characteristics found in earlier works shown in Table 4.1. The assumption in this investigation is that the eight previous friction characterisations can be accurately described by the Modified Gaussian model with the parameter sets from the table.

5.1. Steady State Friction Model

In Figure 5.2 an example of a fit for the different steady state models to the eight earlier modelled steady state friction characteristics is seen. The dotted line is the simulated friction with the friction parameter set #1 in Table 4.1.

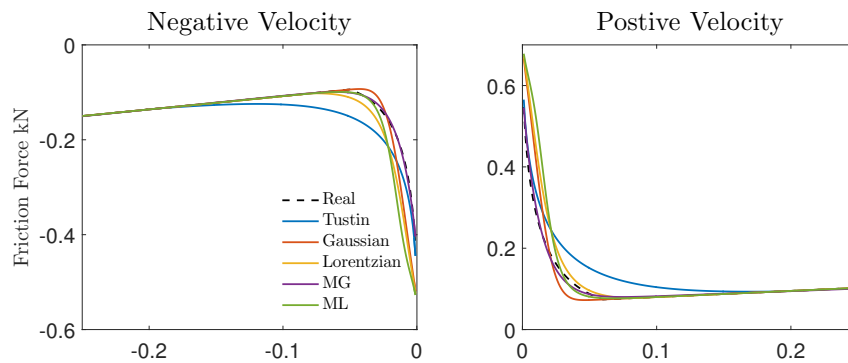


Figure 5.2: An example of the fit of the steady state models and eight earlier described steady state friction forces. This figure illustrates the fit of #1 in Table 4.1.

In Table 5.2 results of fitting the different steady state models to the eight steady state friction force characteristics in Table 4.1 are seen. The fits are made using a NLSM, with points distributed from -0.25 to 0.25 m/s with a sampling interval of 0.001 m/s. RMS represent the Root Mean Square of the residual and Max represents the maximum residual. From this analysis it is seen that the MG model is the most accurate in describing the friction force, assuming that the eight previous found parameter sets are accurately describing this. In the table it is seen that the implementation of the new definition of v_b fits the original data well. Furthermore it is seen that the Gaussian and Lorentzian models yield the worst fit.

		Tustin	Gaussian	Lorentzian	MG	ML
#1	RMS	2,7	6,6	4,4	2,4	4,2
	Max	112,6	187,4	159,2	14,7	39,3
#2	RMS	4,3	12,4	8,1	2,0	3,7
	Max	59,3	140,9	107,8	10,0	42,5
#3	RMS	5,8	24,9	13,5	2,9	6,6
	Max	73,2	221,2	166,2	12,6	68,8
#4	RMS	0,3	1,0	0,5	0,3	0,7
	Max	9,0	22,3	17,4	2,3	6,8
#5	RMS	3,0	6,8	3,7	2,4	5,3
	Max	40,5	207,5	145,9	41,0	96,5
#6	RMS	0,9	5,0	2,8	0,6	2,4
	Max	37,1	149,9	107,8	7,1	43,2
#7	RMS	3,1	4,8	2,6	1,6	4,6
	Max	41,2	176,2	116,4	27,5	82,3
#8	RMS	4,5	9,6	3,3	0,7	4,8
	Max	90,3	150,8	72,5	15,9	62,4
Mean	RMS	3,2	8,9	4,5	1,5	4,1
	MAX	62,6	153,5	104,3	15,7	55,5

Table 5.2: Comparison of fit accuracy for the different steady state models considered.

5.1.3 Sensitivity Analysis of Steady State Models

In this subsection it is investigated how sensitive the different models are with respect to a change in each parameter. This analysis is based on sensitivity equations. Furthermore it is investigated how sensitive the different models are to potential measurement errors.

To conduct these analyses it is chosen to obtain parameter sets for each individual friction model, such the terms for the analyses is the same for the different models. These parameter sets is found by fitting the Tustin model, Gaussian model, Lorentzian model and ML model to the MG model with the expected parameters utilising a NLSM. The results is shown in table 5.3.

Model		F_s	F_c	v_s	n	σ_2
Tustin	$\dot{x} > 0$	2100	191	0.0105	-	349
	$\dot{x} < 0$	-2645	-594	-0.009	-	530
Gaussian	$\dot{x} > 0$	1893	215	0.0126	-	214
	$\dot{x} < 0$	-2293	-612	-0.012	-	431
Lorentzian	$\dot{x} > 0$	1961	201	0.0097	-	291
	$\dot{x} < 0$	-2396	-600	-0.0088	-	496
MG	$\dot{x} > 0$	2000	200	0.01	1.2	300
	$\dot{x} < 0$	-2500	-600	-0.01	1.2	500
ML	$\dot{x} > 0$	1941	190	0.0081	1.96	355
	$\dot{x} < 0$	-2344	-592	-0.0076	2.05	544

Table 5.3: In this table the steady state friction model parameters for the five modelling methods is shown. The parameters are found by fitting the respective models to data generated using the expected parameters for the Modified LuGre model shown in Table 4.1 and 4.2.

The measurement error used in this section is the repeatability error for the friction force measurement, which is based on the accuracy data of the sensors used. The repeatability error for the load cell is $\pm 0.01\%$ $F_s = 5\text{N}$. The repeatability error for the pressure transducers are not stated in the data sheet but is chosen to be $\pm 20\text{N}$ (approximately half of the combined accuracy) for the sake of this analysis. This results in a combined repeatability error of $\pm 25\text{N}$.

In the next section the sensitivity equations for the different steady state models are made to investigate how sensitive the friction force is for changes in each parameter. Subsequently an analysis of the influence of measurement errors for the different Stribeck models is made. The knowledge from this analysis will be used later to determine which method should be used to estimate the different steady state parameters.

Sensitivity Equations

With the use of sensitivity equations it is possible to visualise how the friction force changes when a parameter changes. By this visualising where the different parameters are dominating. It is the parameters for the different models from Table 5.3 which is utilised in this analysis. The parameter vector for the steady state models are: $\theta = [F_s \ F_c \ v_s \ \sigma_2 \ n]$. The sensitivity equations is found by differentiating the friction force with respect to the parameter vector as:

$$\frac{\partial g_s}{\partial \theta} = \left[\frac{\partial g_s}{\partial F_s} \ \frac{\partial g_s}{\partial F_c} \ \frac{\partial g_s}{\partial v_s} \ \frac{\partial g_s}{\partial \sigma_2} \ \frac{\partial g_s}{\partial n} \right] \quad (5.7)$$

In Figure 5.3 the sensitivity of the friction force with respect to each parameter is seen as function of the velocity. As seen the friction force is highly dependent on both F_s , v_s and n at small velocities whereas the friction force is seen to be sensitive to changes in F_c and σ_2 at higher velocities.

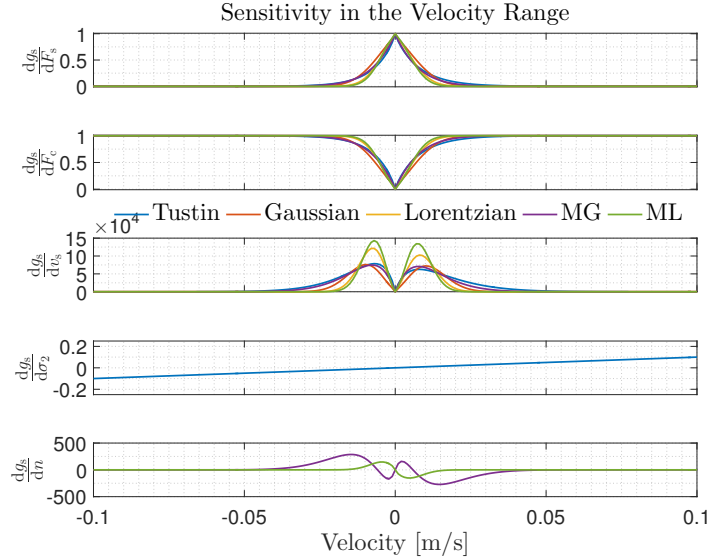


Figure 5.3: Sensitivity of the friction force with respect to each parameter.

The greatest difference between the models is seen for v_s where the Lorentzian and the ML model differs much from the remaining model. Though this is not directly comparable to the other steady state models since the size of v_s is not the same as for the remaining models as can be seen from Table 5.3.

Sensitivity to Measurement Errors

Due to the repeatability accuracy of the sensors used to measure the friction force in the test facility, the measured friction force may change within a certain range even though the actual friction force is not changing. When such small errors are occurring it is desired that the model parameters does not vary much.

To test the influence of this repeatability error a random force error, F_ϵ , is introduced. This is defined as a second order polynomial which varies within $\pm 25N$. This error is added to the simulated friction force of each friction model and the parameters for each model is estimated.

The second order polynomial is constructed from three randomly generated points in the range $\epsilon_{rep} = \pm 25N$, one point at $-5000N$, one point at $0N$ and one point at $+5000N$ as shown in the left plot of Figure 5.4. This range is chosen since it is assumed that the friction force will not exceed this range. The force error polynomial is described as:

$$F_\epsilon(\epsilon) = a + F \cdot b + F^2 \cdot c \quad , \quad \epsilon = [\epsilon(1) \epsilon(2) \epsilon(3)] = rand(1, 3) \leq \epsilon_{rep} \quad (5.8)$$

Where ϵ is three randomly generated numbers within the calculated error range of $\epsilon_{rep} = \pm 25N$.

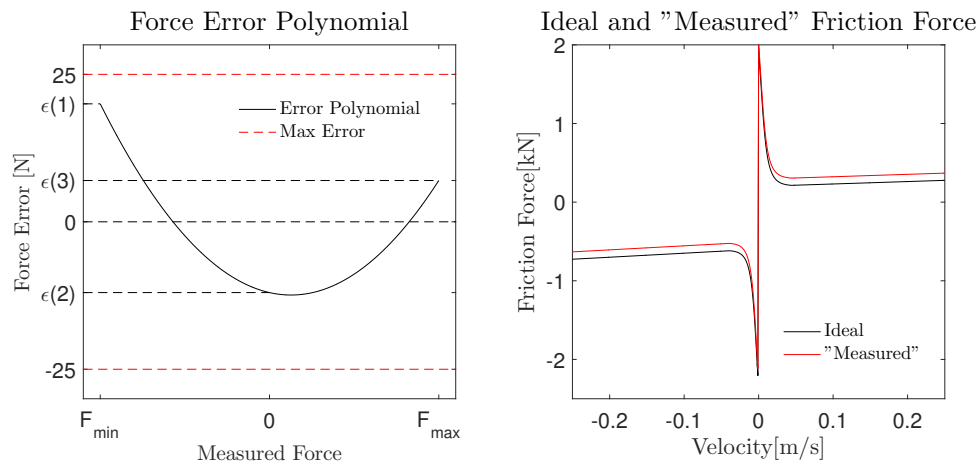


Figure 5.4: Example of error polynomial and example of friction force measurement with and without error. The figure to the right is the simulated steady state friction with and without the simulated error. The error in the plot are scaled to visualise the difference.

To investigate the sensitivity to measurement errors in the different models, each steady state model is fitted to the respective steady state model, utilising the parameters from Table 5.3, with the added error polynomial added to the simulated measurements. This is done 1000 times with random generated error polynomials for each Stribeck model and the results are shown in Table 5.4. This method is used due to a lag of measurements. The method is made to simulate a potential measurement error and investigate how sensitive the different models are to this error. This method will be used in the remaining analyses before measurements are available.

In Table 5.4 the standard deviation, σ , and the maximum error, Max, for each estimated parameter is seen for all the steady state models. It is seen that the parameter estimation error is in the same range for all the models.

Parameter		Tustin	Gaussian	Lorentzian	MG	ML	Mean	
F_s	$x > 0$	σ	12.8	13.2	13.3	13.3	13.0	13.1
		Max	29.7	26.9	29.2	29.2	27.6	28.5
	$x < 0$	σ	12.3	13.0	12.6	12.5	13.1	12.7
		Max	30.1	30.1	29.6	27.7	29.9	29.5
F_c	$x > 0$	σ	14.3	14.5	14.6	14.8	14.8	14.6
		Max	25.4	25.0	26.1	25.6	25.8	25.6
	$x < 0$	σ	14.2	14.5	14.4	14.6	14.7	14.5
		Max	27.0	27.0	27.1	25.6	27.3	26.8
v_s	$x > 0$	σ	7.3e-6	4.9e-6	5.3e-6	7.5e-6	5.5e-6	6.1e-6
		Max	19e-6	13e-6	14e-6	19e-6	14e-6	16e-6
	$x < 0$	σ	5.5e-6	4.1e-6	4.4e-6	7.8e-6	4.7e-6	5.3e-6
		Max	14e-6	11e-6	11e-6	20e-6	12e-6	14e-6
σ_2	$x > 0$	σ	0.70	0.44	0.61	0.61	0.74	0.6
		Max	1.75	1.00	1.39	1.60	1.77	1.5
	$x < 0$	σ	1.12	0.95	1.12	1.10	1.21	1.1
		Max	3.10	2.26	2.86	2.78	2.81	2.8
n	$x > 0$	σ	-	-	-	0.64e-3	0.38e-3	0.51e-3
		Max	-	-	-	1.6e-3	0.95e-3	1.3e-3
	$x < 0$	σ	-	-	-	0.67e-3	0.34e-3	0.51e-3
		Max	-	-	-	1.8e-3	0.89e-3	1.3e-3

Table 5.4: Parameter estimation error due to simulated measurement errors. The fit is made with a NLSM with a sample per 0.001 m/s.

5.1.4 Summary

In this subsection five different methods are described to model the steady state friction of hydraulic cylinders. A method to determine the lubricant film saturation velocity, v_b , as function of the other steady state parameters is proposed to obtain a more robust and consistent parameter estimation. Since v_b is used in the definition of the lubricant fluid film, the placement of v_b affect the curvature of the steady state Stribeck curve but it also has an influence on the dynamical friction force. The method to determine v_b as function of the steady state parameters is based on the knowledge from previous works. The method is revisited when experimental results is obtained from the test bench.

It has been shown that to describe the friction force most accurately the MG model should be used. Furthermore a study of the sensitivity of the parameters is made. This shows that no model is superior compared to the others when considering sensitivity. The MG model is chosen to describe the steady state friction force since this model results in the best fit to previous found friction characteristics.

5.2 Dynamic Friction Model

As Previous mentioned in Section 2.2 the basis of the existing friction models to describe dynamic friction behaviour is the LuGre model. Based on the LuGre model, the Modified LuGre model was proposed to describe the friction in a hydraulic cylinder more accurate by incorporating a dynamic lubricant film thickness, h , which have first order dynamic with respect to velocity. The New Modified LuGre model incorporated an acceleration dependent

friction force and a simple load dependent friction term. The friction model described in this chapter should not incorporate pressure dependency since this model is used to determine the parameters for the velocity dependent model. This will be done for different combinations of pressures and the results are utilised to map the pressure dependency. In this section modifications to the Modified LuGre model are made for greater simplicity of the model. Simplicity and a minimal number of parameters are desired for a robust parametrisation. The modifications regards the acceleration dependency, bristle damping and lubricant film thickness. The modifications to the bristle damping and lubricant film thickness are evaluated in the end of the section.

5.2.1 Neglect of Bristle Damping - σ_1

In previous work different methods are used to determine the bristle damping parameter, σ_1 , which have resulted in very different values for σ_1 as shown in Table 4.2. In two out of three studies a very low value is used which results in a neglectable influence on the overall friction force. From simulations of the eight previous found friction characteristics it is indicated that σ_1 have very little influence on the overall friction force, this is seen in Figure 5.5, where the impact is seen during a fast sine wave where σ_1 have the largest contribution. From the figure it is seen that the bristle damping only contributes with significant friction in one case, though the contribution is very small compared to the total friction force. Since the bristle damping parameter, σ_1 , have not shown to have a clear impact on the modelling accuracy, it is chosen to omit this term. Yet this term is kept in mind and will be discussed again when measurements are available.

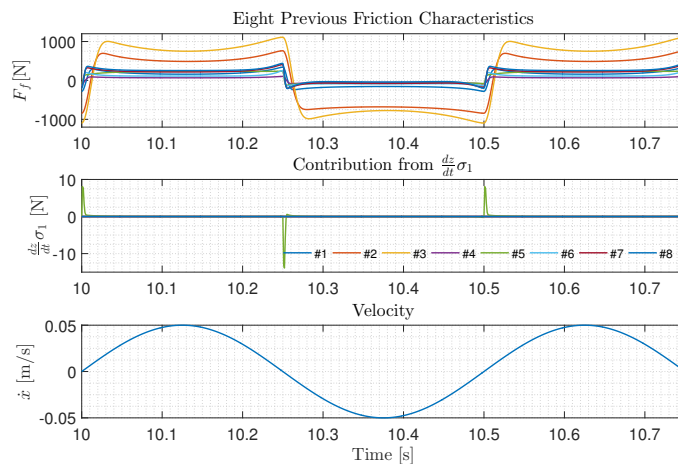


Figure 5.5: Impact from the friction term $\sigma_1 \frac{dz}{dt}$ during a fast sine wave for the eight previous found friction characteristics from Table 4.1 and 4.2.

5.2.2 Neglect of Acceleration Dependent Friction - T

In the New Modified LuGre model an acceleration dependent friction term was implemented in the dynamical friction model. It was seen that the residual between the measured and modelled friction force was proportional to the acceleration with the constant T (Tran et al., 2011).

This proportional parameter, T, was found by making a linear fit of the residual between

the modelled and measured friction force to the acceleration, i.e. it was indicated that the "non modelled" friction force was acceleration dependent. The same method was used in (Pedersen and Jørgensen, 2016) with bad results. In (Pedersen and Jørgensen, 2016) the acceleration dependent friction showed to have a bad influence on the resulting modelled friction force. Though a friction force proportional to the acceleration has been seen, it is not proven that a friction force dependent on the acceleration is present in hydraulic cylinders. The previous found friction force proportional to the acceleration might be an ill defined pressure dependency, since pressures in the cylinder naturally will vary with acceleration. In the following of this project the acceleration dependent friction term will be disregarded. Yet as for the bristle damping parameter, a potential acceleration dependent friction force will be discussed when practical friction force measurements have been obtained.

5.2.3 Reformulation of Lubricant Film Time Constant - τ_{hp}

During parameter estimation of the dynamic parameters, σ_0 , τ_{hp} and τ_{hn} in Section 6.2.2 problems with estimating τ_{hp} was encountered. It is seen in (Yanada and Sekikawa, 2008), (Tran et al., 2011), (Yanada et al., 2010) and (Pedersen and Jørgensen, 2016) that the time constant for rising lubricant film thickness, τ_{hp} , can be estimated by using the steady state parameters. Through simulations with different time constants, it is seen that the simulated friction force differ very little with different values for τ_{hp} as seen in Figure 5.7. This is seen since the difference between steady state and the actual friction force is lower for increasing lubricant film compared to decreasing lubricant film. An example to explain this, taking basis in the steady state friction described by Equation (5.9), is given below both for τ_{hp} and τ_{hn} :

$$g_s(\dot{x}_p, h) = F_c + \underbrace{[(1-h)F_s - F_c]}_{\text{Part 1}} \underbrace{e^{-\left(\frac{\dot{x}_p}{v_s}\right)^n}}_{\text{Part 2}} \quad (5.9)$$

To illustrate the relative higher importance of τ_{hn} relative to τ_{hp} on the friction force, an ideal step from a low velocity to a higher velocity in the negative resistance regime is used as an example. For the purpose of this example the values of part 1 and part 2 in Equation (5.9) are defined at two velocities, seen in Table 5.5. The values in the tables are the friction value contribution from the two parts instantaneously after the step. As seen from the table, a step from 0.01 to 0.1 m/s, governed by τ_{hp} , results in the friction force to change 800 N instantly while the difference between the steady state friction and dynamic friction is 160 N. Though for a step from 0.1 to 0.01, governed by τ_{hn} , the friction changes 160N instantly while the difference between the steady state friction and dynamic friction is 800 N.

	Part 1	Part 2	Total[N]
$\dot{x} = 0.01$	1000	1	1000
$\dot{x} = 0.1$	200	0.2	40
$\dot{x} = 0.01 \Rightarrow \dot{x} = 0.1$	1000	0.2	200
$\dot{x} = 0.1 \Rightarrow \dot{x} = 0.01$	200	1	200

Table 5.5: Examples to emphasise the influence of the dynamic lubricant film thickness during an ideal step.

The greatest impact from the lagging lubricant film thickness is seen during a fast step since the difference between steady state film thickness and dynamic film thickness is at its greatest.

Figure 5.6 and 5.7 illustrates the maximum difference in friction force during different steps for the maximum and minimum time constants according to earlier found parameters in Table 4.2. The difference in the friction force, ΔF_f , for the largest and the smallest time constant is plotted for different initial velocities and different step amplitudes. It should be noted that the contour plots does not have the same magnitude to color ratio of ΔF_f . The velocity step has first order dynamics with a natural frequency of 200 rad/s to simulate actual velocity dynamics. As seen, the difference between the simulated friction force, ΔF_f , with minimum and maximum τ_{hp} is 160 N, and is centred under certain conditions, whereas the influence from the lubricant film dynamics, under conditions governed by τ_{hn} , is seen to have a great impact, up to 1 kN, in a large range of operating conditions.

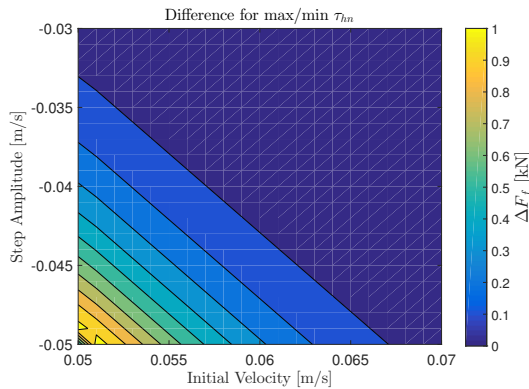


Figure 5.6: Maximum difference in friction force during a step with different initial velocity and amplitude with maximum and minimum time constant respectively $\tau_{hn} = 2.4$ and $\tau_{hn} = 0.2$. Simulated with the proposed model and the expected parameters.

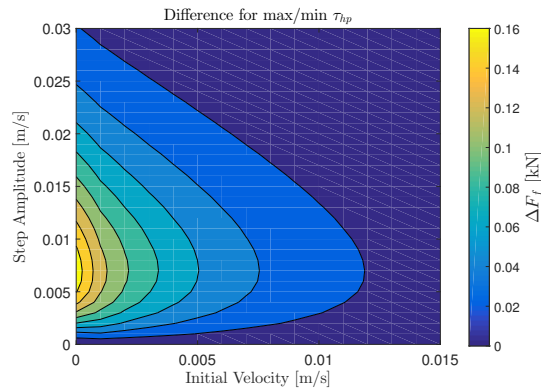


Figure 5.7: Maximum difference in friction force during a step with different initial velocity and amplitude with maximum and minimum time constant respectively $\tau_{hp} = 0.32$ and $\tau_{hp} = 0.033$. Simulated with the proposed model and the expected parameters.

In Figure 5.8 and 5.9 the step is plotted for the case where ΔF_f is largest from Figure 5.6 and 5.7. As seen, the difference in friction force with different τ_{hp} is minimal compared to different τ_{hn} . It should be noted that τ_{hp} is generally smaller than τ_{hn} as seen in Table 4.2.

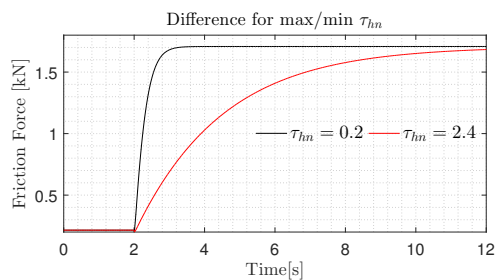


Figure 5.8: Effect in simulated friction force during a step from 0.05 to 0.001 m/s with maximum and minimum τ_{hn} .

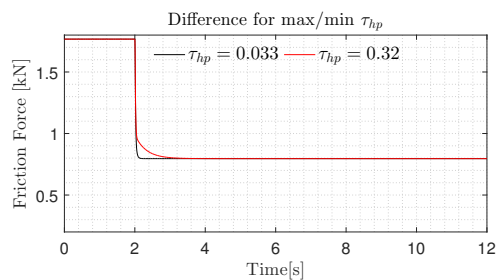


Figure 5.9: Effect in simulated friction force during a step from 0.001 to 0.007 m/s with maximum and minimum τ_{hp} .

Since it is desired to obtain an exact friction model with easy parameter estimation it is chosen to omit the variable τ_{hp} in the parameter estimation based on the reasons elaborated above. It is seen, in Figure 5.9, that changes in τ_{hp} affect the friction force very little and

only under certain conditions.

A method to disregard τ_{hp} is to consider it constant, though it is assumed a more accurate method to consider τ_{hp} to be a function of τ_{hn} which may be indicated by Figure 5.10. Previous found time constants from Table 4.2 are seen in Figure 5.10. This figure indicates a relationship between τ_{hp} and τ_{hn} where $\tau_{hp} = 0.15\tau_{hn}$. The values indicated by the red dot are found in (Yanada and Sekikawa, 2008), though it is described how the time constants are found ad hoc by manually fitting simulations to measurements. According to this section, τ_{hp} has very little influence on the friction force why this method is considered to be inaccurate and the outlier is omitted.

Since it is indicated from figure 5.10 that there is a relation between τ_{hn} and τ_{hp} , it is chosen to define $\tau_{hp} = 0.15\tau_{hn}$ in the proposed model. It is investigated if this relation have in impact on the estimation of the remaining parameters in Section 5.2.4. Furthermore the decision made in this section should be reviewed when experimental measurements is obtained.

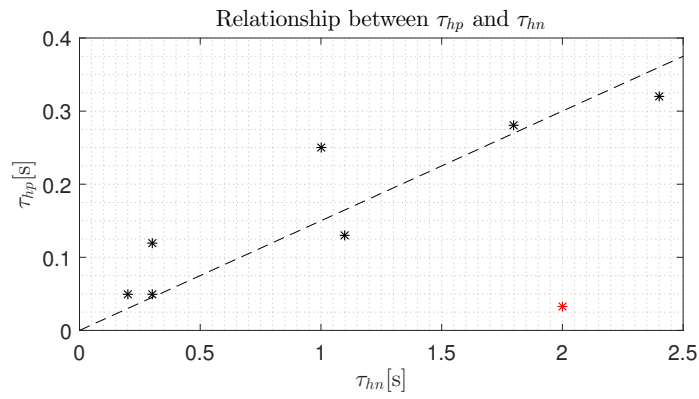


Figure 5.10: Relationship between earlier found lubricant film time constants.

5.2.4 Impact of Dynamic Model Assumptions

In this subsection it is investigated how the simplifications of the dynamic model affect the estimation of the other dynamic parameters. The simplifications include: Exclusion of the bristle damping term $\frac{dz}{dt}\sigma_1$ and the assumption that the relationship between the lubricant film time constants is constant such $\tau_{hp} = k_\tau\tau_{hn}$.

The parameter estimation is made with basis in the trajectory from section 6.2.2, where it is assumed that the steady state parameters can be ideally estimated from the steady state conditions. In Figure 5.11 the estimated parameters are seen when the proposed model is fitted to the Modified LuGre model containing σ_1 and an independent value for τ_{hp} . The fit is made with an NLSM. The two assumptions are varied individually one by one within the bounds of the previous found values from Table 4.2. As seen, the impact from the simplification of the bristle damping is seen to have the greatest impact of the two simplifications. The greatest impact is seen from σ_1 on the estimation of σ_0 . The value of σ_1 is only found to be 10.000 in one case, and in every other case it is found to be 0.1 which have a negligible impact. The time constant for the lubricant film thickness is seen to vary up to approximately 2.5% which is assessed to be negligible. Since the values of the steady state parameters have an influence on how the fluid film will change during a trajectory, it is chosen to make the same analysis when the expected parameters for positive and negative direction is interchanged such the greatest friction force amplitude is during positive velocity. The result from this have shown the same tendency though the error in τ_{hn} is increased with

approximately 50%. Yet it is assessed that the impact of the dynamic model simplifications made, have a negligible influence on the estimation of the parameters.

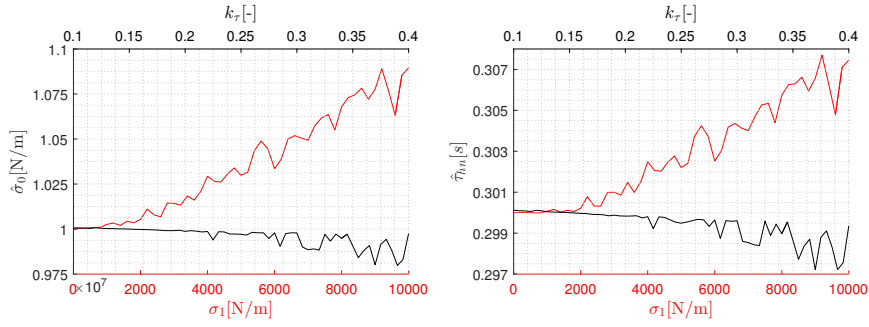


Figure 5.11: Impact from dynamic assumptions on the parameter estimation, $\hat{\sigma}_0$ and $\hat{\tau}_{hn}$ are the estimations of σ_0 and τ_{hn} respectively. The rest of the parameters are the expected parameters.

5.2.5 Summary

The dynamic friction model used in the next parts of this project is described below. An explanation of the different model parameters are given in Section 2.2.

$$\begin{aligned}
 g_s(\dot{x}_p, h) &= F_c + [(1-h)F_s - F_c] e^{-\left(\frac{\dot{x}_p}{v_s}\right)^n} & \frac{dh}{dt} &= \frac{1}{\tau_h} (h_{ss} - h) \\
 \tau_h &= \begin{cases} 0.15\tau_{hn} & \text{for } \dot{x}_p \neq 0, h \leq h_{ss} \\ \tau_{hn} & \text{for } \dot{x}_p \neq 0, h > h_{ss} \\ \tau_{h0} & \text{for } \dot{x}_p = 0 \end{cases} & h_{ss} &= \begin{cases} K_f |\dot{x}_p|^{\frac{2}{3}} & \text{for } |\dot{x}_p| \leq |v_b| \\ K_f |v_b|^{\frac{2}{3}} & \text{for } |\dot{x}_p| > |v_b| \end{cases} \\
 K_f &= \left(1 - \frac{F_c}{F_s}\right) |v_b|^{-\frac{2}{3}} & v_b &= e^{\frac{\ln(-\ln(k))}{n}} v_s \\
 k &= \frac{0.002}{n^{4.5}} & \frac{dz}{dt} &= \dot{x}_p - \frac{\sigma_0 z}{g_s(\dot{x}_p, h)} \dot{x}_p \quad (5.10)
 \end{aligned}$$

6 | Parameter Estimation

In this chapter different parameter estimation methods will be tested and compared in accuracy, sensitivity and simplicity.

Different sequential estimation methods are proposed where the steady state parameters are estimated first and the dynamic parameters are estimated subsequently.

It is also tested if all the parameters can be estimated at the same time using a complete optimisation algorithm which minimises the residual between the model and the measurements. Throughout this chapter the analyses is made with basis in simulation data made with the expected parameters from Table 4.1 and 4.2 if nothing else is stated. In the following, the initial guess for the optimisation algorithms is the expected parameters.

The diagram in Figure 6.1 illustrates how different methods are tested and compared to be able to propose the most accurate, robust and simple estimation method in the end. By a robust method is meant that the optimal parameters should be estimated consistently each time and by simple is meant a combination between the trajectory necessary and the time consumption for data processing.

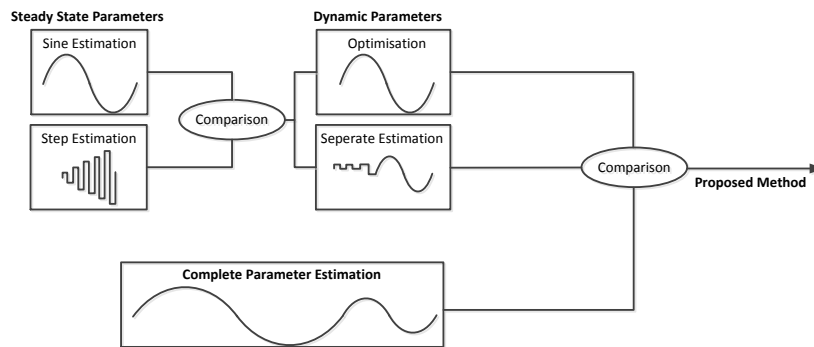


Figure 6.1

6.1 Estimation of Steady State Parameters

To estimate the steady state parameters the model will be fitted to data conducted under steady state conditions. It is investigated which trajectory is necessary to estimate the parameters with adequate accuracy and how measurement errors may affect the parameter estimation. Furthermore it is investigated if it is possible to determine the steady state parameters with adequate accuracy from a simple sine velocity trajectory.

6.1.1 Parameter Estimation from Steady State Conditions

In this subsection the method of estimating the steady state friction parameters from a number of friction measurements during steady state conditions is elaborated. A method to determine at which velocities the friction samples should be made is proposed in Appendix C.1 and it is determined how many friction samples is necessary to estimate the parameters with sufficient accuracy.

As shown in the sensitivity analysis in Figure 5.3, the individual steady state parameters are

influencing the friction force at different velocities. The figure indicates that the friction force is very sensitive to changes in F_s , v_s and n at low velocities why it is necessary to have frequent friction samples in the negative resistance regime. The figure also indicates that the friction force is sensitive to F_c and σ_2 in the whole fluid lubrication regime why samples could be made less frequent in this region.

In Appendix C.1 a method to place the samples in the velocity range is elaborated. The method is developed to ensure that the friction force is sampled more frequently at lower velocities and to have a standardised method.

To determine the number of samples necessary to be able to estimate the steady state parameters accurately, an investigation is made with the following number of samples $n_s = [5, 10, 15, 20, 30, 50]$. The friction data used in this investigation is based on expected measurements. At each sample velocity a random number in the range $\pm 25\text{N}$ is added to the friction force to emulate the repeatability error discussed in Section 5.1.3. The results from estimating the steady state parameters 1000 times with a random repeatability error using a NLSM are shown in Figure 6.2. The results are illustrated with the maximum estimated error $\text{Max}(\tilde{\theta})$, where $\tilde{\theta}$ represents the estimation error, and the standard variance $\sigma(\hat{\theta})$, where $\hat{\theta}$ represents the estimated parameters.

From Figure 6.2 it is seen that a great increase in accuracy is made from 5 to 10 samples. After this the standard variance is approximately decreasing linearly with the number of friction samples. Since it is required that the parameter estimation method should be simple and accurate, it is desired that the least number of sample points are made while obtaining high accuracy. Based on this it is assessed that 15 samples is an adequate compromise.

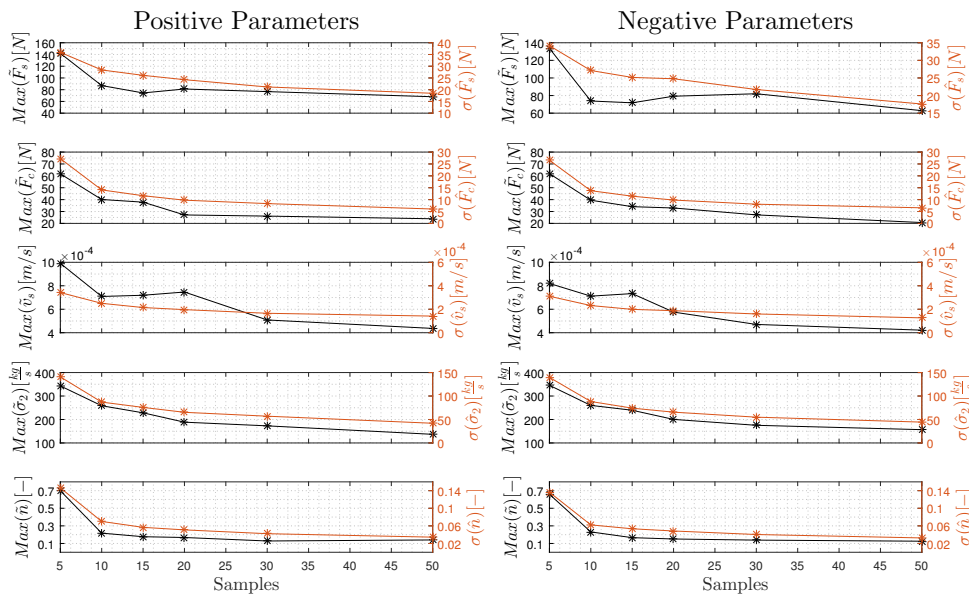


Figure 6.2: Standard variance, σ , and max error due to repeatability error, for each parameter as function of the number of samples. The data is based on 1000 parameter estimations.

6.1.2 Steady State Parameter Estimation from Sine Trajectory

This method is investigated since the necessary trajectory is simpler than the method utilising steady state conditions. A parameter estimation of the steady state parameters will be

performed for a sine wave at different frequencies and amplitudes. In Figure 6.3 a plot of the feasible combinations of frequency and amplitude is seen for the test facility.

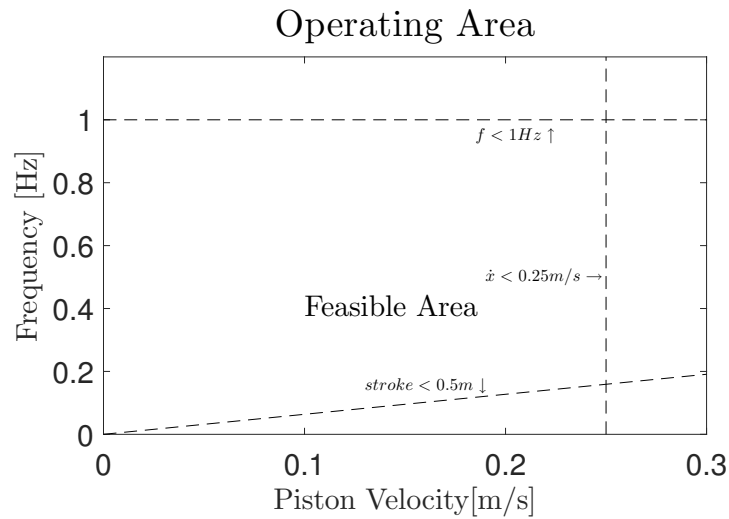


Figure 6.3: Feasible work range for a sine wave.

The dynamics of both the bristles and the lubricant film are influencing the friction force during a sine trajectory. This is seen in Figure 6.4 with a velocity amplitude of 0.05 m/s. The effect of the bristle dynamics is plotted utilising the proposed model without lubricant film dynamics. The effect of the lubricant film dynamics is plotted utilising the steady state friction force equation including lubricant film dynamics. As seen in the top plot, the bristle dynamics have a great impact during change of direction. For a sine wave, a large frequency results in a greater error between the steady state friction and the dynamic friction. The same case is seen for the lubricant film dynamics which influences the friction force more at greater frequencies.

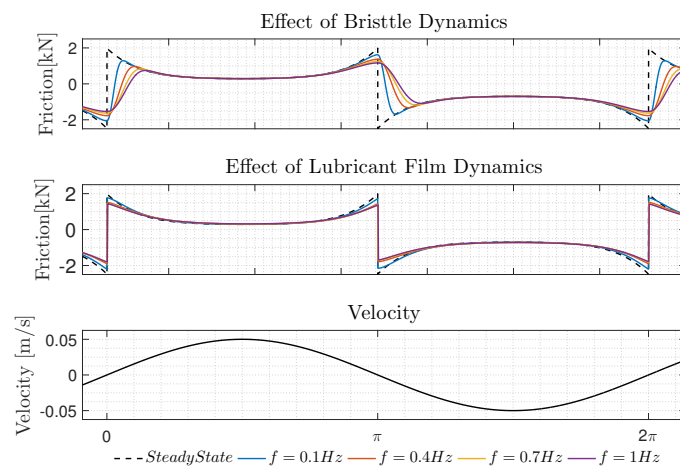


Figure 6.4: Impact of dynamic components in the friction force.

From Figure 6.4 it is seen that the largest difference between steady state and dynamic friction force is seen just after a change in direction. The most accurate estimation will be if the estimation is made from $\pi/2$ to π and from 1.5π to 2π .

The results from the parameter estimation at different frequencies and amplitudes are seen in Figure 6.5 where a NLSM has been utilised and the initial guess is the expected parameters. As seen, the parameters which are sensitive at lower velocities (F_s , v_s and n), according to Section 5.1.3 are estimated wrong, though the parameters are estimated closer to the correct values for lower frequencies. F_c and σ_2 are seen to be estimated in the correct range at higher velocity amplitudes where the fluid lubrication regime is entered.

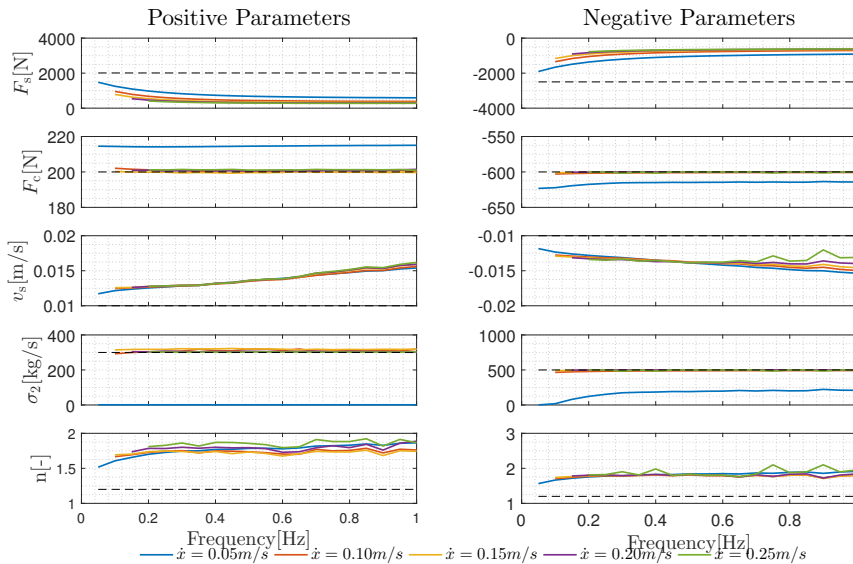


Figure 6.5: Estimated parameters during a sine wave for different frequencies and amplitudes.

From this section it is indicated that by neglecting the dynamics of the friction force while estimating the steady state parameters utilising a sine trajectory shows poor results. Though it is seen that F_c and σ_2 can be estimated in the correct range for higher velocity amplitudes where the fluid lubrication regime is entered.

6.1.3 Summary

If the steady state parameters should be estimated during steady state conditions it is desired that 15 friction samples should be used. When estimating the steady state parameters utilising a sine trajectory only F_c and σ_2 can be estimated in the correct range at velocity amplitudes in the fluid lubrication regime. The method to estimate the steady state parameters for the sequential estimation method will be the estimation method utilising friction measurements from steady state conditions.

6.2 Estimation of Dynamic Parameters

In this section different methods to determine the dynamic parameters, σ_0 and τ_{hn} will be proposed and tested. One method proposed is where τ_{hn} is estimated first during specified operating conditions and σ_0 is determined afterwards by minimising the error between modelled and measured friction during a sine velocity trajectory.

The other proposed method is an optimisation strategy where both parameters are found

at the same time by minimising the error between modelled and measured friction. Both methods requires knowledge of the steady state parameters.

The two methods will be compared on simplicity, sensitivity and accuracy.

The simplicity is a measure of the necessary trajectory and the necessary data processing.

The sensitivity is evaluated by utilising the 1000 different combinations of steady state parameters, found in Section 6.1.1, in the estimation algorithm and at the same time by adding a randomly generated error polynomial to the "simulated measurements" using the expected parameters for each steady state parameter combination, as discussed in Section 5.1.3.

6.2.1 Separate Estimation of Dynamic Parameters

The method described in this subsection to estimate the dynamic parameters, τ_{hn} and σ_0 is based on the methods proposed in (Pedersen and Jørgensen, 2016) and (Yanada et al., 2010). This method showed good results in determining parameters to describe the measured friction force.

Lubricant Film Time Constant - τ_{hn}

The method to determine the lubricant film thickness time constant, τ_{hn} , is based on the dynamic friction model equations described in Section 5.2.5. The method requires measurements under certain conditions where the bristle dynamics can be neglected, such an equation describing the lubricant film thickness can be defined as function of the measured friction force, velocity and steady state parameters. By this, the dynamics of the lubricant film thickness can be found by fitting the response to a first order system. The assumption made is $\frac{dz}{dt} \approx 0$. When a velocity reversal is occurring or when the velocity starts from zero, this results in a large change in z . By omitting these conditions in a trajectory the assumption is valid.

Utilising this assumption in the equations described in Section 5.2.5 results in a description of the lubricant film thickness as described in Equation (6.3).

$$\underbrace{\frac{dz}{dt}}_{=0} = \dot{x}_p - \frac{\sigma_0 z}{g_s(\dot{x}_p, h)} \dot{x}_p \implies g_s(\dot{x}_p, h) = \sigma_0 z \quad \text{for } \dot{x}_p \neq 0 \quad (6.1)$$

With this assumption the friction force can be described in the following way:

$$F_f = \underbrace{\sigma_0 z}_{=g_s(\dot{x}_p, h)} + \sigma_2 \dot{x}_p = g_s + \sigma_2 \dot{x}_p = F_c + [(1-h)F_s - F_c] e^{-\left(\frac{\dot{x}_p}{v_s}\right)^n} + \sigma_2 \dot{x}_p \quad (6.2)$$

From this it is possible to solve the equation for h as:

$$F_f = F_c + [(1-h)F_s - F_c] e^{-\left(\frac{\dot{x}_p}{v_s}\right)^n} + \sigma_2 \dot{x}_p \implies h = 1 - \frac{F_f - F_c \left(1 - e^{-\left(\frac{\dot{x}_p}{v_s}\right)^n}\right) - \dot{x}_p \sigma_2}{F_s e^{-\left(\frac{\dot{x}_p}{v_s}\right)^n}} \quad (6.3)$$

The velocity trajectory used to obtain h over time is a velocity step going towards a lower absolute velocity in the negative resistance regime since this is a simple trajectory which have

shown good results in estimating τ_{hn} , (Yanada and Sekikawa, 2008), (Tran et al., 2011), (Yanada et al., 2010). The dynamics of the lubricant film thickness shown in Equation (6.4) is not linear. Therefore the term $\bar{\dot{x}}_p$ is introduced as input such the lubricant film dynamics is linear and τ_{hn} can be estimated using a first order ARMAX method with second order error dynamics as proposed in (Pedersen and Jørgensen, 2016).

$$\frac{dh}{dt} = \frac{1}{\tau_h} \underbrace{(K_f |\bar{\dot{x}}_p|^{2/3} - h)}_{\bar{\dot{x}}_p} \Rightarrow \frac{dh}{dt} = \frac{1}{\tau_h} (\bar{\dot{x}}_p - h) \quad (6.4)$$

The velocity step to determine the lubricant film dynamics is a negative velocity step with first order dynamics. The velocity at which this step should start and end is elaborated in the following together with the dynamics of the velocity step.

Figure 6.6 shows the estimated value of τ_{hn} as function of the velocity step amplitude and the initial velocity. In this figure the velocity step dynamics has a time constant of 0.2s. From Figure 6.6 it is seen that a good estimation of τ_{hn} , $\hat{\tau}_{hn}$, can be made no matter the initial velocity and the amplitude of the step since the time constant only differs between 0.3-0.35. This will not have a large effect on the total friction force. The step chosen for now is from 0.04-0.02 m/s since a large step in practice will reduce the noise to amplitude ratio.

In Figure 6.7 the impact of the velocity step dynamics regarding the the accuracy of the estimation of the lubricant film time constant is shown. It is seen that the time constant of the velocity step dynamics does not have great impact why it is chosen to 0.2 s such the experiments is fast to execute.

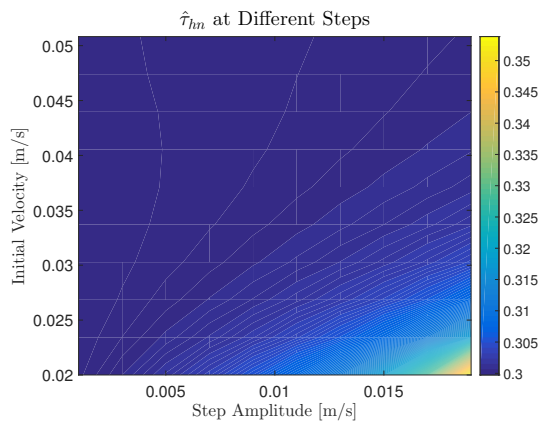


Figure 6.6: Estimated time constant for different step amplitude and initial velocities

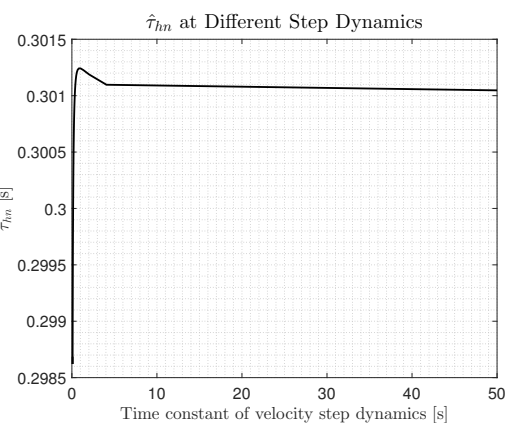


Figure 6.7: Estimated time constant for different velocity step dynamics.

During investigations of the sensitivity of this method, to estimate the lubricant film time constant when utilising the 1000 wrong estimates of the steady state parameters in Equation (6.3), it is experienced that this method is unable to determine the lubricant film time constant consistently. The reason for this is that when utilising the wrong steady state parameter estimates from Section 6.1.1 the estimated lubricant film thickness, from Equation (6.3) in many cases show to lead the defined velocity $\bar{\dot{x}}_p$. This is illustrated below, where Figure 6.8

6.2. Estimation of Dynamic Parameters

show \bar{x}_p and h for an estimation of τ_{hn} when utilising a step from 0.04 m/s to 0.02 m/s and Figure 6.9 show the same for an estimation of τ_{hn} when utilising a step from 0.01 m/s to 0.005 m/s. The same steady state parameter set, estimated in the previous chapter where a error was simulated causing an error in the steady state parameters is used. In both cases a random number between $\pm 25N$ is added to the 15 measurements in each velocity direction. It is seen that the estimated thickness in Figure 6.8 leads the velocity, while the thickness in Figure 6.9 lags the velocity as it should.

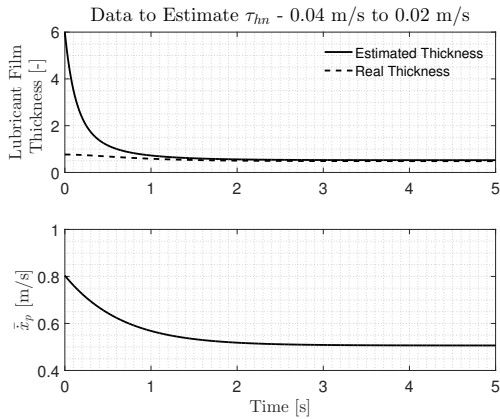


Figure 6.8: \hat{h} and \bar{x}_p for a step from 0.04 m/s to 0.02 m/s.

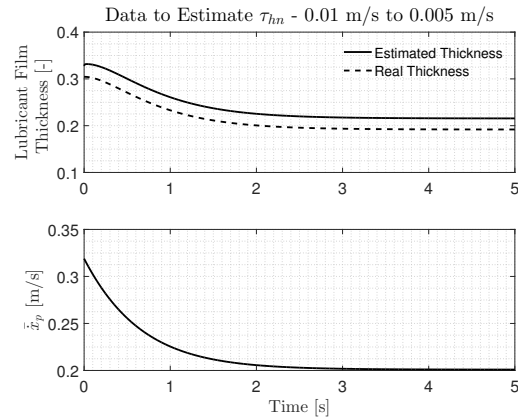


Figure 6.9: \hat{h} and \bar{x}_p for a step from 0.01 m/s to 0.005 m/s.

It has been investigated which steady state parameters is causing the lubricant film to lead the velocity \bar{x}_p . This investigation shows that wrong estimates of the Coulomb friction parameter, F_c , and the viscous friction parameter, σ_2 , results in a wrong estimate of the lubricant film thickness.

To avoid the influence on the lubricant film thickness of wrong parameter estimates of F_c and σ_2 it is chosen to make the velocity step at lower velocities such these steady state parameters does not have a great influence on the total friction force as indicated from the sensitivity analysis in Section 5.1.3. It is found that a step from 0.01 m/s to 0.005 m/s results in a lubricant film thickness which is lagging the velocity \bar{x}_p in every case. In Figure 6.10 it is shown for different values of τ_{hn} how the estimation of τ_{hn} is as function of the dynamics of the velocity step. The mean, standard variance and maximum error of the estimated τ_{hn} is defined from estimating τ_{hn} using the first 10 steady state parameter combinations of the series of 1000 steady state parameter combinations mentioned before. From the figure it is seen that the optimal velocity step dynamics depends upon the actual value of τ_{hn} . Yet it is seen that a velocity step with a time constant, $\tau_{vel} = 0.6s$ results in a good parameter estimation of τ_{hn} in most cases.

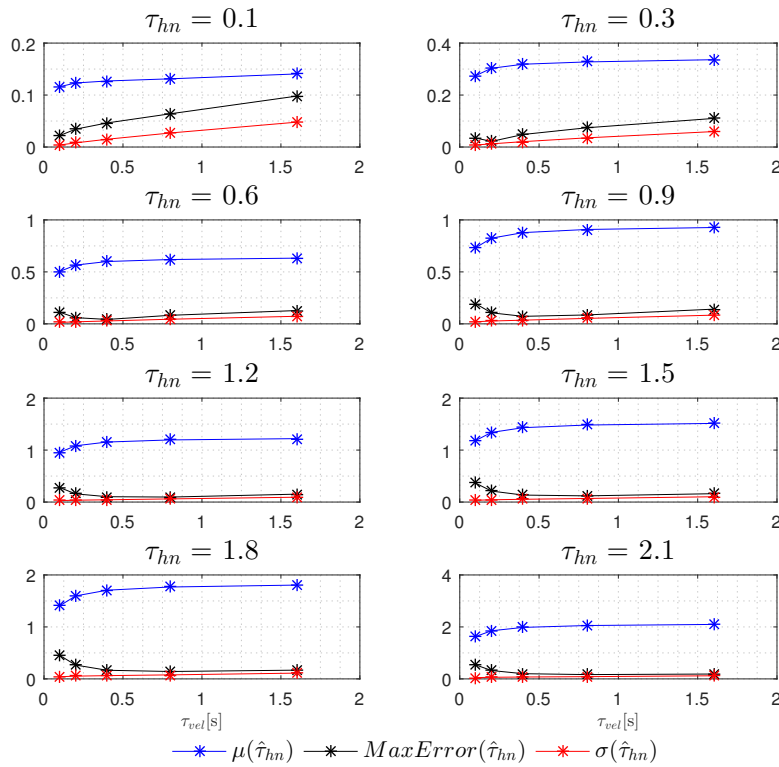


Figure 6.10: Estimation of different values of τ_{hn} at different velocity step dynamics.

Bristle Stiffness Parameter - σ_0

The methods used to estimate the parameter σ_0 in (Pedersen and Jørgensen, 2016) and (Yanada et al., 2010) is respectively based on a method utilising the mean squared error between measured and modelled friction force during a sine trajectory for different values of σ_0 and a method of manually comparing measured data with simulated data with different values of σ_0 . To obtain a simple, consistent and accurate parameter estimation scheme it is preferred to use a NLSM to estimate the value of σ_0 utilising a sine trajectory where the cost function is the sum of squared residuals. The sine velocity trajectory is defined as in Subsection 6.2.2 and the optimisation algorithm is the same as utilised in Subsection 6.2.2.

The results obtained using this parameter estimation method is compared in subsection 6.4 to the method described in the next subsection.

6.2.2 Optimisation Based Estimation of Dynamic Parameters

This section investigates the possibility of estimating the dynamic parameters through an optimisation algorithm. It is desired to use a gradient based search algorithm to minimise the computation time. To ensure that the minimum is found it is desired to minimise a convex problem. The proposed cost function, $S(\theta)$, is the sum of squared residuals described as:

$$S(\theta) = \sum_{i=1}^m [y_i - F_f(x_i, \theta)]^2 \quad (6.5)$$

6.2. Estimation of Dynamic Parameters

Where y is the measured friction force and $F_f(x_i, \theta)$ is the modelled friction force with the parameters $\theta = [\sigma_0 \ \tau_{hn}]$.

It is desired to define a trajectory where both dynamic parameters have a great influence on the friction force. The influence from σ_0 is seen when the change in friction force is large i.e. during a change in direction, why the trajectory includes a fast sine wave. The change in friction force due to τ_{hn} is seen to have a large impact during a step from a velocity to a smaller velocity. The impact of both parameters are seen in the negative resistance regime why the amplitude is chosen as 0.05 m/s. The velocity trajectory and the effect of the dynamic parameters are seen in Figure 6.11.

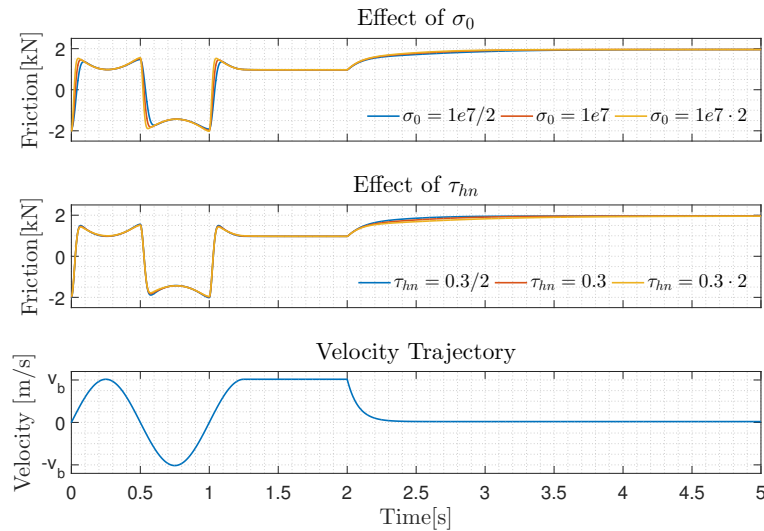


Figure 6.11: Trajectory for determining the dynamic parameters through optimisation.

In Figure 6.12 the cost function is shown for different combinations of dynamic parameters. As seen, the cost function is convex for all σ_0 , though it is only convex for approximately $\tau_{hn} < 5$. Since the largest time constant seen in the eight previous friction models is 2.1 seconds it is assumed that 5s is a reasonable bound such optimality can be ensured. Yet it should be noted that this optimality is only valid when all the steady state parameters are correct.

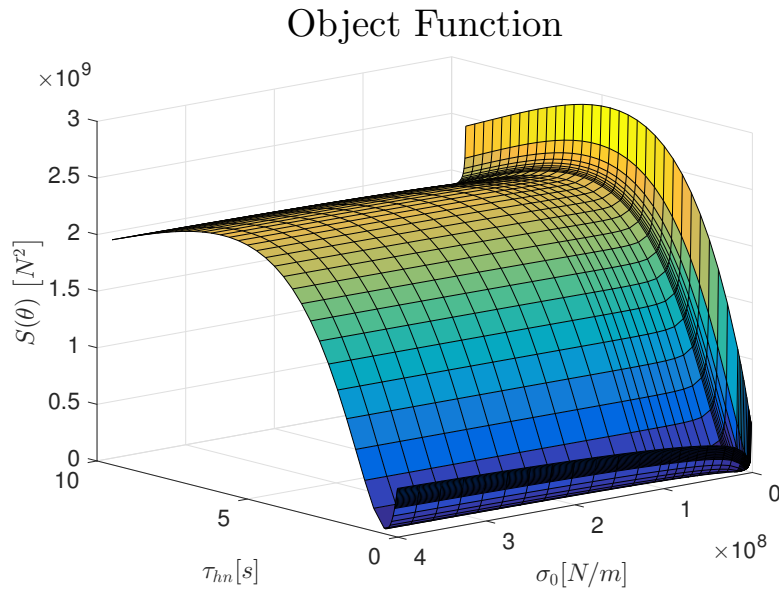


Figure 6.12: Convexity of object function.

In Section 6.3 an evaluation of different optimisation algorithms is made. The one chosen there, is used for this purpose as well: a NLSM with Trust-region-reflective algorithm with a step size tolerance of 10^{-3} .

The results from this estimation method are seen in Section 6.4 where the estimation methods will be compared.

6.3 Complete Parameter Estimation

It is desired to investigate the possibilities of estimating the parameters globally through an optimisation algorithm. This way it is not necessary to obtain measurements where certain conditions are met e.g. steady state conditions.

As in Section 6.2.2 it is desired to design a trajectory where changes in every parameter is visible. The same trajectory is used, though a slow sine with a large amplitude is added to have an impact from σ_2 , and a slow ramp in the low velocity range is added to include a large impact from F_s , v_s and n . In Figure 6.13 the velocity trajectory is seen along with the change in friction force due to changes in each parameter. As seen from the figure, every parameter has an impact on the friction force.

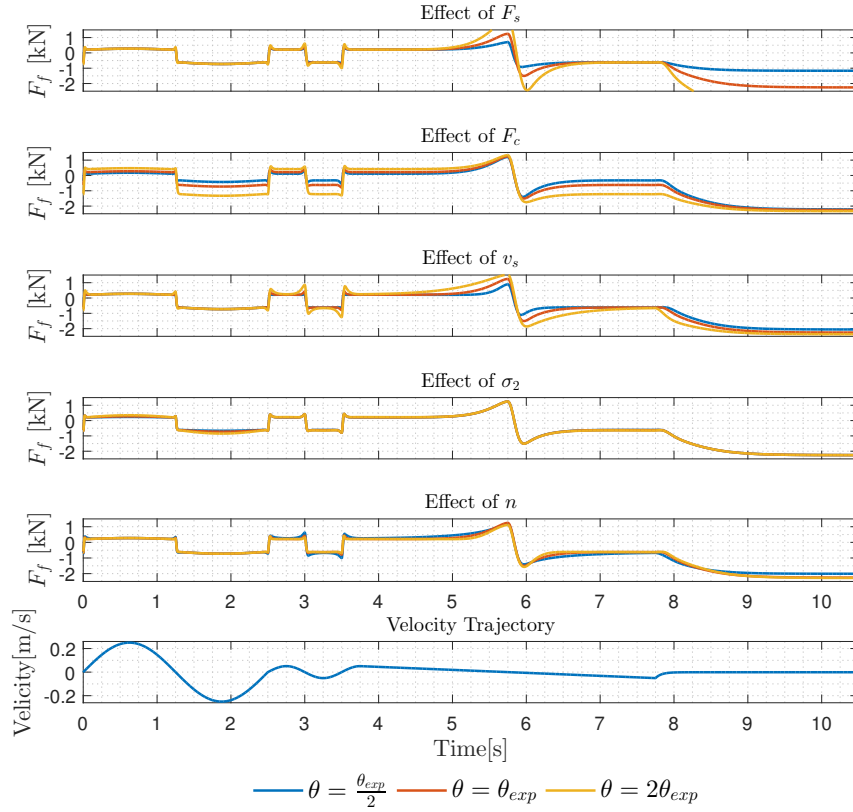


Figure 6.13: Trajectory for complete parameter estimation and the impact of changes in the parameters.

The cost function to be minimised, $S(\theta)$, is the sum of squared errors:

$$S(\theta) = \sum_{i=1}^m [y_i - F_f(x_i, \theta)]^2, \quad \theta_{\text{exp}} = \text{argmin}(S(\theta)) \quad (6.6)$$

Where y is the friction force measurements, F_f is the simulated friction, θ is the parameter vector and θ_{exp} is the expected parameters from Table 4.1 and 4.2 which results in the minimum of the cost function

It is desired to use a gradient based search algorithm to minimise the computation effort. A gradient based search algorithm only locates a local minimum if several minima is available. To ensure that the search algorithm locates the global minimum, the cost function should be convex. Since the problem consists of non-linear differential equations with discontinuities it is not possible to prove convexity analytically. In Figure 6.14 an indication of the convexity of the cost function is seen. The cost function is seen where each parameter is changed. The simulated measurements, y , is made with the expected parameters and the fitted model, F_f , is made with the same parameters except the varying parameter. Sweeps are also made where the remaining parameters for the fitted model, F_f , are changed 20% up and 20% down. The cost function with respect to F_s , F_c , v_s and σ_2 is seen to be convex in every case. $S(\theta)$ with varied n and τ_{hn} is seen to be convex for $\theta = \theta_{\text{exp}}$ and $\theta = 1.2\theta_{\text{exp}}$ though no local minima is seen for $\theta = 0.8\theta_{\text{exp}}$. $S(\theta)$ with varied σ_0 is seen to have multiple minima which indicate that the search algorithm might converge to a non global minimum.

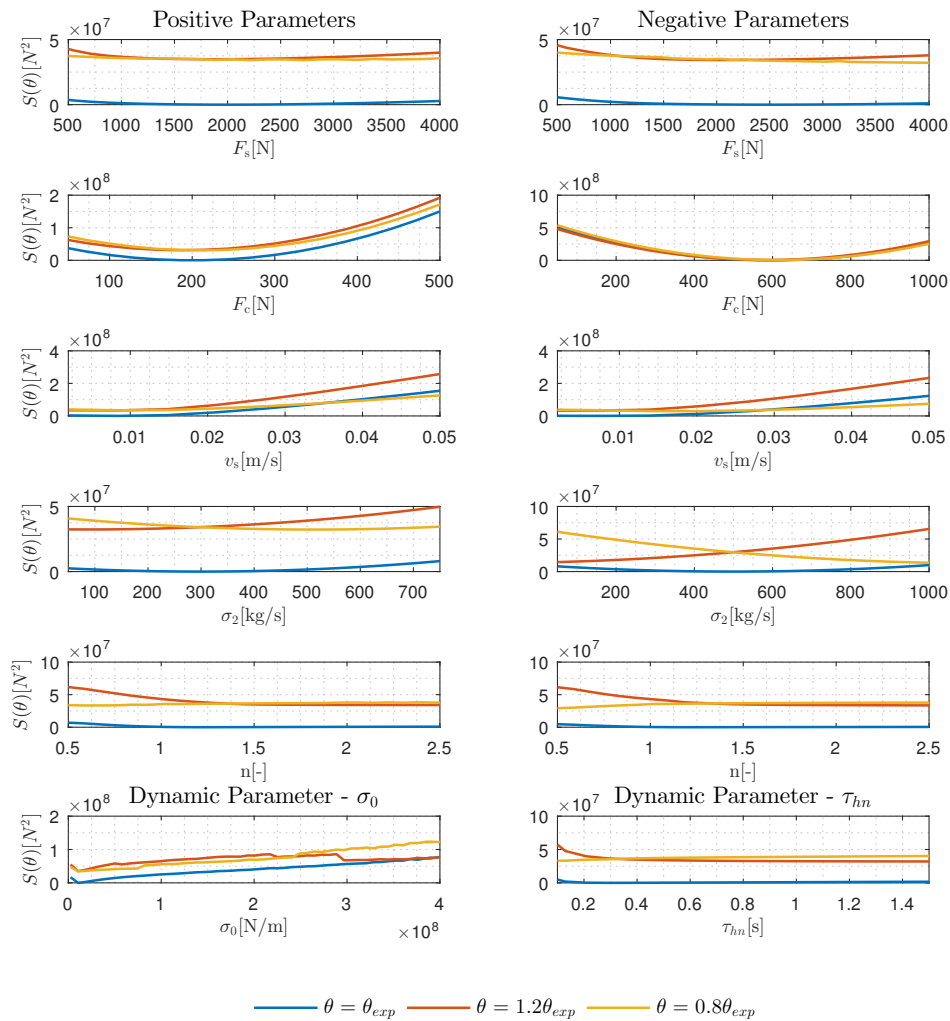


Figure 6.14: Indication of convexity of cost function where the cost function is evaluated while varying each parameter.

It is desired to obtain an algorithm which uses the least amount of function evaluations to converge. For the purpose of least squares minimisation Mathworks suggest LSQNONLIN or fmincon (Mathworks). Different optimisation methods can be utilised for each (Mathworks, -). The different algorithms and methods have been tested at three different starting points where the variables have been normalised with normalisation constants equal to the expected parameters. In Table 6.1 the results of the test are seen. As seen the LSQNONLIN algorithm is best in most cases. The sqp method with the fmincon algorithm is seen not to converge in one case, and the fmincon algorithm requires in general many function evaluations. The function tolerance is set to 0 such that the step tolerance is the only stopping criteria, this is set to 0.001. The LSQNONLIN algorithm will be used for the optimisation problem.

Starting Point:	1.01		1.4		0.6	
	Count	Value	Count	Value	Count	Value
	LSQNONLIN					
Trust-region-reflective	273	481.2	676	534.5	585	1296.8
	FMINCON					
Interior point	271	4173	1149	1.98	892	7.9
SQP	823	1.2	Inf	Inf	1224	14.1
Active-set	581	9.8	955	434.0	939	10.6

Table 6.1: Test of different optimisation methods.

6.4 Comparison of Parameter Estimation Methods

In this section the different estimation methods are compared. The estimated parameters are compared based on the mean estimated value, standard deviation and the max deviation. The results of the different methods are seen in Table 6.2.

As seen from the table, the complete parameter estimation method yields the most accurate and consistent estimation. The reason for this, is that the two methods where the steady state parameters are found separately, is subjected to more uncertainty than the complete estimation method. These have both wrong estimated steady state parameters and an error polynomial added to the measurement series for the dynamic parameters. The premises for this investigation is that friction samples at steady state conditions are subjected to random errors and continuous measurement series are subject to an error polynomial. This method might yield uncertainties since it is not proven that measurement errors can be simulated this way. Though for now this method is considered valid. The results in Table 6.2 is based on 1000 estimations of the parameters utilising the simulated error described in Section 5.1.3 for the error polynomial and Section 6.1.1 for the measurement error at steady state conditions. The complete parameter estimation yields a higher simplicity since it only requires a single 11 second trajectory which is evaluated by one algorithm which is already a Matlab application. The pressure fluctuations during a transient trajectory is greater than during steady state measurements which might influence the parameter estimation. This will be considered in the next section where the influence of pressure dependent friction on the estimation methods will be analysed.

Parameter		Step+Sequential	Step+Opti	Total Opti
F_s	$x > 0$	σ	25.7 (1.3%)	26.1 (1.3%)
		μ	2001.0	2000.1
		Max	69.0 (3.5%)	58.0 (2.9%)
	$x < 0$	σ	27.0(1.1%)	5.7 (0.2%)
		μ	2502.2	2500.1
		Max	81.5 (3.3%)	13.3 (0.5%)
F_c	$x > 0$	σ	12.1 (6.1%)	13.9 (7.0%)
		μ	200.2	200.2
		Max	37.7 (18.9%)	25.2 (12.6%)
	$x < 0$	σ	11.5 (1.9%)	14.6 (2.4%)
		μ	599.7	600.0
		Max	31.6 (5.3%)	27.1 (4.5%)
v_s	$x > 0$	σ	0.22e-3 (2.2%)	0.082e-3 (0.8%)
		μ	0.010	0.010
		Max	0.73e-3 (1.5%)	0.22e-3 (2.2%)
	$x < 0$	σ	0.21e-3 (2.1%)	0.033e-3 (0.3%)
		μ	0.010	0.010
		Max	0.001 (10%)	0.078e-3 (0.8%)
σ_2	$x > 0$	σ	78.4 (26%)	2.8 (0.9%)
		μ	296.5	299.5
		Max	217.6 (72.5%)	13.6 (4.5%)
	$x < 0$	σ	73.4 (14.7%)	2.8 (0.5%)
		μ	501.4	499.9
		Max	210.0 (42%)	7.3 (7.3%)
n	$x > 0$	σ	0.056 (5.6%)	0.015 (1.3%)
		μ	1.2	1.2
		Max	0.18 (15%)	0.041 (3.4%)
	$x < 0$	σ	0.057 (4.8%)	0.0058 (0.5%)
		μ	1.2	1.2
		Max	0.23 (19.2%)	0.0163 (1.3%)
σ_0	σ	1.05e5 (1.0%)	2.58e5 (2.6%)	0.709e5 (0.7%)
	μ	9.96e6	9.99e6	10.01e6
	Max	4.93e5 (4.9%)	8.16e5 (8.2%)	1.57e5 (1.6%)
τ_{hn}	σ	0.04 (13%)	0.013 (4.2%)	0.00062 (0.2%)
	μ	0.32	0.30	0.30
	Max	0.165 (55 %)	0.04 (13.3%)	0.0020 (0.7%)

Table 6.2: Comparison of different estimation methods

6.4.1 Impact of Pressure Dependent Friction in the Estimation

To investigate the impact of non-modelled pressure dependency in the friction force a simple pressure dependency is incorporated in the complete system model. This will effect the parameter estimation since it is not incorporated in the proposed friction model which the data is fitted to.

A linear pressure dependency is incorporated on all the parameters and is dependent on both chamber pressures . The pressure dependent parameters, θ_{pd} , are modelled such, that they change away from the normalised parameters, θ_n , when the pressures changes away from the

normalised pressures, p_n , such:

$$\theta_{pd} = \theta_n + \Delta p_{pm} C1 + \Delta p_{rm} C2 \quad (6.7)$$

Where the pressure difference is calculated as:

$$\Delta p_{pm} = p_{pm} - p_{pm,n} \quad , \quad \Delta p_{rm} = p_{rm} - p_{rm,n} \quad (6.8)$$

In this case the pressures are controlled to 50 bar such $p_{pm,n} = p_{rm,n} = 50\text{bar}$. The pressure dependency coefficients C1 and C2 are calculated such the parameter change is a percentage, k_p , of the normal value, θ_n , per change in pressure such:

$$C1 = C2 = k_p \theta_n \quad (6.9)$$

The estimation methods are tested with a pressure dependency of 0.5%, 1% and 2% such k_p equals 0.005, 0.01 and 0.02. This is tested in the complete system model including noise on the measurements. The results, which are stated as the estimation error for each parameter, are seen in Table 6.3 and 6.4 for the dynamic parameters and the steady state parameters respectively. It is assumed that steady state samples can be made without pressure fluctuations why the steady state parameters has zero error for the two first methods. As seen from the table, the pressure dependency has almost no impact on the steady state parameters in the complete parameter estimation. The error in the steady state parameters are seen to be lower compared to the error caused by measurement errors seen in the previous section. Furthermore the dynamic parameters σ_0 and τ_{hn} are seen to be estimated most exact for the complete estimation and with no remarkable error as well.

It is chosen to use the complete parameter estimation method to map the pressure dependencies, since it is indicated that this method will yield the most accurate estimations of the parameters and since this method only need a simple 11 second trajectory to determine all the parameters.

Yet this method yields weaknesses, since it can not be proven that the optimisation algorithm converges to the correct parameters.

A further investigation of the convergence of the method will be made in the next chapter.

Parameter	k_p	Step+Seperate	Step+Opti	Total Opti
σ_0	0.005	1.44e5 (1.4%)	0.02e5 (0.02%)	0.043e5 (0.04%)
	0.01	0.99e5 (0.99%)	0.06e5 (0.06%)	0.07e5 (0.07%)
	0.02	0.87e5 (0.87%)	0.19e5 (0.19%)	0.17e5 (0.17%)
τ_{hn}	0.005	45e-3 (15%)	0.1e-3 (0.03%)	0.32e-3 (0.1%)
	0.01	38e-3 (12.6%)	0.3e-3 (0.09%)	0.58e-3 (0.2%)
	0.02	34e-3 (11.3%)	0.6e-3 (0.2%)	1.2e-3 (0.4%)

Table 6.3: Error in parameter estimation of dynamic parameters due to pressure dependent friction.

Parameter	Total Opti					
	$\dot{x} > 0$			$\dot{x} < 0$		
	0.005	0.01	0.02	0.005	0.01	0.02
F_s	0.75 (0.04%)	0.66 (0.03%)	1.45 (0.07%)	0.79 (0.04%)	1.47 (0.06%)	2.57 (0.1%)
F_c	0.0058 (0.00%)	0.022 (0.01%)	0.010 (0.00%)	0.062 (0.01%)	0.14 (0.02%)	0.23 (0.04%)
v_s	1.56e-5 (0.16%)	3.92e-5 (0.40%)	3.01e-5 (0.30%)	10.9e-5 (1.0%)	20.2e-5 (1.0%)	34.5e-5 (3.5%)
σ_2	0.64 (0.21%)	1.15 (0.38%)	1.52 (0.50%)	0.36 (0.07%)	0.95 (0.19%)	1.70 (0.34%)
n	0.18e-3 (0.02%)	0.57e-3 (0.05%)	0.96e-3 (0.08%)	2.3e-3 (0.19%)	4.6e-3 (0.38%)	8.3e-3 (0.69%)

Table 6.4: Error in parameter estimation of steady state parameters due to pressure dependent friction.

6.5 Parameter Estimation Evaluation

In this chapter the chosen parameter estimation method will be examined further. An evaluation of the robustness of the parameter estimation will be made to ensure that it converges to the correct parameters. During this investigation it is seen that the optimisation algorithm at first does not converge to the correct parameters. Two schemes for estimating a good initial guess are utilised which improves the accuracy of the estimated parameters. Yet the optimisation algorithm does not converge to the correct parameters for any of the applied methods. It is therefore concluded that the sequential estimation method should be used to estimate the friction model parameters.

6.5.1 Convergence of the Parameter Estimation

As shown in Figure 6.14 the problem is not convex since the convergence is dependent on the initial points for the optimisation algorithm. Though in Figure 6.14 it is seen that the problem is convex in a large range with respect to each variable when the remaining variables are correct. This indicates that the convergence of the parameter estimation is dependent on the initial guess.

To investigate the convergence of the algorithm, it is tested if the algorithm converges to the correct parameters for the 8 sets of parameters from Table 4.1 and 4.2, where v_b is calculated in the proposed way from Section 5.1.1.

All the variables in the optimisation are scaled with the values of the expected parameters. Initially the convergence is tested utilising the initial parameters, θ_{init} , equal to the expected parameters from Table 4.1 and 4.2. From this test it is seen that none of the tests converges to a set of parameters in the vicinity of the correct parameters.

From this it is clear that the convergence to the correct parameters are highly dependent on the initial guess. Two different methods to determine initial guesses of the parameters will be tested. One where initial guesses are estimated from parts of the trajectory and one where the initial guesses are estimated from velocity step estimation prior to the trajectory.

Initial Guess Using Existing Trajectory

The method elaborated in this subsection can deduce an initial guess of the steady state parameters from the exciting trajectory.

- F_c and σ_2

As seen from Section 6.1.2 the parameters F_c and σ_2 can be estimated in the correct range utilising a sine velocity trajectory. This estimation is done for the first sine wave of the trajectory seen in Figure 6.13 utilising a NLSM.

- F_s , v_s and n

Since it is not possible to obtain correct initial guesses on F_s , v_s and n from the sine trajectory a further initial parameter estimation of these parameters are performed. This estimation is done for the ramp seen in the trajectory in Figure 6.13. The impact from the dynamic components of the friction is greatest just after a direction change. The positive parameters are thus estimated from 3.75s to 5.75s before velocity reversal. Another ramp in the other direction is added to the trajectory such the negative parameters can be estimated from these using the same method. A NLSM is used to fit the friction measurements to the steady state friction equations. The initial guess of the dynamic parameters is set to the expected parameters.

The results from this method is seen in Table 6.5. It is seen that the initial guesses on the steady state parameters are in the correct range, though the optimisation algorithm still does not converge to the correct values.

Initial Guess From Prior Steady State Evaluation

It is possible to do steady state measurements prior to the trajectory. From this it is possible to estimate the steady state parameters as seen in Section 6.1.1. 10 velocity steps is made in each direction since this results in a much lower error than the case for 5 steps, and since this is assessed to be adequate for a good initial guess of the steady state parameters. This method may still yield some error in the initial guess as seen from Figure 6.2 due to measurement errors. To make the initial guess of the steady state parameters the mean error, σ , from the figure is added to the correct value of F_s and F_c , and the percentage mean error of v_s , n and σ_2 is added to the actual values of these three parameters to simulate the estimation error. When the steady state parameters are estimated with this accuracy it is possible to conduct a sweep of the cost function for different values of σ_0 and τ_{hn} . This sweep is made utilising the part of the trajectory with a fast sine wave and the velocity step since it is seen that σ_0 and τ_{hn} have a great impact at these occasions. The initial guess of σ_0 and τ_{hn} is the parameter set which yields the lowest error from this sweep. The results utilising the initial guess from this method is shown in Table 6.6.

Even though the initial guess is good, the algorithm does not converge to the correct values. From the table it is seen that the residual from the algorithm is very small compared to the values in Table 6.5, though ideally it should be zero. The optimisation algorithm has so far been made with a step size tolerance of 10^{-3} . If the algorithm should further converge to more exact parameters, the step size tolerance should be lowered significantly. This is shown in Table 6.7, where the optimised parameters are found with a step size tolerance of 10^{-10} , the initial guess is the optimised parameters from Table 6.6. The step size tolerance was not met after 20.000 function evaluations and did not make further progress. As seen in the table some parameter sets have converged to almost zero error while others have a large error. This is either due to a non-convex problem or a very complex optimisation problem. Due to time limitations it has not been possible to examine other object functions or test other optimisation algorithms.

6.5.2 Sub Conclusion

In Table 6.6 the error in the estimated parameters are seen with a step size tolerance of 10^{-3} which is seen to cause significant estimation errors in the parameters. These errors are greater than the resulting error from the sequential method. The sequential method is thus more accurate. Furthermore the sequential method is as simple as the complete parameter estimation when it is necessary to run steady state tests prior the trajectory to obtain initial guesses.

Since it is too time consuming to run the algorithm with a lower tolerance for greater estimation accuracy, the estimation method for the remainder of this project will be the sequential method.

Parameter set:	#1		#2		#3		#4		#5		#6		#7		#8		
Error in %	$\tilde{\theta}_{init}$	$\tilde{\theta}$															
F_s	$\dot{x} > 0$	19.3	11.7	6.5	0.1	4.8	0.6	10.3	20.9	12.0	17.8	21.2	19.0	12.3	21.6	8.7	22.3
	$\dot{x} < 0$	29.5	22.5	11.3	1.2	9.8	0.1	16.5	19.1	64.5	13.5	57.2	30.7	53.4	34.8	54.5	36.7
F_c	$\dot{x} > 0$	1.0	50.2	1.0	1.0	712.0	672.4	0.3	14.1	2.0	6.5	0.1	16.7	0.3	9.9	4.6	22.9
	$\dot{x} < 0$	0.4	60.5	502.0	437.1	129.2	91.1	0.3	9.5	0.1	22.5	0.0	2.5	0.1	28.8	6.3	100.0
v_s	$\dot{x} > 0$	123.1	2.6	0.9	0.5	53.0	21.3	120.1	71.6	3.0	32.9	9.9	24.8	4.4	36.4	2.1	40.7
	$\dot{x} < 0$	479.3	1.5	66.8	36.7	36.7	9.4	765.0	701.0	17.7	0.3	9.5	20.2	1038.2	145.6	5.4	14.4
σ_2	$\dot{x} > 0$	1.2	65.5	13.1	11.6	100.0	100.0	0.5	21.4	22.2	75.6	0.2	49.5	2.1	82.7	5791.2	32887.0
	$\dot{x} < 0$	0.5	73.5	35.3	38.4	36.2	29.8	0.3	10.1	0.1	30.2	0.1	5.0	0.0	8.3	0.1	1.8
n	$\dot{x} > 0$	49.6	26.3	31.6	1.6	89.0	8.7	61.8	58.3	14.7	37.1	18.6	31.2	13.6	41.0	11.3	49.3
	$\dot{x} < 0$	65.1	49.5	60.6	10.0	39.6	3.1	72.0	71.7	24.8	26.3	17.8	45.3	81.0	78.1	11.0	5.8
σ_0		50.0	9.3	33.3	0.2	33.3	0.2	0.0	3.4	90.0	47.9	90.0	72.7	90.0	70.8	90.0	80.4
τ_{hn}		66.7	25.5	0.0	3.5	50.0	0.2	0.0	41.4	85.0	1.8	72.7	5.8	83.3	5.0	87.5	8.8
Res		1267310		161104		294137		131133		3798926		7471119		15063198		42696670	

Table 6.5: Percentage error of the initial parameter, $\tilde{\theta}_{init}$, and the optimised parameter, $\tilde{\theta}$, compared to the correct parameters.

Parameter set:	#1		#2		#3		#4		#5		#6		#7		#8		
Error in %	$\tilde{\theta}_{init}$	$\tilde{\theta}$															
F_s	$\dot{x} > 0$	4.3	3.7	2.7	0.7	2.1	0.1	19.0	4.3	2.0	1.8	2.6	3.5	2.0	1.9	1.4	0.5
	$\dot{x} < 0$	6.0	4.3	2.6	2.1	2.0	0.2	21.2	7.3	2.3	1.8	3.9	1.5	3.7	0.1	2.4	1.6
F_c	$\dot{x} > 0$	27.8	15.8	4.3	1.9	50.8	80.3	30.6	3.6	6.5	0.0	15.2	6.0	7.7	0.3	5.9	1.1
	$\dot{x} < 0$	19.7	6.5	33.3	80.1	18.1	38.4	43.4	5.3	24.7	12.4	20.4	8.4	31.5	23.6	876.5	895.6
v_s	$\dot{x} > 0$	2.5	4.1	2.5	1.0	2.5	2.3	2.5	27.5	2.5	8.2	2.5	6.4	2.5	8.8	2.5	5.7
	$\dot{x} < 0$	2.0	7.5	2.0	6.3	2.0	3.2	2.0	18.3	2.0	4.5	2.0	3.2	2.0	1.0	2.0	1.8
σ_2	$\dot{x} > 0$	33.3	20.3	33.3	23.8	33.3	11.3	33.3	6.9	33.3	0.8	33.3	19.3	33.3	3.4	33.3	100.0
	$\dot{x} < 0$	18.0	8.0	18.0	3.6	18.0	13.3	18.0	5.4	18.0	18.1	18.0	16.5	18.0	13.4	18.0	13.5
n	$\dot{x} > 0$	6.7	12.0	6.7	5.8	6.7	1.1	6.7	26.0	6.7	8.1	6.7	10.8	6.7	8.9	6.7	5.4
	$\dot{x} < 0$	6.3	16.6	6.3	7.3	6.3	1.1	6.2	44.4	6.3	13.3	6.3	14.5	6.3	14.8	6.3	7.3
σ_0		0.0	0.6	0.0	0.3	0.0	0.2	0.0	23.7	0.0	5.7	0.0	4.6	0.0	7.1	0.0	2.0
τ_{hn}		66.7	1.7	133.3	5.1	50.0	8.9	533.3	9.1	5.0	0.0	0.0	0.6	11.1	0.1	4.2	2.3
Res		66710		83423		86867		68726		196881		180993		430736		936951	

Table 6.6: Percentage error of the initial parameter, $\tilde{\theta}_{init}$, and the optimised parameter, $\tilde{\theta}$, compared to the correct parameters.

Error in %	$\tilde{\theta}(\#1)$	$\tilde{\theta}(\#2)$	$\tilde{\theta}(\#3)$	$\tilde{\theta}(\#4)$	$\tilde{\theta}(\#5)$	$\tilde{\theta}(\#6)$	$\tilde{\theta}(\#7)$	$\tilde{\theta}(\#8)$
F_s	$\dot{x} > 0$	0.7	0.1	0.1	3.8	1.2	4.1	0.5
	$\dot{x} < 0$	0.8	0.6	0.2	6.4	4.2	2.0	0.8
F_c	$\dot{x} > 0$	3.5	0.7	85.9	3.5	0.1	2.1	0.3
	$\dot{x} < 0$	1.1	92.6	41.6	6.6	6.7	3.5	923.1
v_s	$\dot{x} > 0$	0.5	0.3	2.9	13.0	5.6	9.8	3.7
	$\dot{x} < 0$	1.3	8.7	4.1	15.1	8.7	6.9	0.0
σ_2	$\dot{x} > 0$	4.6	8.3	11.6	5.6	0.8	6.2	0.2
	$\dot{x} < 0$	1.3	6.4	13.5	6.9	9.2	6.5	6.7
n	$\dot{x} > 0$	2.1	0.9	1.1	27.2	5.4	11.6	3.7
	$\dot{x} < 0$	2.6	2.7	1.6	45.1	13.8	13.8	4.3
σ_0		0.1	0.0	0.0	9.5	6.1	5.7	6.0
τ_{hn}		0.4	1.3	1.0	10.2	0.2	0.5	0.1
Res		2140	5745	7034	33499	97687	65155	216176

Table 6.7: Percentage error of the initial parameter, $\tilde{\theta}_{init}$, and the optimised parameter, $\tilde{\theta}$, compared to the correct parameters with a convergence step tolerance of $1 \cdot 10^{-10}$.

6.5.3 Complete Estimation Utilising Sequential Method

In this section the estimation of the friction parameters utilising the sequential method will be elaborated. First it will be investigated, utilising the full non-linear model, how long each velocity step should last to estimate the correct steady state parameters utilising 15 steady state velocities in each direction. The duration of the velocity steps influences the accuracy

of the parameter estimation since steady state conditions should be obtained. A sequential trajectory containing 15 steps in each direction, sine velocities and a first order step will be introduced and an estimation of the expected parameters in the complete model utilising this trajectory will be made to evaluate the trajectory.

Time Duration of Velocity Steps

This test will be made such each of the 15 velocity steps in each direction have the same time duration, yet some of the higher velocities can only be obtained for a certain time due to the cylinder stroke length. The time duration for these velocities will be the maximum obtainable. A NLSM with a step size tolerance of 10^{-3} is used to estimate the steady state parameters from velocity data and friction data from the last 0.1s of each steady state velocity. The friction data is calculated as:

$$F_{f,m} = p_{pm}A_{pm} - p_{rm}A_{rm} - F_L - m_m\ddot{x}_p \quad (6.10)$$

From Figure 6.15 the results are shown where the percentage error of the parameter estimation is plotted as function of the time duration of each velocity step. In the simulations the largest value of τ_{hn} , 2.4s, seen in table 4.2 is used, since this results in the slowest development of the friction force. It is seen from the figure that the estimation error is decaying approximately linearly from a 2 second time duration. The longest step time duration yields the most accurate parameter estimation, but due to the time consumption it is assessed that a time duration of 4 seconds is adequate since this result in a small estimation error.

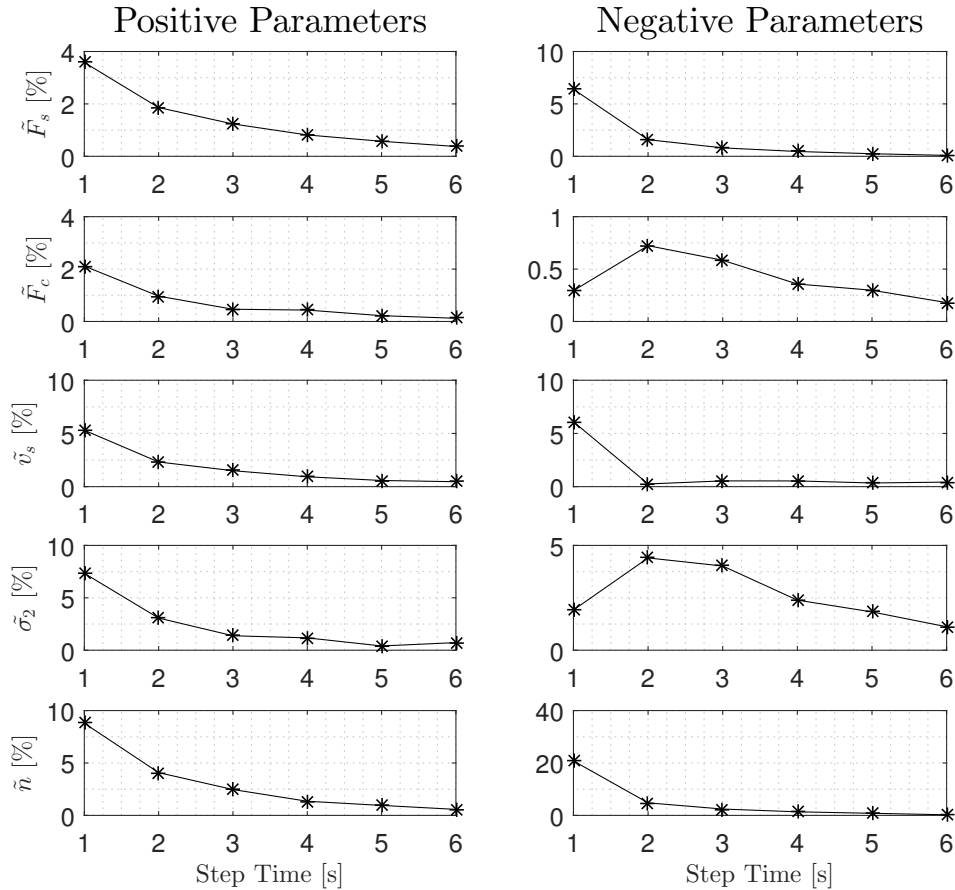


Figure 6.15: Estimation error of steady state parameters at different velocity step duration. The parameters are estimated utilising data from the complete model with noise and a lubricant film time constant of $\tau_{hn} = 2.4$.

Estimation of Friction Parameters From Complete Model

In this subsection it is investigated if it is possible to estimate the expected friction model parameters utilising a complete system simulation where noise is added to the measurements. This is done to investigate how noise on the measurements and control errors in tracking the velocity trajectory affect the parameter estimation algorithm.

A trajectory with a 4 second step time duration, is utilised in the complete non-linear model with noise, and the load force, F_L , main pressures, p_{pm} and p_{rm} , and acceleration, \ddot{x}_p from the model is used to calculate the friction force.

The friction force in the main cylinder is calculated as:

$$F_{f,\text{main}} = p_{pm}A_{pm} - p_{rm}A_{rm} - F_L - m_{\text{main}}\ddot{x}_p \quad (6.11)$$

In the optimisation algorithm the velocity input used for the friction model is the "measured" velocity from the complete system model simulation. In Table 6.8 the actual and estimated friction parameters are listed. As shown in the table, the noise and the control errors does not affect the parameter estimation much.

	Estimated		Actual	
	Positive	Negative	Positive	Negative
F_s	1999.6	-2499.4	2000	-2500
F_c	200.1	-599.7	200	-600
v_s	0.01	-0.01	0.01	-0.01
σ_2	300.3	501.9	300	500
n	1.197	1.199	1.2	1.2
σ_0	$1.0043 \cdot 10^7$		$1 \cdot 10^7$	
τ_{hn}	0.3002		0.3	

Table 6.8: Results from estimating the friction parameters from "measurements" of a simulation of the full model with noise added to the signals. The pressures are controlled to 20 bar.

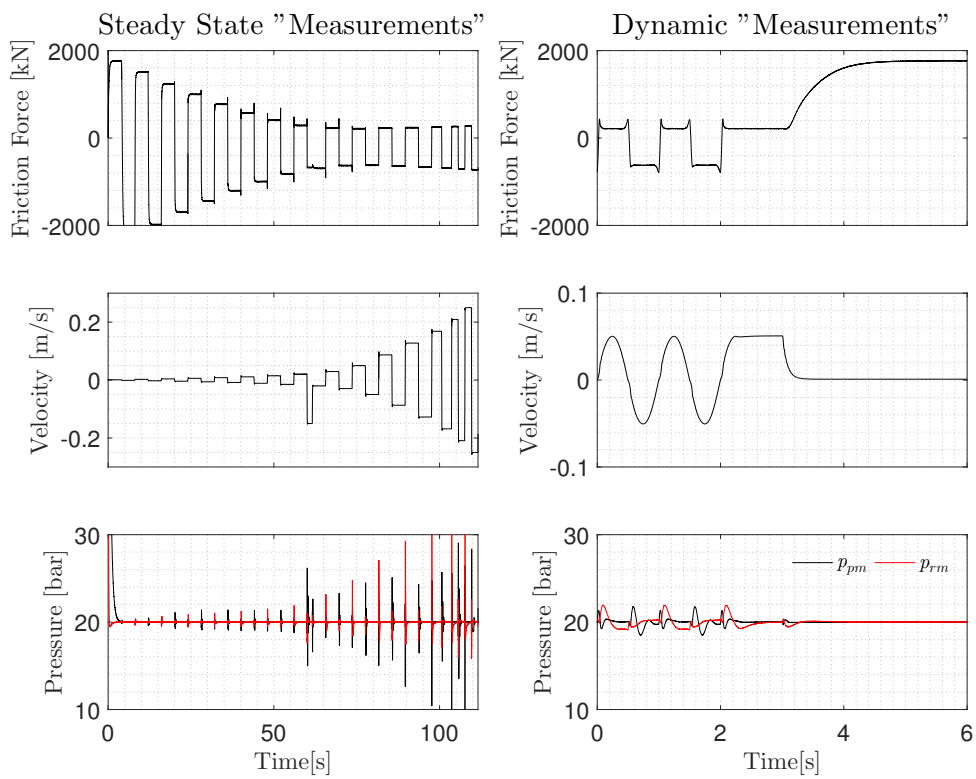


Figure 6.16: Simulated measurements used to estimate the parameters from the model with noise and pressure references of 20bar.

7 | Validation of Proposed Friction Model

A validation of the proposed friction model summarised in Section 5.2.5 is evaluated in this chapter to investigate if the proposed model is able to describe the friction force in the main cylinder. This chapter will consist of two sections. A validation of the steady state friction model and a validation of the full friction model.

Prior to the final measurements, the cylinder should be run to break it in. The break in period is the period before the friction force is constant over time. This is elaborated in Appendix D.1 where the trajectory utilised during break in is described and some measurements made during break in are shown. From these measurements it is indicated that the cylinder is still in the break in period after a travel distance of 2675m where the final measurements are started. This causes the friction force to behave different than expected, though due to time limitations further break in has not been possible. Therefore the measurements presented in this thesis are measured during the break in period. Due to time limitations it has only been possible to conduct measurements one time. Subsequent to submission further break in of the cylinder will be made and the measurements will be conducted again and presented in the examination. The measurements will be conducted three times to assure repeatability of the measurements.

Problems regarding the control of the pressures at low pressure references is also seen during the experiments. The problems related to a lack of break in and the pressure control are elaborated in Appendix D.1 to D.4, and a summary of the investigations are given below.

- Break in - Appendix D.1
 - A trajectory used during break in is designed and measurements during the break in period is shown. It is seen that the main cylinder is in the break in period.
- Evaluation of Velocity Step Duration for Steady State Measurements. - Appendix D.2
 - The desired velocity step duration found in Section 6.5.3 of 4 seconds is evaluated by measurements. It is seen that the friction force is not constant after 4 seconds and an investigation leads to a new trajectory with a 30 second velocity step duration, or as long as possible, to be utilised for the resulting measurements.
- Steady State Friction Sampling Instance - Appendix D.3
 - During the resulting measurements the steady state friction samples for negative velocities are made at a cylinder position of approximately -0.25m. From the measurements it is seen that the friction force changes a lot at this point why it is assumed that a position dependent friction is acting in this point. To circumvent the influence of this it is chosen to sample the friction force before this large change in the friction force.
 - From the measurements with low pressure references of 20 bar it is observed that the system is unable to maintain the pressures during high steady state velocities. Therefore for $p_{rm,ref} = 20$ bar, the three friction force samplings at high negative velocities are disregarded together with the two friction force samplings at high negative velocities for $p_{pm,ref} = 20$ bar. This problem may be caused by a

undesired disabling of the flow feed forward to the main valves.

- Position Dependency - Appendix D.4
 - Since it was assessed that a position dependent friction force was present in the main cylinder an investigation is made with constant pressures and constant velocities during the whole stroke length at 0.005 m/s and 0.025 m/s. This investigation showed that a position dependent friction appears.

All the measurement data illustrated in this chapter have been filtered with a 2nd order Savitzky-Golay filter with 51 frames, due to noise on the measurements. Yet unfiltered signals are used for data processing.

7.1 Steady State Friction Model Validation

To validate the steady state friction model, a trajectory with 30 velocity steps from 0.001 to 0.25 m/s for positive and negative velocities are utilised to obtain a detailed characteristic of the steady state friction behaviour. These measurements are conducted with a pressure reference of 100 bar for both the rod side and piston side of the main cylinder. In Figure D.4 the measurement data from this experiment are shown and Figure D.5 is a zoom of these data at the high velocities. In Appendix D.3 some considerations about the sampling instances for the steady state friction are made and the results from this appendix is applied here.

The resulting steady state friction curve from the data shown in Figure D.4 is illustrated in Figure 7.1. It is seen that the friction curve for positive velocities can be well described by the steady state friction model proposed in Section 5.2.5. Yet the fit for negative velocities is not as good since the friction force of the four points at low velocities are very low. These four points are sampled in the middle of the cylinder where the remaining points are sampled at approximately -0.25m. Either this is due to non-modelled friction characteristics or a position dependency. When measuring the combined friction of several surfaces, which is the case for a hydraulic cylinder which has multiple seals, the different surfaces might have different Stribeck characteristics (Armstrong-Helouvry, 1991). In this case it is assessed that it is more plausible that the characteristics are due to a position dependency. This assumption is confirmed in the analysis in Appendix D.4 where the friction force is seen to change with position during steady state conditions.

Two methods to overcome this problem are investigated. Either the first sample points which have a lower value than the maximum value are disregarded in the model estimation or either they are not. Both methods are illustrated in Figure 7.1, where the Modified Estimation is where the points lower than the maximum are disregarded in the estimation. The choice of method is further elaborated in the next subsection where the two methods will be evaluated based on measurements obtained using the trajectory shown in Figure 7.2 at different pressure combinations.

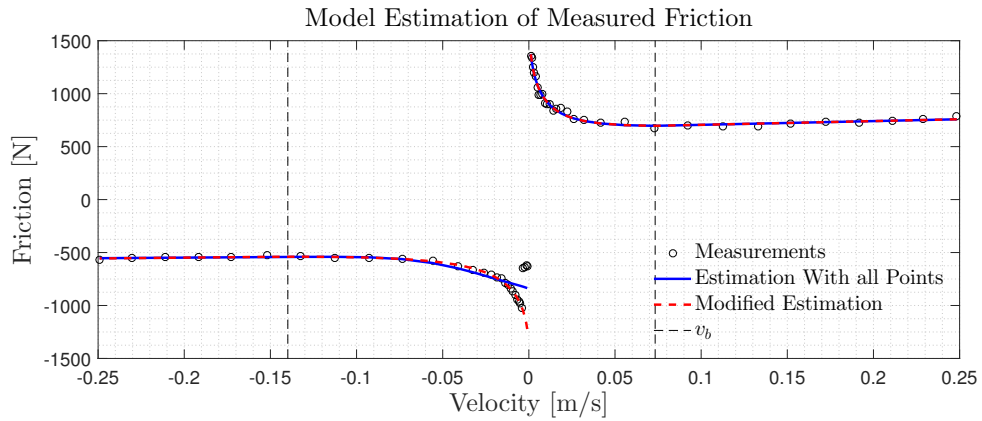


Figure 7.1: Estimation of steady state friction model from the measurements shown in Figure D.4.

7.1.1 Evaluation at Different Pressure Combinations

The resulting trajectory used to estimate the friction parameters for the model described in Section 5.2.5 is shown in Figure 7.2 which is a result of the investigation in Appendix D.2. This trajectory will be utilised to determine the pressure dependencies of the individual friction parameters by estimating the parameters for the velocity dependent friction model for varying pressure combinations.

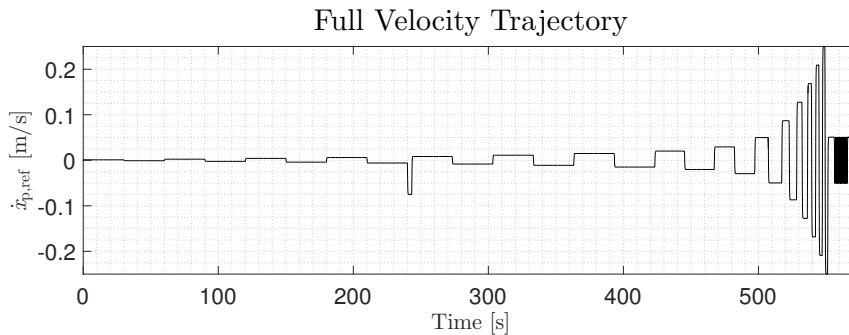


Figure 7.2: Final velocity trajectory used for the sequential friction parameters estimation.

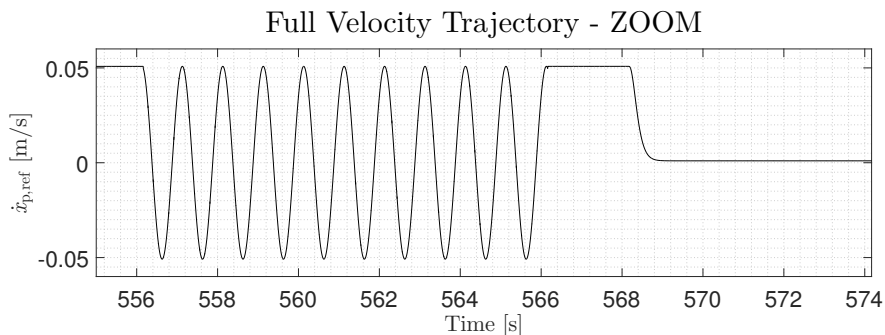


Figure 7.3: Zoom of Figure 7.2.

In Figure 7.4 the steady state friction measurements and model estimation for six represen-

tative pressure combinations are shown. The black circles illustrates the friction samples, the blue line is the friction model estimation including all the sampling points, the dashed red line is the friction model estimation excluding the first sampling points, which is lower than the maximum friction force, and the dashed black line is where v_b is placed.

From Figure 7.4 it is seen that the steady state friction for positive velocities can be well described by the proposed friction model from Section 5.2.5. For negative velocities it is seen that the friction curve without the first samples, prior to the maximum friction sample, behaves like the proposed friction model and that the measurements can be fitted well using this method.

It is chosen to disregard the first samples, prior to the maximum friction sample, since it is assessed that this will yield the best results regarding the robustness of the parameter estimation. Since these points are measured at a piston position different from the other measurements this is assumed to be reasonable due to the position dependency stated in Appendix D.4.

The value of v_b is seen to be placed approximately at the velocities where the fluid lubrication regime begins. v_b is placed at different velocities since the Stribeck curve changes with pressures. This justifies the method elaborated in Section 5.1.1.

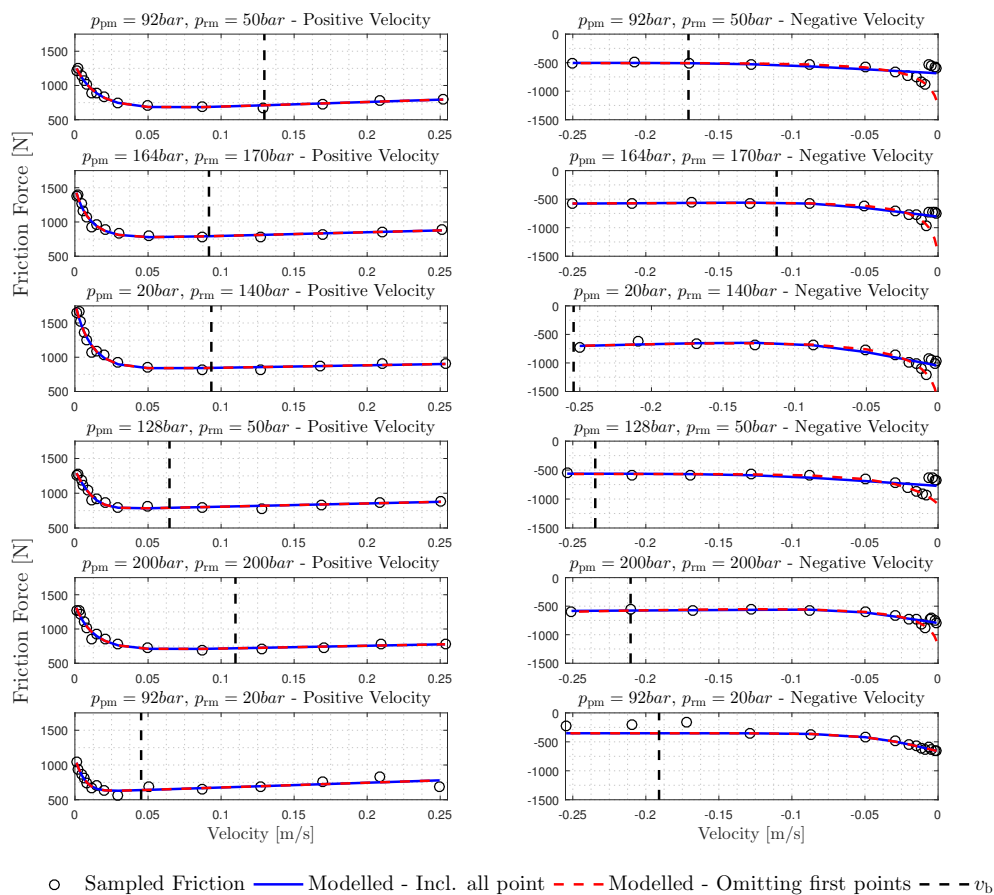


Figure 7.4: Results from estimating the steady state parameters for six representative pressure combinations where the estimation is conducted with and without the first sampling points, prior to the maximum friction sample.

7.2 Complete Friction Model Validation

The dynamic parameters are estimated from a minimisation of the sum of squared residuals between the measured friction and the modelled friction with the measured velocity as input, where the steady state measurements are sampled during steady state conditions. In the previous section it has been shown that the proposed steady state model is unable to accurately describe the friction force for low velocities in negative direction. This is assumed to be caused by a position dependency in the friction force described in Appendix D.4. A modelling error in the steady state friction will affect the estimation of the dynamic parameters since the dynamic parameters will be found such they compensate for the steady state error.

From Figure 7.5 the friction force during a sine wave is seen. It is seen that the modelled friction force fits the measurements poorly. This is probably due to the inaccurate steady state model, since the steady state model is used for the complete model. The full friction model can not be validated with the data obtained prior to project submission, yet it is attempted to validate the model prior to the examination utilising new measurements.

Besides the obvious error between the model and the measurements, a lag between measured and modelled friction is seen during a direction change. An investigation of this shows that this is caused by a temporary stand still in the measured velocity during a direction change. This is shown in the bottom plot of Figure 7.5. This stand still was also observed in the former work done by the authors. In this work it was proposed that the stand still was primarily due to axial play in the velocity sensor (Pedersen and Jørgensen, 2016). In this thesis the cylinder velocity is measured with a no contact linear encoder with a resolution of $5 \mu\text{m}$, why it can be concluded that the temporary stand still is not due to axial play in the sensor. During a direction change in the pre-sliding regime, before the break away force is met, the friction is behaving as a stress/strain relation such the friction is a function of position more than velocity. If the resolution of the sensor is too low to detect the changes in the pre-sliding regime, the pre-sliding regime will appear as a stand still. As seen from the bottom plot in Figure 7.5 the velocity is constant for approximately 30ms during a direction change. The velocity is showing the value obtained from the last detected change in position and from the position measurement it has been seen that the position is constant. Since the direction of the proposed friction model is controlled by the direction of the measured velocity, the stand still in the velocity appear as a lag between the modelled and measured friction. This lag might cause the bristle stiffness, σ_0 , to be estimated too high. This is seen in Figure 7.5 where the estimated bristle stiffness, $\hat{\sigma}_0$, does not result in the correct slope during the direction change, though if the friction is modelled with a tenth of the estimated bristle stiffness, the slope seems to fit. From these observations it is indicated that an estimation of σ_0 will result in a wrong value due to the lag between measured and modelled friction. Regarding the lubricant film thickness, τ_{hn} , the estimation of this parameter also depend on the steady state parameters and will be affected by the position dependency too, why the estimated values and the development with pressure should be evaluated with care.

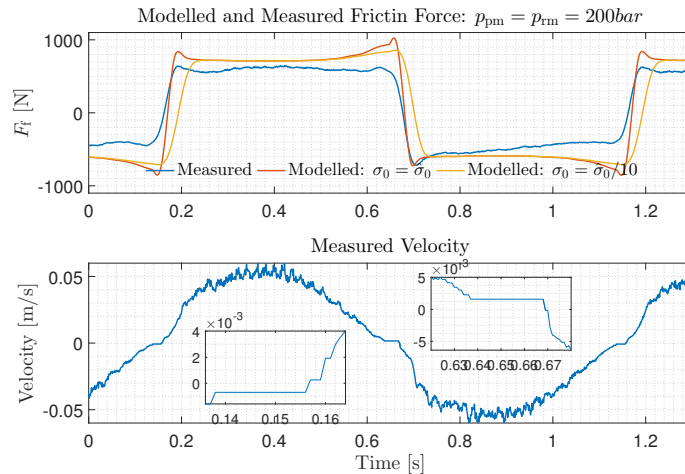


Figure 7.5: Modelled and measured friction during a sine wave of 1Hz and an amplitude of 0.05 m/s.

7.2.1 Evaluation at Different Pressure Combinations

In Figure 7.6 the six examples, used for steady state estimation in the previous section, is shown for the measured and modelled friction force utilising the trajectory shown in Figure 7.3 and the estimation method elaborated in Section 6.2.2. As seen in the figure the measured friction force levels differs from the modelled. This is due to an inaccurate steady state model, which is properly caused by a position dependency, since the measurements for the dynamic friction model estimation are made at a different position than the steady state measurements. The dynamics of the friction force differs from the measured during the sine wave from 14s to 16s, though during the step from 16s to 20s the dynamics of the modelled friction seems to fit the measurements in most cases yet no conclusions can be drawn. From this it is indicated that estimation of the dynamic parameters are wrong. Though new measurements subsequent to submission will be presented the examination.

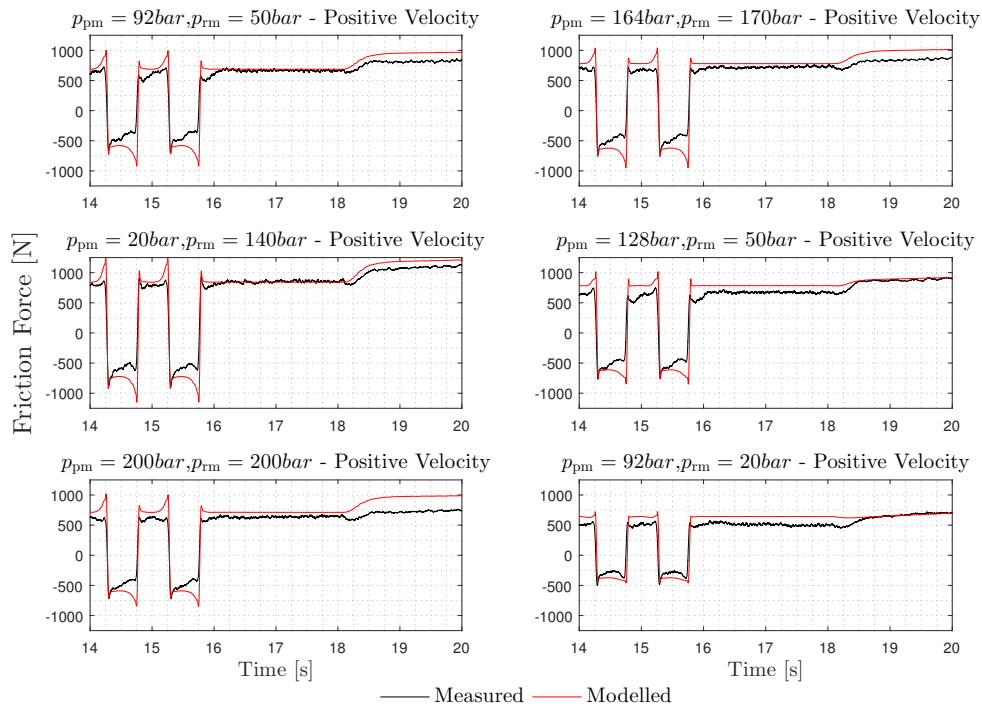


Figure 7.6: Six representative examples of the modelled and measured friction force during a sine wave of 1Hz with an amplitude of 0.05 m/s and a step from 0.05 m/s to 0.001 m/s.

Summary

The steady state parameter estimations for negative velocities should be evaluated with care since a lot uncertainty is associated with the sampling of the friction force. This is due to the sudden changes of the friction force around the sampling instance which made it necessary to change the steady state sampling instance. This problem is assessed to be caused by a position dependent friction due to a lack of break in. Furthermore when disregarding the first friction sampling points for negative velocities which is lower prior to the maximum measured friction force, the values of n , F_s and v_s may be estimated wrong. The parameter values for positive direction should also be evaluated with care since an potential position dependency will have an influence of the usability of the friction model which is not position dependent. Yet it is shown that, under these circumstances, the proposed steady state friction model can describe the steady state friction behaviour.

Regardless of a potential position dependency, it may still be possible to characterise the pressure dependency of the steady state parameters locally at certain piston positions since the sampling instances for all the trajectories are made at the same piston position.

Regarding the estimation of the dynamic parameters a great uncertainty may affect the results. A position dependent steady state friction and a disability to measure velocities during the pre-sliding regime may result in an estimation of the dynamic parameters which is not robust since the model can not fit the measurements.

8 | Validation of Parameter Estimation Methods

In this chapter the chosen sequential parameter estimation method is validated. Furthermore the optimisation based method is compared to the results obtained with the sequential estimation method. The validation is based on three measurement series conducted after each other with pressure references of 100 bar. The trajectory in Figure 7.2 is utilised for the sequential method and the trajectory in Figure 6.13, with an extra ramp, is utilised for the optimisation method. The optimisation method is evaluated with an step tolerance of 10^{-3} and 10^{-10} .

The results are shown in Table 8.1 where the mean and standard variance of the estimated parameters are shown. The three steady state measurements used in the estimation for the sequential method are shown in Figure 8.1 and the dynamic measurements used for the optimisation based method are shown in Figure 8.2.

From the table it is seen that the values of F_s and F_c are estimated with a standard variance below 10% for the sequential method. Yet the Stribeck shaping parameters n and v_s and the viscous friction σ_2 are varying more in the estimations regardless of the friction sampling points being consistent as seen in Figure 8.1. The variation in the parameter estimation should be compared to the change in the parameters, observed for different main cylinder pressure combinations, which will be investigated in the next chapter.

The estimation of the dynamic parameters are also estimated with good consistency for the sequential method. Yet the values are found during an optimisation, elaborated in Section 6.2.2, which is dependent on the steady state parameters as discussed in Section 7.2, where it was seen that the modelled steady state friction did not fit the measured friction force during a sine trajectory due to a position dependency. This results in a disability to model the dynamic friction force accurately and an potential change in the dynamic parameters for different pressures, seen in the next chapter, can not be used to model a pressure dependency when a position dependent friction is present.

The parameter estimation using the optimisation based method generally results in a less consistent parameter estimation. The reason for this may be that the parameters are found from a friction force measured over a large range of the stroke where the friction force changes with position. By this, the proposed friction model can not be fitted well to the measurements. The measurement data, seen in Figure 8.2, used for the optimisation based method is generally consistent, yet one irregularity is observed in "Measurement 1". This may have an influence in the larger standard variance of the estimated parameters compared to the sequential method. The fits of "Measurement 2" with two different stopping tolerances are seen in the Figure as well, as seen the fits does not describe the measurement.

From the table it is seen that the mean parameters found with the different methods differs much from each other. This might be due to the complex optimisation problem as described in Section 6.5.1 which resulted in wrong estimates of some parameters. Furthermore the trajectories for the sequential and optimisation based estimation are not conducted at the same piston positions which may have an influence.

In the next section the parameter estimation variance for the sequential method in this section will be discussed regarding how large the changes in the parameters are due to pressure. To indicate a pressure dependency of the parameters, the change in the parameters due to pressure should be larger than the estimation standard variance shown in Table 8.1.

		Positive			Negative		
		Sequential	Opti. Tol: 10^{-3}	Opti. Tol: 10^{-10}	Sequential	Opti. Tol: 10^{-3}	Opti. Tol: 10^{-10}
F_s	μ	1392	1315	1641	-1248	-314	-635
	σ	113	282	717	100	35	516
	$\sigma(\%)$	8.1%	21.4%	43.7%	8%	11.2%	81.3%
F_c	μ	582	609	625	-447	-281	338
	σ	19	20	4	28	9	109
	$\sigma(\%)$	3.3%	3.3%	0.6%	6.3%	3.2%	32.3%
v_s	μ	0.0168	0.0027	0.0023	-0.0164	$-3.1 \cdot 10^{-6}$	$-0.1 \cdot 10^{-3}$
	σ	0.0035	0.0027	0.0021	0.004	$2.7 \cdot 10^{-6}$	$0.2 \cdot 10^{-3}$
	$\sigma(\%)$	20.8%	100%	91.3%	24.4%	87.1%	200%
σ_2	μ	790	609	517	436	1699	1316
	σ	95	100	81	164	76	756
	$\sigma(\%)$	12%	16.4%	15.7%	37.6%	4.5%	57.5%
n	μ	0.71	0.5	0.6	0.51	0.5	0.5
	σ	0.187	0	0.19	0.0093	0	0
	$\sigma(\%)$	26.3%	0%	31.7%	1.8%	0%	0%
σ_0	μ	$1.3 \cdot 10^7$	$0.8 \cdot 10^7$	$1.4 \cdot 10^7$			
	σ	$6.2 \cdot 10^5$	$0.2 \cdot 10^7$	$0.1 \cdot 10^7$			
	$\sigma(\%)$	4.8%	25%	7.1%			
τ_{hn}	μ	22.9	1.0	2.65			
	σ	2	0.55	0.56			
	$\sigma(\%)$	8.7%	55%	21.1%			

Table 8.1: Validation of the sequential and optimisation based parameter estimation. The values in the table is based on three measurement series.

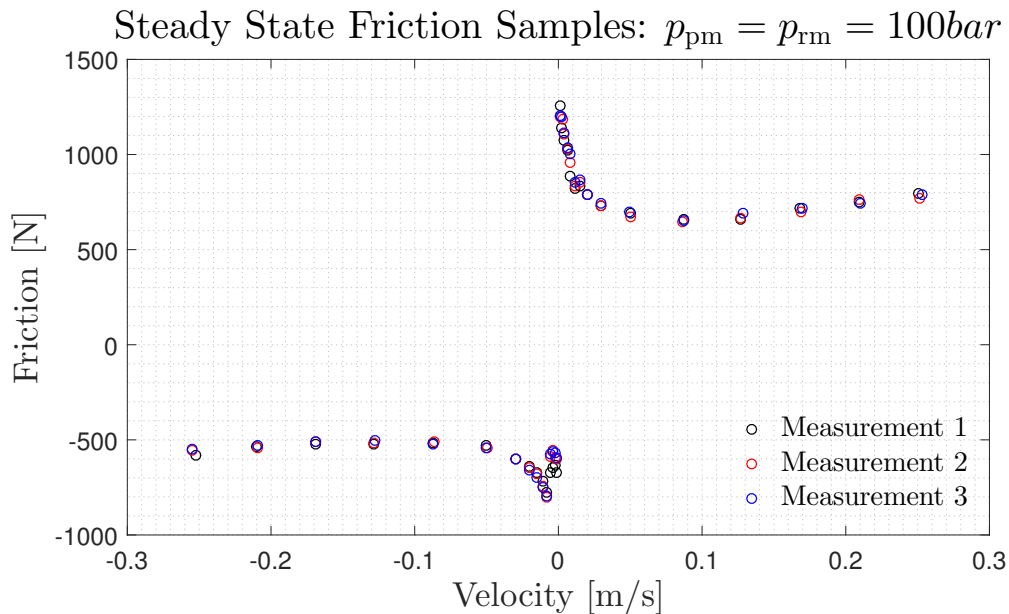


Figure 8.1: Steady state friction samples used for the sequential estimation of the friction force parameters.

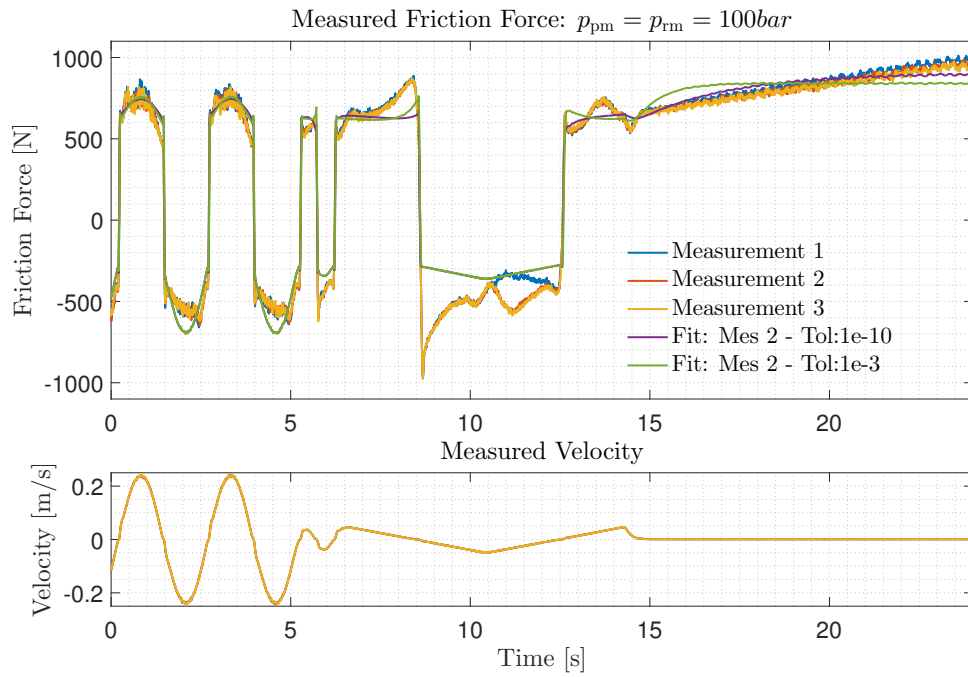


Figure 8.2: Measurement data used to estimate the friction parameters, and the fit for measurement 2 with different stopping tolerances utilising the optimisation based method from Section 6.5.1.

9 | Pressure Dependency in the Friction Force

In Chapter 7 it is described that some unexpected tendencies are occurring during the friction measurements. These observations regards a position dependent friction force and a disability to measure very small displacements smaller than $5 \mu\text{m}$. This position dependent friction may result in a wrong steady state curve. Yet since the measurements are sampled at the same cylinder position each time, the "error" is assumed to be consistent, why it might be possible to indicate a pressure dependency utilising the available measurements. Regarding the dynamic parameters, a development of σ_0 due to a pressure dependency may not give an indication of an actual pressure dependency due to the lag between measured and estimated friction and the position dependent steady state friction. A pressure dependency in τ_{hn} might be difficult to detect since the accuracy of the steady state model might cause the estimation of τ_{hn} to vary. Due to time limitations it has only been possible to conduct each measurement once why these data can not be used to conclude any pressure dependencies since it is not shown that the measurements are consistent. Yet indications of the pressure dependencies may be seen.

9.1 Static Pressure Dependency

The pressure dependency at steady state pressures are investigated by estimating the proposed friction model parameters at various pressure combinations. The rod side chamber are varied from 20 to 200 bar with 30 bars interval while the piston side chamber are varied from 20 to 200 bar with 36 bars interval. In this section the variation in each parameter is presented. Some tendencies are seen in the pressure dependency, though the tendencies are not consistent why a model of the pressure dependency will not be proposed.

In Figure 9.1 the pressure dependency of the Stribeck parameter, F_s , is seen. From the state of the art investigation it was indicated that the amplitude of this parameter should increase with pressure. From the figure it is indicated that the parameter, as expected, increases with pressure. Furthermore the figure indicates that the parameters might saturate for higher pressures in p_{rm} though this tendency is not seen for all pressures e.g. $p_{\text{pm}} = 56\text{bar}$ and 92bar in positive direction. The variation in F_s for negative and positive velocity is approximately 1000N and 1500N respectively. From Table 8.1 it is seen that the standard variance for the estimation of F_s for negative and positive velocity is 113N and 100N respectively. This indicates a pressure dependency of F_s .

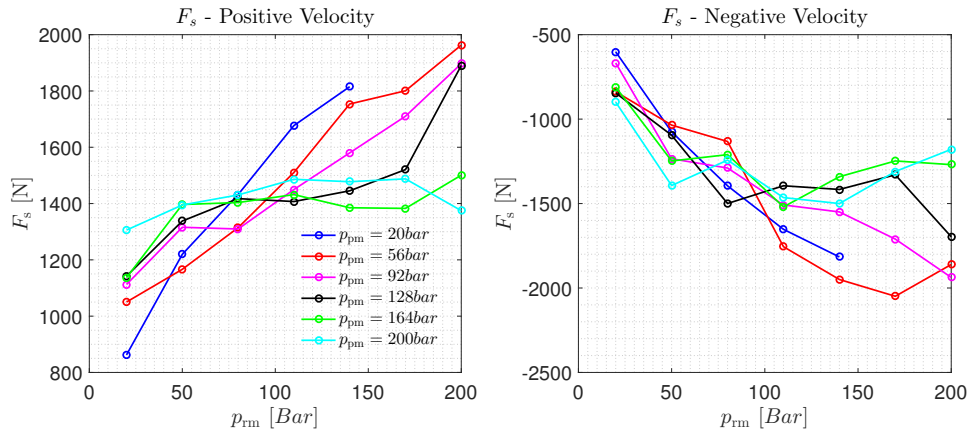


Figure 9.1: F_s for different parameter combinations.

The change in the Coulomb friction, F_c , is seen in Figure 9.2. As for F_s , it is indicated in the state of the investigation that this parameter should increase with pressure. This is also the general tendency seen from the figure, though for some piston side pressures, $p_{pm} = 128\text{bar}$ and 164bar , the parameter is seen to decrease with the rod side pressure. The variation in F_c is approximately 600N for both directions. From Table 8.1 it is seen that the standard variance for the estimation of F_c for negative and positive velocity is 19N and 28N respectively. This indicates a pressure dependency of F_c .

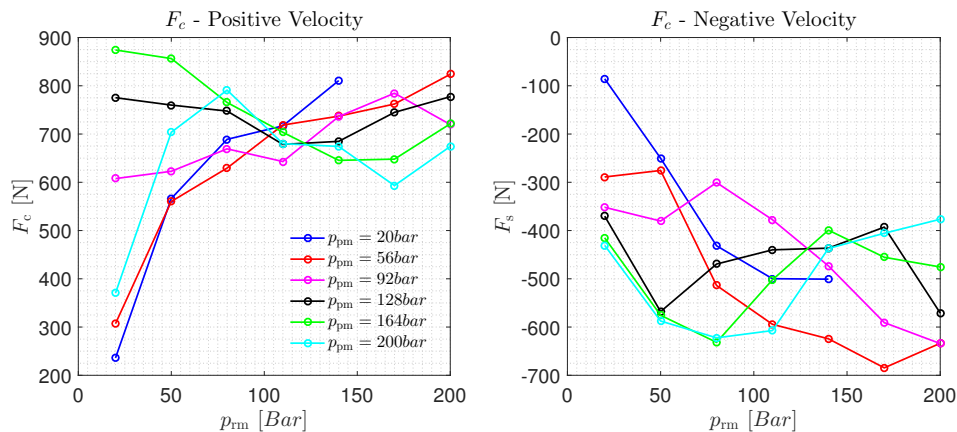


Figure 9.2: F_c for different parameter combinations.

In Figure 9.3 the change in the shaping parameter v_s is seen. From the state of the art investigation no clear indication of how this parameter varies with pressure was seen. This is also what is indicated in this investigation. The variation in v_s for negative and positive velocity is approximately 0.02 m/s and 0.07 m/s respectively. From Table 8.1 it is seen that the standard variance for the estimation of v_s for negative and positive velocity is 0.0035 m/s and 0.004 m/s respectively. Yet no tendency is seen in the parameter either from the variation in p_{rm} or p_{pm} .

9.1. Static Pressure Dependency

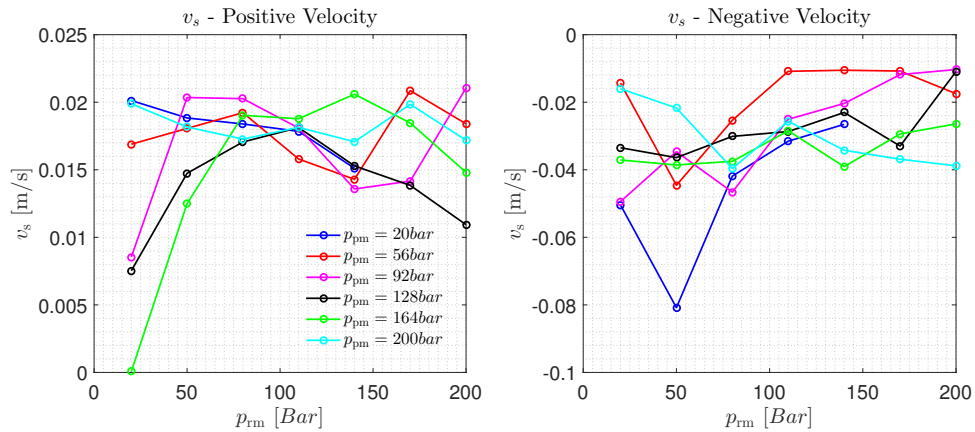


Figure 9.3: v_s for different parameter combinations.

In Figure 9.4 the change in the viscous friction parameter σ_2 is seen. From the state of the art investigation it was indicated that this parameter should increase with pressure for negative velocities while it should decrease for positive velocities. For positive velocities it is seen that the parameter is estimated in the same range for higher rod side pressures, though for $p_{rm} = 20\text{bar}$ a great variation is seen. For negative direction the parameter is seen to differ greatly, though no tendency is seen.

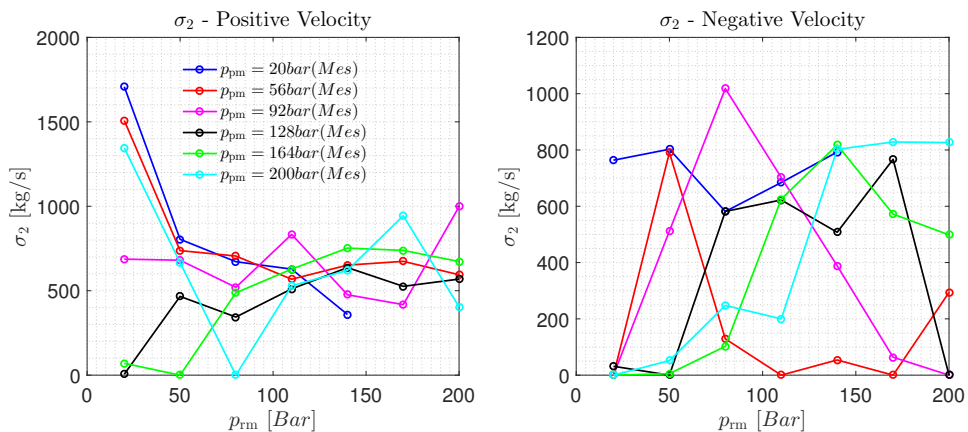


Figure 9.4: σ_2 for different parameter combinations.

In Figure 9.5 the change in the shaping parameter n is seen. From the state of the art investigation it is indicated that this parameter should increase with pressure. The variation in n for negative and positive velocity is approximately 2.5 and 1 respectively. From Table 8.1 it is seen that the standard variance for the estimation of n for negative and positive velocity is 0.187 and 0.0093 respectively. For positive direction it might be indicated that n decreases with p_{rm} except for $p_{rm} = 20\text{bar}$. Furthermore the figure indicates that n increases with p_{pm} . In negative direction no clear indication of the tendency is seen though in many cases the estimation of n is seen estimated at the boundary of 0.5. This boundary was incorporated for the scheme to determine v_b to be accurate. The reason for this may be due to a lack of sampling points at low velocities in the parameter estimation. This is seen in all cases for $p_{pm} = 20\text{bar}$ in negative direction.

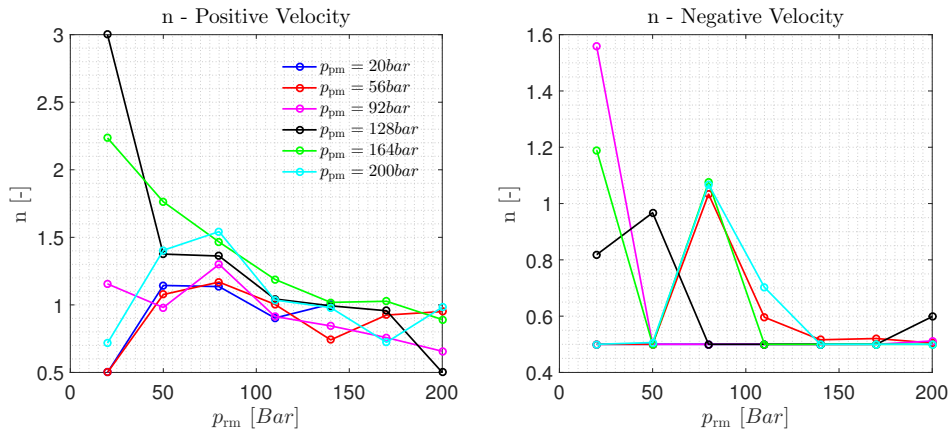


Figure 9.5: n for different parameter combinations.

In Figure 9.6 the change in the dynamic parameters σ_0 and τ_{hn} are seen. No indication was seen of the pressure dependency in σ_0 in the state of the art investigation. The variation in σ_0 is approximately $2.5 \cdot 10^{-7}$. From Table 8.1 it is seen that the standard variance for the estimation of σ_0 is $0.062 \cdot 10^{-7}$. Figure 9.6 might indicate that σ_0 increases with p_{rm} , though no tendency is seen for varying p_{pm} .

From the state of the art investigation it is indicated that τ_{hn} increases with pressure. Figure 9.6 indicates no relationship between τ_{hn} and the pressures.

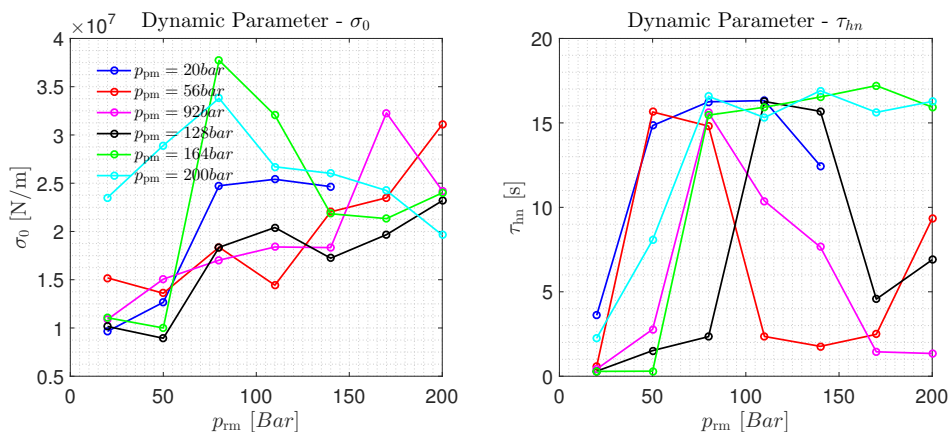


Figure 9.6: σ_0 and τ_{hn} for different parameter combinations.

9.2 Dynamic Pressure Dependency

In this section it is investigated if the friction force is dynamically dependent to the chamber pressures. This is investigated by maintaining constant velocity and pressure in one chamber, while the other pressure is varied. This way it can be investigated how the friction force changes with the change in pressure. In this analysis the piston velocity is controlled to 0.005 m/s while one chamber pressure is controlled to 100 bar. The other pressure is varied with a sine wave of 0.25 Hz for p_{rm} and 0.5 Hz p_{pm} around 100 bar with an amplitude of 20 bar. The difference in frequency is due to an error when designing the trajectories which was discovered subsequent to experiments. The frequency is chosen as fast as possible without

influencing the other pressure and the velocity. During examination of the measurements it is seen that the influence on the velocity is negligible.

The measurements are, as the previous presented measurements, made before the break in period of the cylinder is over. This might be the cause of the measured position dependency present in Appendix D.4. In this experiment a position dependency will influence the results, since the friction force not only varies with the variation in pressure, but also with position. The measurements are presented in Figure 9.7 and 9.8. In general it is seen that the friction force is dependent on the varied pressure, except when p_{rm} is varied during negative velocity. In this case a clear pressure dependency is not seen. In most cases a dynamic dependency is not clearly seen. This would have been seen as a hysteresis loop in the right plot where the friction force is plotted as function of pressure. When varying p_{pm} during a positive velocity, as seen in Figure 9.7, a hysteresis loop appear in the right plot. The figure indicates that the pressure dependent friction force is greater for decreasing pressures, this is also indicated by the left figure, where it is seen that the friction lags the pressure. While the friction changes with pressure it also changes with position why a dynamic behavior for the remaining pressure/velocity combinations in the figures might not be visible.

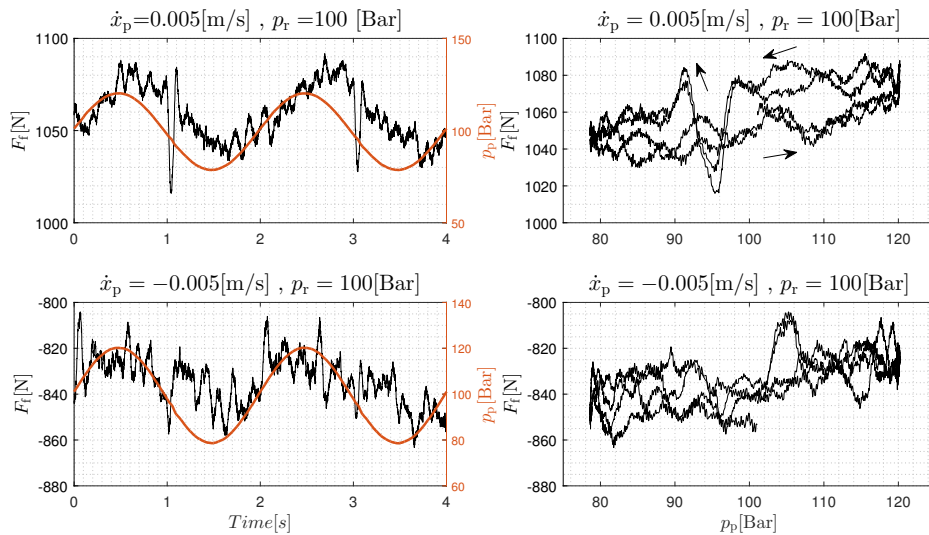


Figure 9.7: Dynamic investigation the dynamic pressure dependency of the piston side chamber pressure, p_{pm} . Constant velocity and rod side chamber pressure while varying the piston side chamber pressure with a sine wave.

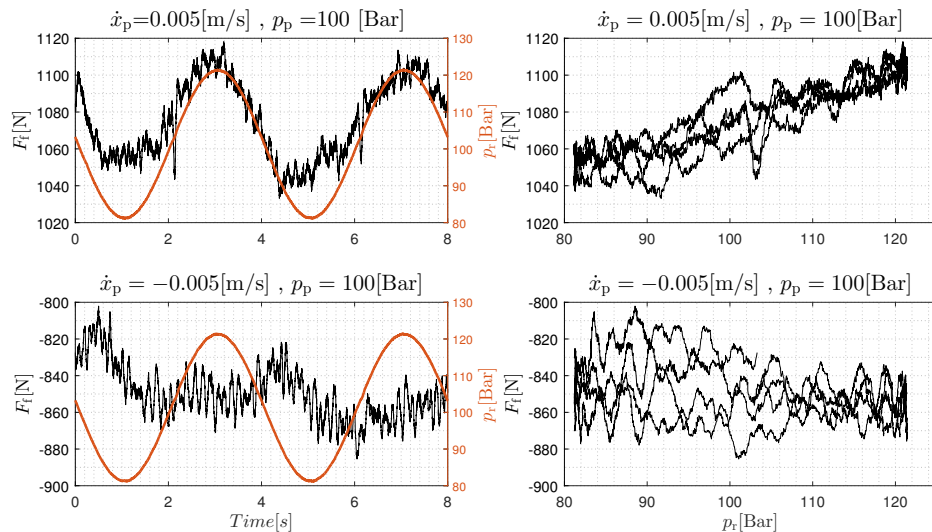


Figure 9.8: Dynamic investigation the dynamic pressure dependency of the rod side chamber pressure, p_{rm} . Constant velocity and piston side chamber pressure while varying the rod side chamber pressure with a sine wave.

A dynamic connection between the pressure and the friction force might not be directly linked to the pressure. In the current friction models describing the friction force in hydraulic cylinders with dynamic lubricant film thickness, the thickness h changes if the parameters F_c , F_s or v_b changes. As indicated by Chapter 9.1 the parameters F_c and F_s changes with pressure. This causes the amplitude of the steady state lubricant film thickness to change which causes the friction force to change dynamically.

One way to investigate how the dynamical connection between pressure and friction force can be described, is to develop a pressure dependent friction model and compare the dynamics of the model with the dynamics of the measurement. This has not been possible with the measurements presented in this thesis.

In the figure where the hysteresis loop is seen, it is seen that the difference in the friction is approximately 25N, why the contribution from this might be negligible though this might increase for larger pressure variations or operation cycles.

A lump in the friction force is seen in the same place in each cycle for some of the measurements. During examination of the measurements it has been seen that the velocity has a lump at the same instance. It is not deduced what the cause for this is.

Part II

Closure

10 | Discussion

In this chapter the methods and results from the thesis is discussed. The chapter covers discussions of the friction modelling and parameter estimation, system design and results.

10.1 Friction Modelling and Parameter Estimation

The analyses of different friction models and different parameter estimation methods are made with "simulated measurements" since no measurements were available at the time. The "simulated measurements" are made with a set of parameters in the range of the expected friction force for the main cylinder. Yet eight earlier found friction characteristics are used during the analyses, to test the models and estimation methods for different parameter sets. This analysis is thus not a general analysis of the friction force and parameter estimation, but can only be used as an indication.

10.1.1 Simulated Error In Parameter Estimation Analysis

In Chapter 6, different parameter estimation methods are evaluated. Since no test facility was available at the time, a measurement error was simulated to evaluate the robustness of the different parameter estimation methods. This error was simulated from the assumed repeatability error of the test facility, $\pm 25\text{N}$. The error simulation is not proven to be correct, but is used in lack of measurements. It is assumed that during continuous measurements, the error changes as a second order polynomial since it is assumed that the repeatability error is changing continuously. One problem utilising this polynomial is that the friction force error is the same for a repeated friction force level e.i. The error changes with force but not change with time. This means that e.g. during a sine wave, the "measured" friction force will be the same for every repeated sine wave, which is not necessarily correct.

Furthermore it is assumed that during sampling of the friction force e.g. during steady state sampling of the friction force, the repeatability error can be simulated with a random error within $\pm 25\text{N}$ on each friction force sampling.

The error is simulated in different ways, weather it is a continuous measurement or if it is sampling of measurements, yet the estimation error is stilled compared to each other. It is not proven that this method is valid but it is assessed that it is a reasonable assumption to compare the estimation methods.

10.1.2 Convergence of Parameter Estimation

In every of the different parameter estimation methods a NLSM is utilised. In no case the optimisation problems are shown to be convex. It is thus not proven that the global optimum is found. In the analysis of different parameter estimation methods a step size tolerance is set to 0.001. This showed good results in the analysis where the expected parameters were used. This tolerance might be too high since large estimation errors was seen with this tolerance, when the algorithm was tested on other sets of parameters.

A lower stopping tolerance was seen to increase the accuracy but the resulting estimation error was still large. From the parameter estimation of the practical measurements the

algorithm is seen to converge differently depending on the initial guess. This is seen in Figure 10.1, where two different initial guesses are used in the optimisation utilising a step size tolerance of 10^{-10} . Another algorithm, cost function or trajectory might yield more consistent results, though due to time limitations this has not been investigated.

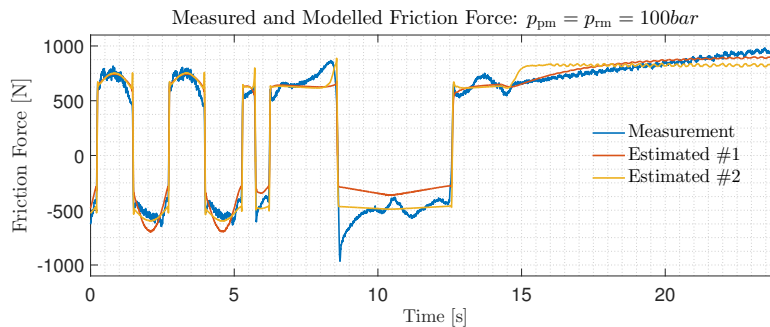


Figure 10.1: Measured and Modelled friction where parameters are estimated with the complete parameter estimation using two different initial guesses.

10.1.3 Proposed Friction Model

The proposed friction model consists of a steady state model which is validated and describes the measured friction well. The remaining model has not been validated due to the position dependency described in Appendix D.4. It is indicated, from the steady state measurements, that v_b is estimated correct with the assumption that v_b should be estimated to the velocity where the friction enters the fluid lubrication regime. The placement of v_b should also be tested in a full model estimation to validate the impact from v_b on the lubricant film dynamics. The other dynamic components of the friction model have not been validated as well, why the proposed model and model simplifications have not been proven to be able to describe the dynamic friction force.

10.2 System Design

10.2.1 Encoder Tolerance

To measure the position and velocity a linear encoder is mounted. This encoder has a vertical tolerance of 0.6 mm. A small misalignment would cause the tolerance to be exceeded. The alignment coupler can cause the vertical distance from the encoder to the magnet band to vary. This might cause the encoder to malfunction. Furthermore the encoder is mounted such a rotation of the piston would cause a malfunction of the encoder. So far no problems with the encoder has been encountered but it might be more robust to measure the position and velocity with another sensor.

10.2.2 Encoder Resolution

In Section 7.2 it is seen that a too low resolution of the encoder results in a lag between the modelled and measured friction during a direction change. This is seen since the encoder can not detect velocity changes in the pre-sliding regime. Since the direction of the modelled

friction is dependent on the direction of the velocity, which can not be measured at displacements lower than $5 \mu\text{m}$, a lag is seen. For accurate modelling it might be necessary to mount an encoder with higher resolution, though the mounted encoder yields the highest resolution of the ones considered. It might be better to mount an analogue sensor to measure the velocity. Yes noise should be considered since this would result in switching of the direction in the modelled friction during a change in velocity direction.

10.2.3 Pre Tensioning of Bolted Friction Joint

The bolted friction joint between the struts and the end plates should be pre tensioned with approximately 250 kN. This is a large pre tensioning which require special tools. It might have been possible to design the struts in another way where more bolts could have been used. This way each bolt should be pre tensioned less than the proposed design. For this design it is though assessed that this was the best solution since more bolts would require a larger strut. A larger strut would result in the center of mass to be moved up, thus increasing the dynamic load on the guidance solution.

10.2.4 Dynamic Load

The test facility is dimensioned to withstand the maximum static load from the load cylinder. Though the dynamic load of the system is only calculated as the resulting force for the acceleration of a sine wave velocity of 1Hz and an amplitude of 0.25 m/s, $\ddot{x}_p = 1.6\text{m/s}^2$. For the purpose of evaluating the friction it is not necessary to obtain larger accelerations, though in reality the dynamic load of the system can be much higher if not controlled correctly. Either the system should have been designed to withstand the maximum dynamic load, or an adequate safety system should be implemented to avoid large dynamic loads. The governing limitation for the dynamic load is the guidance system which can withstand dynamic loads from acceleration up to 6.4 m/s^2 following the supplier.

10.2.5 control

The control of the system is elaborated in Section B.2.3. The pressures are controlled with PID controllers and the velocity is controlled with a PI controller with high pass leakage. Furthermore flow feed forward is added in all control loops. The bandwidth of the different control loops are chosen such large interference between the control loops are avoided while obtaining a bandwidth high enough to meet the requirements stated in Section 3.1.3. The control of the system might yield better response if different control loops were controlled to attain a high bandwidth, e.g. if the two pressure loops were controlled to the highest bandwidth, this might yield a better response since the two valves for the pressures are faster than the load valve. Another way to obtain better control performance might be to design centralised control. Even though it might be possible obtain a better control performance, the designed control meets the requirements that pressures during transient response should be within 10 bar of the reference and 5 bar during steady state. This is seen in Figure 10.2, where it is seen that the controlled pressures are well within the requirements during a transient response.

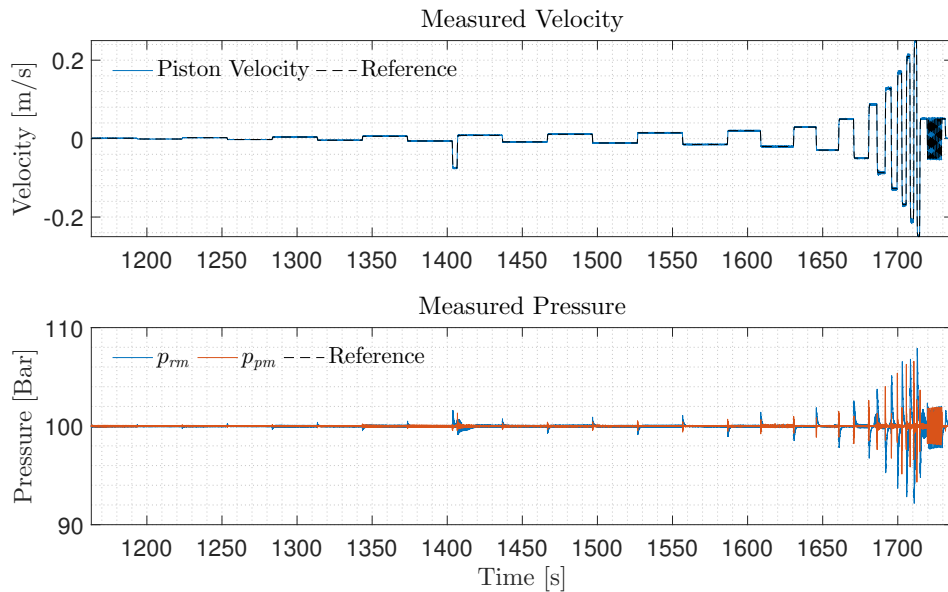


Figure 10.2: Control performance with pressure references of 100 bar during the full trajectory in Figure 7.2.

10.3 Experimental Measurements

10.3.1 Break In

Prior to the final measurements, break in of the cylinder is performed such consistent measurements are made. In Appendix D.1 this process is elaborated. It is seen that the break in period is not over for the cylinder. Measurements have been performed despite this due to time limitations. The lack of break in is the assumed cause of the position dependency seen in Appendix D.4. This position dependent friction force affect all the measurements and since the position dependency is not characterised it is not possible to disregard it in the conclusion since the impact is unknown. It has to some extent been possible to validate the proposed model, but further validation of the model has not been possible. Since the proposed model is not validated it is not possible to evaluate the accuracy of the model.

10.3.2 Consistency of Results

Due to time limitations it has only been possible to conduct measurements once. Since the measurements are only conducted once, consistency can not be ensured. The measurements of the pressure dependency is thus inconclusive and can merely be used as an indication of the tendency in pressure dependency.

10.3.3 Temperature

The temperature of the oil affects the friction since the viscosity changes with temperature as shown in Section 2.1.3. The oil temperature affecting the friction is the temperature of the oil between the sealing and the cylinder since these are the sliding surfaces. The oil

temperature of the supply line is monitored, but this oil temperature is not necessarily the same as the oil temperature between the sealing and the cylinder. If this oil temperature is not constant this will affect the measured friction characteristics. As seen in Figure 10.3 the oil temperature in the supply line is almost constant and is only varying 0.5 degrees. In Section 2.1.3 it is shown how the friction force changes with temperature, though it is indicated that a change of 0.5 degrees is negligible.

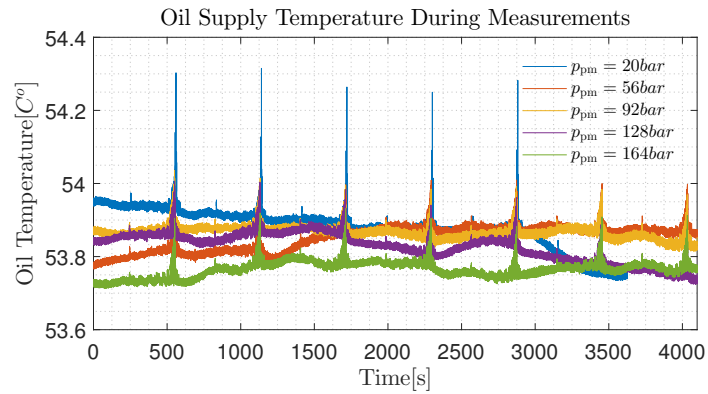


Figure 10.3: Oil temperature at supply line during measurements.

11 | Conclusion

This thesis has concerned an investigation of the pressure dependency in the friction force in an asymmetric hydraulic cylinder. For this purpose a test facility is designed in which the friction can be measured. To obtain the desired operating range it has been assessed the best solution is to load the cylinder with another cylinder. This topology has shown to meet the desired requirements to operating range and performance. Accurate sensors yield an accuracy of the friction force of 50N. The position and velocity measurement are obtained from a linear encoder with a resolution of $5\mu\text{m}$. This resolution has shown to be inadequate since the velocity in the pre-sliding domain is undetectable.

It is chosen to investigate the pressure dependency in each parameter of a velocity dependent friction model. This is done by estimating the parameters at various pressure combinations. For this purpose a velocity dependent model is proposed. Different steady state models are investigated and compared on accuracy and robustness. From this analysis it is seen that the most accurate model, when comparing the models to previous found friction characteristics, is the Modified Gaussian model. Furthermore no model is superior to the other when considering robustness why the Modified Gaussian is chosen. With basis in the state of the art in dynamic friction modelling, a model which reduces the number of variables by three is proposed. The modifications to the state of the art models concern: Reformulation of the lubricant film thickness saturation velocity, neglect of bristle dynamics and reformulation of the dynamics of the lubricant film thickness. From measurements it is validated that the steady state model can describe the measured steady state friction. Though due to a lack of break in of the cylinder, resulting in a large position dependency, it has not been possible to validate the complete proposed friction model.

To estimate the parameters for the proposed model, different estimation methods are investigated. To test the different methods an error is simulated and the most accurate method, despite the simulated error, was seen to be a full optimisation of all the parameters from a 13s measurement series. Further investigation of this method shows that the algorithm does not converge to the correct parameters. Since the full optimisation method is not consistent it is chosen to estimate the parameters with the second most accurate method. This method estimates the steady state parameters from steady state conditions. Subsequent the dynamic parameters are estimated using a Non-linear Least Squares Method. The two different methods are tested with practical measurements. This indicates the same as the theoretical analysis, that the full optimisation method does not converge to the correct parameters.

The proposed model and parameter estimation are used to investigate the pressure dependency in each parameter by estimating the parameters at different pressure combinations. Due to time limitations a complete break in is not seen. This is assessed to be the cause of a measured position dependency. Furthermore the measurements are only performed once why consistency can not be shown. These reasons cause the results to be inconclusive.

Tendencies are showing that F_s and F_c increases with pressure and n for positive velocities decreases with pressure. Furthermore it is indicated that p_{rm} has the greatest impact on the friction force of the two pressures. Though no tendency is clear enough to be modelled.

It is tested if the friction force is dynamically dependent on the pressures. It is shown in one case that the friction force lags a variation in the pressure, though due to the position dependency further evaluation has not been possible. Due to a lack of break in and non-repeated measurements no conclusions regarding the pressure dependency in the friction force can be drawn. Therefore a pressure dependent friction model has not been proposed.

Bibliography

- B. Armstrong-Helouvry, *Control of Machines With Friction*. Kluwer Academic Publishers, 1991.
- J. S. Courtney-Pratt and E. Eisner, *The Effect of a Tangential Force on the Contact of Metallic Bodies*. The Royal Society, 1957.
- P. Dahl, *A Solid Friction Model*. The Aerospace Corporation, 1969.
- C. de Wit, H. Olsson, K. J. Åström, and P. Lischinsky, *A New Model for Control of Systems with Friction*. IEEE Transactions on Automatic Control, Vol. 40, No. 3, 1995.
- J. Swevers, F. Al-Bender, C. G. Ganseman, and T. Prajogo, *An Integrated Friction Model Structure with Improved Pre-sliding Behaviour for Accurate Friction Compensation*. IEEE Transactions on Automatic Control, 2000.
- V. Lampaert, F. Al-Bender, and J. Swevers, *Experimental characterization of dry friction at low velocities on a developed tribometer setup for macroscopic measurements*. Katholieke University Leuven, 2003.
- F. Al-Bender, V. Lampaert, and J. Swevers, *The Generalized Maxwell-Slip Model: A Novel Model for Friction Simulation and Compensation*. IEEE Transactions on Automatic Control, 2005.
- V. Lampaert, J. Swevers, and F. Al-Bender, *Modification of the Leuven Integrated Friction Model Structure*. IEEE Transactions on Automatic Control, 2002.
- P. Dupont, V. Hayward, and F. A. Brian Armstrong, *Single State Elastoplastic Friction Models*. IEEE Transactions on Automatic Control, 2014.
- A. Merola, C. C. Domenico Colacino, and F. Amato, *A parsimonious friction model for efficient identification and compensation of hysteresis with non-local memory*. Int. J. Modelling, Identification and Control, 2015.
- H. Yanada and Y. Sekikawa, *Modeling of dynamic behaviors of friction*. Elsevier, 2008.
- D. P. Hess and A. Soom, *Friction at a Lubricated Line Contact Operating at Oscillating Sliding Velocities*. Journal of Tribology, 1990.
- Z. J. Jianyong Yao, Wenxiang Deng, *Adaptive Control of Hydraulic Actuators With LuGre Model-Based Friction Compensation*. IEEE transactions on industrial electronics, 2015.
- X. B. Tran, N. Hafizah, and H. Yanada, *Modeling of dynamic friction behaviors of hydraulic cylinders*. Elsevier, 2011.
- J. Sugimura and H. Spikes, *Technique for measuring EHD film thickness in non-steady state contact conditions*. Elsevier Science, 1997.
- N. Pedersen and S. M. Jørgensen, *Friction Modelling and Parameter Estimation for Hydraulic Cylinders*. AAU, 2016.
- Parker, *HL Rod Seals*. Parker, 2010.
- S. H. Cho, O. Niemi-Pynttari, and M. Linjama, *Friction characteristics of a multi-chamber cylinder for digital hydraulics*. Journal of mechanical engineering and science, 2015.
- A. Bullock, *Fundamental Concepts Associated with Hydraulic Seals for High Bandwidth Actuation*. University of Bath, 2010.
- H. Yanada, K. Takahashi, and A. Matsui, *Identification of dynamic parameters of modified LuGre model and application to hydraulic actuator*. Transactions of the Japan Fluid Power system society, 2010.
- Y. S. Hideki Yanada, *Effects of viscosity and type of oil on dynamic behaviour of friction of hydraulic cylinders*. Hideki Yanada and Yuta Sekikawa, 2010.

- P. Dahl, *Solid Friction damping of spacecraft oscillations*. AIAA guidance and control conference, 1975.
- V. Lampaert, J. Swevers, and F. Al-Bender, *A Smoothed GMS Friction Model Suited for Gradient-Based Friction State and Parameter Estimation*. IEEE Transactions on Mechatronics, 2014.
- Mathworks, *Optimization decision table*. Mathworks.
- , *Choosing the algorithm*. Mathworks, -.
- DNV-GL-AS, *CLASS GUIDELINE -Hydraulic cylinders*. DNV-GL-AS, 2015.
- P. W. Rasmussen, *Hydraulik Ståbi*. TEKNISK FORLAG, 1996.
- E. C. F. S. CEN, *Eurocode 3: Design of steel structures - Part 1-8: Design of joint*. EUROPEAN COMMITTEE FOR STANDARDIZATION, 1993.
- Fastenal, *Mechanical Properties*. Fastenal, 1993.
- R. L. Norton, *Machine Design*. Prentice Hall, 2000.
- J. M. Gere and B. J. Goodno, *Mechanics of material*. Cengage Learning, 2009.
- Moog, *Direct Drive Servovalves, D633/D634*. Moog, 2009.
- T. O. Andersen and M. R. Hansen, *Fluid Power Circuits, System Design and Analysis*, 3rd ed. Aalborg University, 2007.
- T. O. Andersen, *Fluid Power Systems, Modelling and Analysis*, 2nd ed. Aalborg University, 2003.
- I. P. Sigurd Skogestad, *Multivariable Feedback Control*. John Wiley and Sons, 2001.
- C. L. Phillips and J. M. Parr, *Feedback Control Systems*, 5th ed. Pearson Education, 2011.
- A. Zmitrowicz, *WEAR PATTERNS AND LAWS OF WEAR - A REVIEW*. Journal of Theoretical and Applied Mechanics 44, 2, pp.219-253, Warsaw, 2006.
- W. A. Y.M El-Sherbiny, A.T Hasouna, *FRICTION COEFFICIENT OF RUBBER SLIDING AGAINST FLOORING MATERIALS*. ARPN Journal of Engineering and Applied Sciences, 2012.

Part III

Appendix

Appendix A System Design	91
A.1 Mechanical Setup	92
A.1.1 Hydraulic Cylinders	93
A.1.2 Structural Design	95
A.1.3 Strut Dimensioning	95
A.1.4 Slider System	97
A.1.5 Couplings	100
A.1.6 Summary	101
A.2 Hydraulic Setup	101
A.2.1 Valves	102
A.2.2 Accumulator Dimensioning	104
A.2.3 Hoses	105
A.3 Sensor Setup	106
A.3.1 Position/Velocity/Acceleration Measurement	106
A.3.2 Force Measurement	107
A.3.3 Pressure Transducer	107
A.3.4 Temperature Sensor	108
A.3.5 Summary	108
Appendix B System Modelling and Analysis	109
B.1 System Model	109
B.1.1 Mechanical Model	110
B.1.2 Valves	110
B.1.3 Pressure Dynamics	111
B.1.4 Model Validation	111
B.2 Analysis and Control	112
B.2.1 Linear Model	113
B.2.2 Analysis of Linear Model	116
B.2.3 Control Design	118
Appendix C Appendix for Part I	125
C.1 Method to Place Sampling Points	125
Appendix D Experimental Measurements	127
D.1 Break in	127
D.1.1 Trajectory Planning	127
D.1.2 Change in Friction During Break in Period	128
D.2 Evaluation of Velocity Step Duration for Steady State Measurements	128
D.3 Steady State Friction Sampling Instance	129
D.4 Position Dependency	132

A | System Design

This chapter will concern the design and construction of a test facility such the friction force can be measured in the desired range with the highest possible accuracy.

Requirements to the velocity range, pressure range, dynamic performance and accuracy are formulated in Section 3.1.3. To be able to control two pressures and the velocity it is necessary to have three input possibilities. Therefore a topology to load the main cylinder should be chosen.

Load Topology

It is necessary to vary the load force acting on the cylinder to fulfil the requirements. In Supplement E an analysis of different system topologies is made. The considered loading options are:

Mass as load Systems where a mass is used to load the cylinder is investigated. With this load system it is not necessary to measure the load force, thus increasing accuracy. Yet problems emerge with this topology since it is only possible to load the system in one direction, thus limiting the operating area. Furthermore it is not possible to change the load dynamically, thus not being able to maintain constant chamber pressures during transient response.

Dynamic Load It is investigated how the system can be loaded with both an electric machine and a hydraulic cylinder. In both cases the whole required operating range can be reached. The electrical machine is an expensive solution compared to the hydraulic cylinder, though the electrical machine presumably yields a better system response.

A further investigation of the dynamic performance of the system with a load cylinder is made in Supplement E.3. This investigation indicates that a hydraulic cylinder load can fulfil the requirements formulated in Section 3.1.3. Since the load cylinder is the cheapest solution which can fulfil the requirements, this solution is chosen. The chosen topology is seen in Figure A.1 and consist of the main cylinder and the load cylinder mounted rod to rod. Between the cylinders a mass, m , is placed to influence the natural frequency and a load cell is mounted to measure the load force acting on the main cylinder.

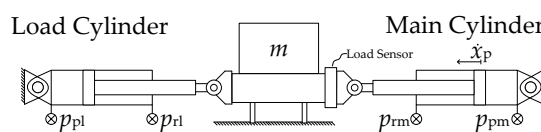


Figure A.1: The chosen topology where a hydraulic cylinder is used as load.

Test object

It is desired to construct a test facility which can test cylinders up to $\text{Ø}80\text{mm}$. Due to this, a $\text{Ø}80$ cylinder is chosen as the load to be able to fulfil the load requirements up to a $\text{Ø}80$ main cylinder.

The accuracy increases as the cylinder size decreases since the forces acting in the cylinder increases with size. This is seen in Table A.1 where the measurement accuracy for the friction force is seen for different cylinder sizes.

Cyl \varnothing	$p_p A_p$	$p_r A_r$	F_l	Total
40/25	12.57	7.65	20	40.2 N
50/35	19.63	10.01	20	49.6 N
63/40	31.17	18.6	50	99.8 N
80/50	50.26	30.6	50	130.9 N

Table A.1: Measurement accuracy for the friction force for different cylinder sizes with 0.05% Fs. accuracy on the pressure measurements and 0.04% Fs accuracy of load cells for $\varnothing 40$ and $\varnothing 50$ cylinders and 0.05% Fs accuracy for larger cylinders.

A leap is seen from $\varnothing 50$ to $\varnothing 63$. In a $\varnothing 40$ and $\varnothing 50$ a 50 kN load cell with 0.04% Fs. accuracy can be used. When moving up to $\varnothing 63$ it is necessary to use a 100 kN load cell which provides an accuracy of 0.05 % Fs. Due to this leap in accuracy the highest accuracy compared to the cylinder size can be obtained with a $\varnothing 50$ cylinder why this is chosen as the main cylinder in which the friction will be measured.

The following of this chapter will consist of 3 section:

Mechanical Setup	The mechanical setup is designed and dimensioned to meet the requirements with appropriate safety factors.
Hydraulic Setup	The hydraulic setup is described and dimensioned to meet the requirements.
Sensor Setup	Different sensor configurations are discussed, and the most accurate sensor setup is described.

A.1 Mechanical Setup

The main mechanical parts are:

- Main cylinder
- Load cylinder
- The structural design of the test bench
- The sliding system

The mechanical construction is mounted on a precision bench available at the institute. The mounting on the precision bench is chosen, since this bench support easy mounting and aligning. Different topologies will be discussed and the chosen topologies will be designed and dimensioned.

The mechanical system is seen in Figure A.2. The system consists from right to left of: A load cylinder ($\varnothing 80 \times 40 \text{mm}$ - stroke: 680mm) with front flange mount connected to the slider through an alignment coupler. On the other side of the slider is an additional alignment coupler connected through a reduction coupling to a load cell, which through another coupling is connected to the main cylinder ($\varnothing 50 \times 35 \text{mm}$ - stroke: 700mm). On the coupling between the load cell and the main cylinder a linear encoder is mounted to measure position and velocity.

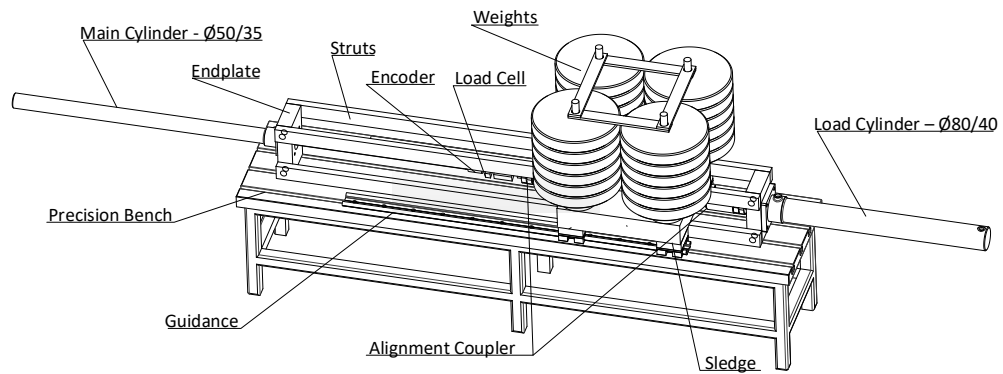


Figure A.2: Complete mechanical system.

The main cylinder is designed to have a stroke 2 cm shorter than the load cylinder. This way the cylinders can be aligned such the load cylinder goes to end stop before the main cylinder to ensure that the load on the main cylinder does not exceed the limitations during steady state.

A.1.1 Hydraulic Cylinders

In this section different cylinder mounting topologies will be discussed. When considering the mounting of the cylinder and piston rod, different aspects should be considered, such as: axial play, alignment, buckling of the cylinder etc. A choice of mounting method for both the main and the load cylinder will be elaborated. Afterwards a buckling analysis is made for the cylinders.

Hydraulic Cylinder Mount

In Figure A.3 the cylinder mounting methods considered are seen. When considering the cylinder mount, the most important factor is the ability to measure the load force and the velocity precisely without undesired characteristics such as axial play. The front flange mount is chosen for the cylinders since this will not result in axial play as the bearing solutions in a,b and c will. Furthermore this solution results in a symmetrical distribution of the cylinder reaction force around the centre of the piston rod which method f does not. This is preferred since a symmetric reaction force will simplify the structural design. Method e with a rear flange is disregarded since this results in a longer buckling length.

When a flange mount is utilised for the cylinders, aligning problems in the construction phase should be absorbed in a coupling mounted on the piston rod end. The considered rod coupling methods are illustrated in Figure A.4. For this purpose the self aligning rod coupler, method a, will be utilised since this is the only method which allows radial misalignments. Using these mounting methods the velocity and load force can be measured directly between the cylinder rod end and the alignment coupler. Since the alignment coupler allows some radial and angular misalignments, axial play in the range 0.05-0.25mm may influence the control performance. This is investigated in Supplement E.3 where it is seen that the impact is negligible. The same mounting method will be utilised for the main and load cylinder.

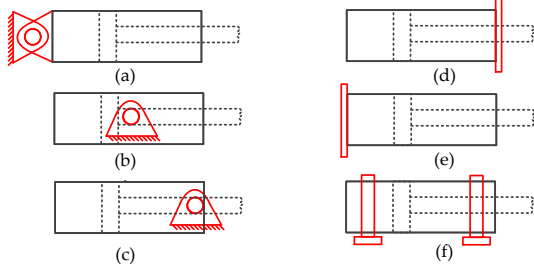


Figure A.3: Cylinder mounting methods considered. a) Rear pivot mount b) Center trunion mount c) Front Trunion mount d) Front flange mount e) Rear flange mount f) Foot bracket mount.

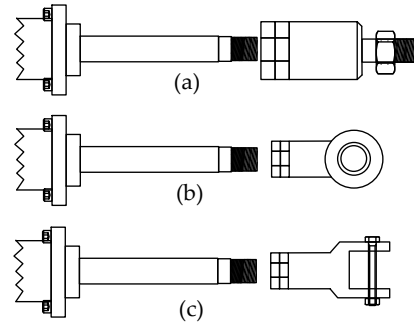


Figure A.4: Rod Mounting Topologies: a) Self-aligning rod coupler b) Rod eye c) Rod clevis.

Cylinder Buckling

Buckling calculations are done in order to ensure no buckling of the main cylinder. Buckling calculations is provided from the supplier, though the buckling length of the cylinder column is extended due to the mount of sensors and alignment coupler, why further buckling analysis is required. Buckling is calculated according to (DNV-GL-AS, 2015)(Rasmussen, 1996). The cylinder column is seen in Figure A.5.

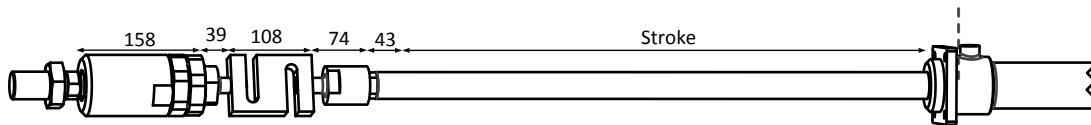


Figure A.5: Column for calculating the buckling.

The length L is calculated without the threads, since these are screwed inside the other parts, and the diameter used for calculating buckling in the column is the diameter of the piston rod. This is justified since the area moment of inertia for all the parts are assumed to be greater than the piston rod, thus using the following dimensions: $d = 35\text{mm}$, $L = 1122\text{mm}$ and $\text{Stroke} = 700\text{mm}$. This is calculated with Young's modulus for steel of $E = 210 \cdot 10^9\text{N/m}^2$. The area moment of inertia for the rod column is calculated as:

$$I = \frac{\pi d^4}{64} \quad (\text{A.1})$$

The buckling resistance, F_E , is calculated according to (DNV-GL-AS, 2015) and (Rasmussen, 1996) for a fixed / pinned column as:

$$F_E = \frac{2E\pi^2 I}{L^2} = 242\text{kN} \quad (\text{A.2})$$

The maximum reaction force from the main cylinder, F_r , is 40kN, at a load pressure of 200 bar assuming that the dynamic load on the column is negligible due to a low mass of the column and piston. This results in the following safety factor, SF_b :

$$SF_b = \frac{F_E}{F_r} = 6 \quad (\text{A.3})$$

According to (DNV-GL-AS, 2015) and (Rasmussen, 1996) the safety factor should be above 4 and 3.5 respectively, why the calculated safety factor is adequate even though some assumptions regarding the column thickness is made.

A.1.2 Structural Design

In this section different structural designs will be discussed. When designing the structure, different limitations have to be met:

- The alignment rod coupler have a maximum radial displacement of 1mm
- The linear encoder chosen to measure the velocity has a vertical tolerance of 0.6mm

For the purpose of easing the alignment process a precision work bench is available. The bench is seen in Figure A.2 and is 500x2250 mm with 4 grooves for mounting.

Four structural topologies have been considered in the design process. These are shown in Figure A.6, A.7, A.8 and A.9. The topology with four struts, Figure A.9, is chosen for the purpose of this thesis. Utilising this structural topology a symmetrical reaction force distribution is realised due to the four struts being distributed in each corner of the end plates. This results in equal displacements in the four struts i.e. an equal distribution of the reaction force. By this the vertical tolerance for the linear encoder of 0.6 mm can be met. Utilising four struts instead of two struts, as in A.7 and A.8, secures a symmetric load distribution but it also makes the requirements to the strut dimension lower.

Contrary to the three topologies with angle brackets, the chosen topology should be mounted to the precision bench through the mid point of the lower struts. The bolts should be pre tensioned such the construction does not move during dynamic response. This is elaborated in Supplement F.1.3.

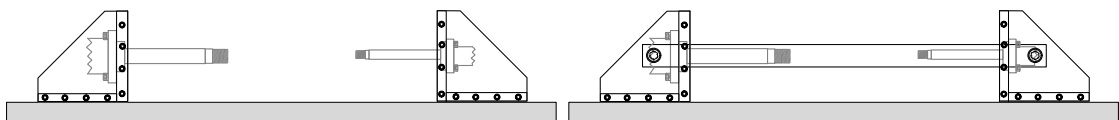


Figure A.6: Angle Bracket topology mounted on the precision bench (grey).

Figure A.7: Angle Bracket with center mounted struts mounted on the precision bench (grey).

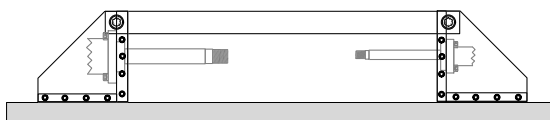


Figure A.8: Angle Bracket with upper mounted struts mounted on the precision bench (grey).

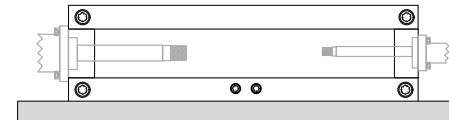


Figure A.9: Symmetrical design with 4 struts mounted on the precision bench (grey).

A.1.3 Strut Dimensioning

The height of the strut is dimensioned to support the mount of the strut, which is a bolted friction joint, while the width of the strut is dimensioned to avoid buckling.

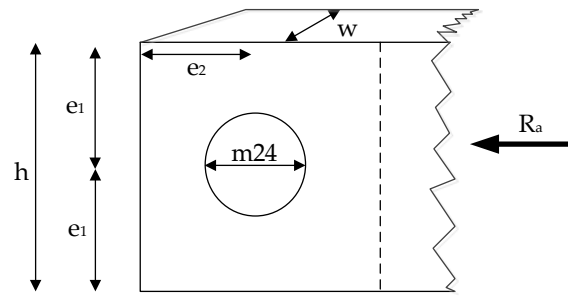


Figure A.10: Strut joint where R_a is the maximum reaction force

Bolted Friction Joint

The joint in each end of the strut is a bolted friction joint which is held together by a single m24 bolt. This minimises the dimensions of the strut, since more bolts would require a larger surface area. In the design presented in A.2, a higher strut will result in a higher centre of mass resulting in an increased dynamic load on the guidance system which is undesired. Each joint is dimensioned with oversized holes for easy alignment. A conservative way of dimensioning the pretension of the bolts, is to design the joint such all tension is transferred to the strut through the friction in the joint such no radial tension is transferred to the bolt (CEN, 1993). The slip resistance, $F_{s,Rd}$, in the joint should be greater than the maximum load force acting on each joint, $F_{R,max}$, with a safety factor of two why the following condition should be fulfilled:

$$F_{s,Rd} \geq 2F_{R,max} \quad (A.4)$$

The maximum reaction force on each joint is calculated as:

$$F_{R,max} = \frac{F_a}{4} = 25\text{kN} \quad (A.5)$$

Where F_a is the maximum reaction force from the load cylinder, and divided by 4 to obtain the maximum reaction force acting on each joint. The friction force, $F_{s,Rd}$ is directly proportional to the pre tension of the bolt, though the bolt should only be pre tensioned up to 70% of the ultimate tensile strength (CEN, 1993). 10.9 class bolts have an ultimate tensile strength of $\sigma_{ub} = 1000\text{N/mm}^2$, thus calculating the maximum pretension allowed, $F_{p,c}$, as:

$$F_{p,c} = 0.7\sigma_{ub}A_b = 247\text{ kN} \quad (A.6)$$

Where A_b is the tensile stress area, 353 mm^2 for m24 (Fastenal, 1993).

The friction acting in the joint is calculated as:

$$F_{s,rd} = \frac{k_s n \mu_s}{\gamma_{m3}} F_{p,c} = 50.41\text{kN} \quad (A.7)$$

With the hole factor, $k_s = 0.85$, for oversized holes, number of surfaces $n=1$, safety factor $\gamma_{m3} = 1.25$ and the friction factor $\mu_s = 0.3$ for steel/steel surfaces.

Thus concluding that a single m24 bolt can be pre tensioned enough to result in a joint friction force greater than the force acting on the joint. In the construction phase it was chosen to fabricate the end plates in aluminium to ease the manufacturing process. The necessary applied torque to obtain the required pretension is elaborated in Supplement F.1. According to (Norton, 2000) the friction coefficient for steel / aluminium surfaces is 0.61 why the pre tensioning is adequate.

Hole Placement

The height of the strut is dimensioned from the bolt dimension, since a certain distance from the bolt center to each boundary of the strut is required (CEN, 1993). e_1 and e_2 seen in Figure A.10, should be within the following range:

$$\begin{aligned} d_0 1.2 &\leq e_1 \leq 40\text{mm} \\ d_0 1.2 &\leq e_2 \leq 40\text{mm} \end{aligned} \tag{A.8}$$

Where d_0 is the hole diameter.

For the strut seen in Figure A.10, e_1 and e_2 should be minimum $25 \cdot 1.2 = 30\text{mm}$, thus choosing the strut to have a height $h=60$ mm.

Buckling

The thickness of the strut is dimensioned to resist buckling with a safety factor of two. Thus calculating the minimum strut thickness from the critical buckling force, F_{cr} , on the struts where the following relationship should hold:

$$F_{cr} > 2F_{R,max} \tag{A.9}$$

The buckling is calculated in the w direction, according to Figure A.10, since this results in the lowest buckling resistance. The area moment of inertia is calculated as (Gere and Goodno, 2009):

$$I_w = \frac{w^3 h}{12} \tag{A.10}$$

The critical buckling force is calculated as a pinned-pinned column according to (Gere and Goodno, 2009):

$$F_{cr} = \frac{\pi^2 E I}{L^2} > 2F_{R,max} \tag{A.11}$$

With $F_{R,max} = 25\text{kN}$, $L = 1965\text{mm}$, $h = 60\text{mm}$ and $E = 210 \cdot 10^9$ results in the following minimum strut width.

$$w > 26.4\text{mm} \tag{A.12}$$

Thus choosing the width, w , to be 30 mm to avoid buckling in all directions.

This dimension with a yield strength of steel of $\sigma = 235\text{N/mm}^2$ and an area of $A = 60\text{mm} \cdot 30\text{mm} = 1800\text{mm}^2$ results in a critical load of 423kN per strut. Since the maximum reaction force in each strut is 25kN this results in a safety factor of 17, thus concluding that the strength of the struts is adequate. The buckling is calculated as a pinned / pinned connection even though the buckling characteristics may be more like a fixed / fixed column to ensure no buckling.

A.1.4 Slider System

In this section the slider system will be elaborated and designed. The slider system, seen in Figure A.11, consists of a linear guidance system consisting of four carriages sliding on two rails. On top of the guidance system, spacers are placed between the carriages and sledge. The sledge is designed with threaded holes in each end for direct mounting of the alignment

couplers. Spacers are placed on top of the sledge before the weights such the two upper struts can go through. The weights are secured on the sledge by a threaded pole through the weights and the top spacers into the sledge.

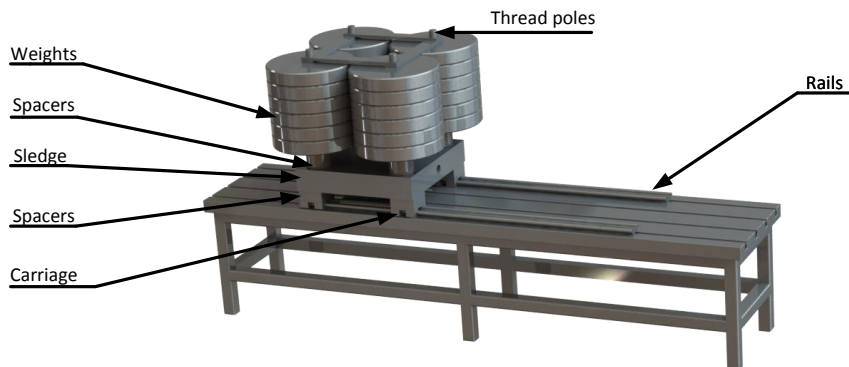


Figure A.11: Sliding system mounted on the bench.

Guidance

The guidance system should be able to guide the mass and cylinders in a desired horizontal direction and fulfil the following requirements:

- The rail carriage system should be flexible such small misalignments in the installation process does not have a great impact on the guidance.
- The total guide system should be able to work with a static vertical load force of 700kg.
- The guidance system should work in the range of dynamic forces equivalent to an acceleration of $1.6 \frac{m}{s^2}$.
- The guide solution should be able to work in an environment with hydraulic oil.

For this purpose a rail and carriage solution is desired. Since the centre of mass will be located at a vertical distance to the carriages, as shown in Figure A.12, the carriages will be subjected to a moment during acceleration. To obtain a minimal moment on each carriage and to distribute the load it is desired to have four carriages, one in each corner of the sledge. This dynamic load force is a result of the acceleration and deceleration of the mass. Since the sledge system is made symmetrical, a torque will act in the middle of the four carriages when the mass accelerates and decelerates. Figure A.12 shows a cross section of the sliding system. The vertical length from the carriages to the centre of mass is $L_{CM} = 351.16mm$. The maximum acceleration required is at a sine trajectory of 1Hz and a velocity amplitude of $0.25 \frac{m}{s}$ which results in an acceleration of $1.6 \frac{m}{s^2}$. This results in a torque in the plane of the carriages top, $\tau_{dynamic}$, which is calculated as:

$$\tau_{dynamic} = L_{CM} \cdot m \cdot \ddot{x} = 404.5Nm \quad (A.13)$$

Where $m = 720kg$ and $\ddot{x} = 1.6 \frac{m}{s^2}$. This torque results in a dynamic load force, $F_{dynamic}$, on each carriage, calculated as the moment divided by the horizontal distance from centre of mass to the carriage. This force is divided by two carriages:

$$F_{dynamic} = \frac{\tau_{dynamic}}{0.2 \cdot 2} = 1011N \quad (A.14)$$

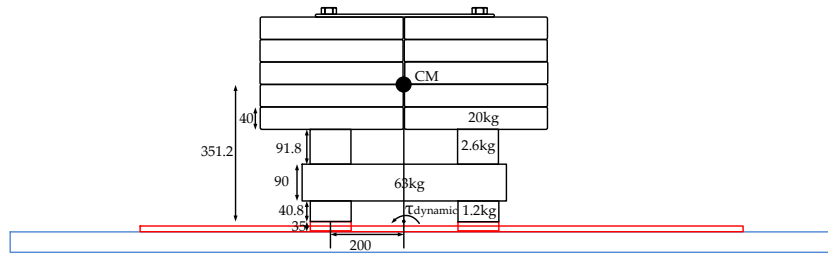


Figure A.12: The centre of mass of the moving mass on the carriages.

A guidance solution able to fulfil all these requirements is a linear sliding guidance system made by IGUS. Figure A.11 shows the guidance system with four carriages. The carriage model chosen, WW-16-60-10, has a static load force limit of 8400N. Since the static load of 700kg is distributed equally on the 4 carriages the total maximum allowable load is 33600N, which is much more than required.

The maximum allowable dynamic vertical load force on each carriage is 4000N.

This rail/carriage system can compensate for small misalignments in the installation process since the carriage and rail have a possibility of mounting loose bearings, WJ200UM-01-16-LL, which results in a clearance of $\pm 0.2\text{mm}$ in the horizontal direction. Furthermore the guidance system is described as a dirt and corrosion resistant system why it will work in an environment with hydraulic oil.

Sledge

The sledge is designed in aluminium, to ease the manufacturing process, and is 500x500mm. The sledge should have a thickness which supports the tapping of a m36 thread in each end. According to (CEN, 1993) this requires a thickness of minimum $2.4 \cdot d_0$, where d_0 is the hole diameter, in this case 36 mm, thus requiring a thickness of minimum 86.4 mm. An aluminium plate can be purchased in 90 mm thickness why this is chosen. The sledge is seen in Figure A.13 where different holes are drilled. The three small holes in each corner are countersunk and are used to mount the sledge to the carriages with m8 bolts. The large hole in each corner is a m30 tapped hole for the thread pole going all the way through the weights into the sledge.

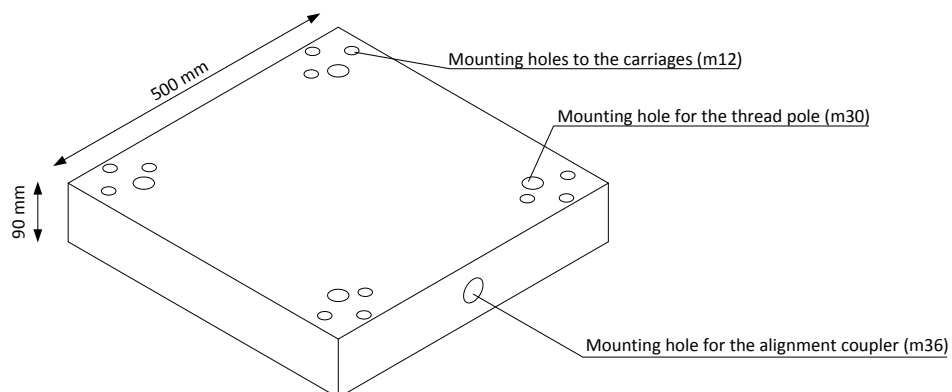


Figure A.13: Sledge.

To verify that the m36 threads can withstand the forces acting on the thread, the pretension is calculated as if the bolt was made of aluminium. Since the maximum tensile load on the bolt is $F_{R,max}=75.4$ kN, the bolt should be pre tensioned with 75.4 kN times a safety factor of 2. The required yield strength of the material is calculated as:

$$\sigma = \frac{2F_{R,max}}{A_b} = 184.6\text{N/mm}^2 \quad (\text{A.15})$$

Where $A_b = 817\text{mm}^2$ is the tensile stress area of a m36 bolt. The yield strength of Hokotol aluminium is $\sigma_{ub} = 550\text{N/mm}^2$ which is adequate.

Weights

The weights used is of 20 kg each with a height of 40mm, a diameter of 340mm and a hole diameter of 31 mm. To support the weights, a m30 thread pole is mounted through the weights into the sledge. 32 weights are distributed on the four thread poles.

To ensure that no bending force, from an acceleration of the weight, is acting on the thread pole and to ensure rigidity of the weights, the pretension of the nut, $F_{p,c}$, is dimensioned as a bolted friction joint. The maximum acceleration of the slider is 1.6 m/s^2 and each pole supports one fourth of the weights, approximately 160 kg assuming that the mass is rigid. This corresponds to a force between the surfaces of $F_r = 1.6\text{m/s}^2 \cdot 160\text{kg} = 256\text{N}$. A safety factor of 3 is introduced thus requiring a friction force of $F_{s,rd} = 768\text{N}$.

The required pretension of the bolts to achieve this friction force, disregarding the normal force from the gravitation, is calculated as (CEN, 1993):

$$F_{p,c} = \frac{F_{s,rd} \gamma_{m3}}{k_s n \mu_s} = 3.8\text{kN} \quad (\text{A.16})$$

With the hole factor, $k_s = 0.85$, for oversized holes, number of surfaces $n=1$, safety factor $\gamma_{m3} = 1.25$ and the friction factor $\mu_s = 0.3$ for steel/steel surfaces.

The required pretension is 3.8 kN, but the bolts will be pre tensioned as much as possible with standard tools.

A.1.5 Couplings

Coupling From Main Cylinder to Load Cell

This coupling reduces from a m22x2 female to a m20x1.5 male and is seen in Figure A.14. The male part is designed with space for a jam nut. The tension calculations is done to ensure that the steel can withstand the tension.

The maximum tensile load from the main cylinder, $F_{R,max}$, is 20 kN. With a safety factor of two, the required yield strength is calculated as:

$$\sigma = \frac{2F_{R,max}}{A_b} = 163\text{N/mm}^2 \quad (\text{A.17})$$

Where $A_b = 245\text{mm}^2$ is the tensile stress area of a m20 bolt. The steel type used is DIN 42CrMo4 steel which has a yield strength of $\sigma = 600\text{N/mm}^2$ which is adequate.



Figure A.14: Coupling between main cylinder and load cell.

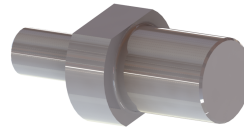


Figure A.15: Coupling between load cell and alignment coupler.

Coupling From Load Cell to Alignment Coupler

The coupling goes from a male m20x1.5 to a male m36x2 and is seen in Figure A.15. On the load cell side space is made for a jam nut. The tensile strength calculations are the same as in the prior section why the same steel, DIN 42CrMo4, is chosen.

A.1.6 Summary

In this section a mechanical structure is designed with two plates for cylinder mounting, supported by a strut in each corner. This is chosen since the deflection is evenly distributed due to symmetry, thus avoiding misalignments. It is concluded, on basis of a bolted friction joint analysis, that the struts should be bolted to the plates with a single m24 bolt with a pretension of 247kN. The m24 bolt requires a height of the strut of 60mm. A buckling analysis with a safety factor of 2, concludes that the width of the strut should be 30mm to avoid buckling.

The slider system was designed. A suitable guidance system from IGUS was chosen which complies with the requirements. It was concluded that a 90mm aluminium plate is adequate to withstand the force acting on the sledge, and the pretension of both the alignment couplers and the nut on top of the weights was calculated.

A.2 Hydraulic Setup

The hydraulic system consist of two hydraulic cylinders, three valves, an accumulator and hoses to connect the parts. The system is seen in Figure A.16.

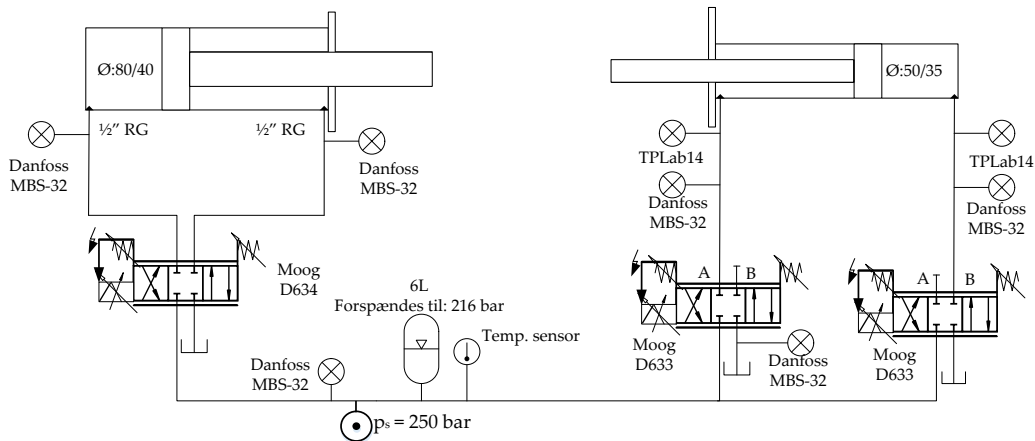


Figure A.16: Diagram showing the components used in the hydraulic setup.

In the following sections the different parts will be discussed. First the choice of valves will be described based on the requirements stated in chapter 3.1. Afterwards an accumulator is dimensioned to the system and at last the hose dimensions is chosen.

A.2.1 Valves

The choice of valves for the two cylinders is based on the requirements in chapter 3.1. The system should be able to reach velocities of 0.25 m/s and each chamber pressure should be individually controlled up to 200 bar. Furthermore it is desired that the bandwidth of the valves is greater than the system natural frequency to be able to obtain fast control of the system. As seen in Figure A.16 it is chosen to have one valve for the load cylinder and two valves for the main cylinder to be able to control each chamber pressure and the velocity individually. In the next two subsections the load side valve and two main side valves will be chosen.

Load Valve

The load valve should deliver the necessary flow to obtain the maximum velocity of 0.25 $\frac{m}{s}$ for a 80x40 cylinder.

$$Q_{load,max} = A_{pl} \cdot \dot{x}_{p,max} = 75.4 \frac{L}{min} \quad (A.18)$$

A MOOG D634 valve is available. This valve is capable of delivering this flow according to the datasheet (Moog, 2009). As seen in Figure A.20 a flow of 75.4 L/min requires a pressure drop of 40bar. The valve bandwidth at a 10 % step is 30Hz as seen in Figure A.18. During simulation, shown in Section B.2.3, it has been shown that this valve is adequate to fulfil the requirements.

Main Valves

The necessary flow required of the main valves is calculated as the required maximum velocity times the main cylinder piston area.

$$Q_{\text{main,max}} = A_{\text{pm}} \cdot \dot{x}_{\text{p,max}} = 29.5 \frac{\text{L}}{\text{min}} \quad (\text{A.19})$$

A MOOG D633 (Moog, 2009) able to deliver the required flow is available as seen in Figure A.19. At a step of 10 % this valve has a bandwidth of 60Hz , (Moog, 2009), as seen in Figure A.17. During simulation, shown in Section B.2.3, it has been shown that this valve is adequate to fulfil the requirements. It is required that each chamber pressure can be controlled individually up to 200 bar. In the datasheet, the pressure drop across the valve at a flow of $30 \frac{\text{L}}{\text{min}}$ is approximately 40 bar, why the supply pressure should be at least 240 bar to ensure the ability to obtain a chamber pressure of 200 bar during 0.25 m/s.

Furthermore it is desired that the hydraulic system should be connected to a pump able to deliver a flow of more than $91 \frac{\text{L}}{\text{min}}$ and maintain a pressure of at least 240 bar.

Frequency response

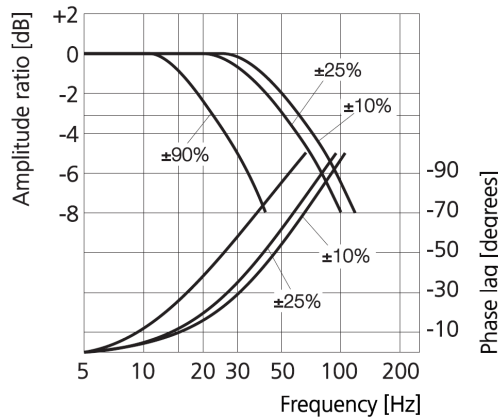


Figure A.17: Frequency response for MOOG D633.

Frequency response

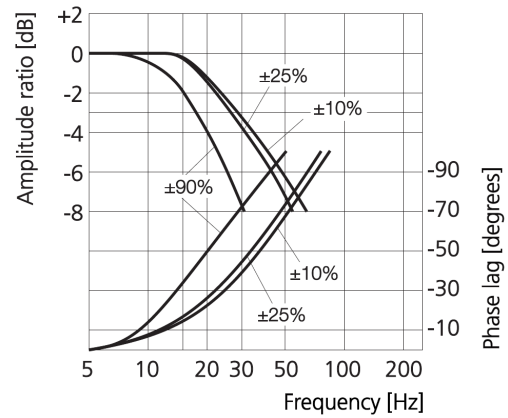


Figure A.18: Frequency response for MOOG D634.

Valve flow diagram

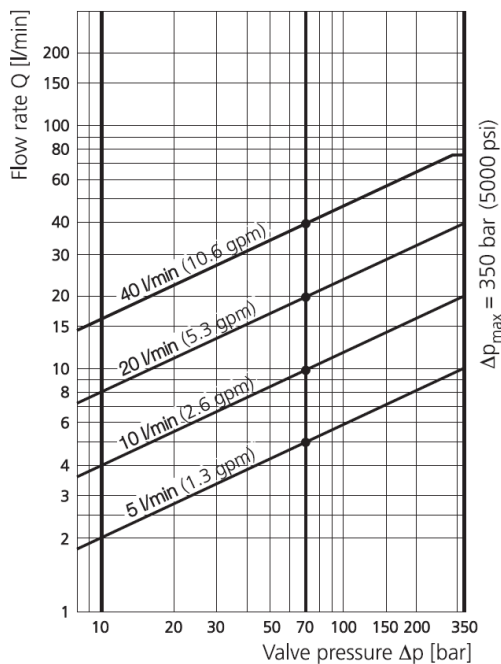


Figure A.19: Flow diagram for MOOG D633.

Valve flow diagram

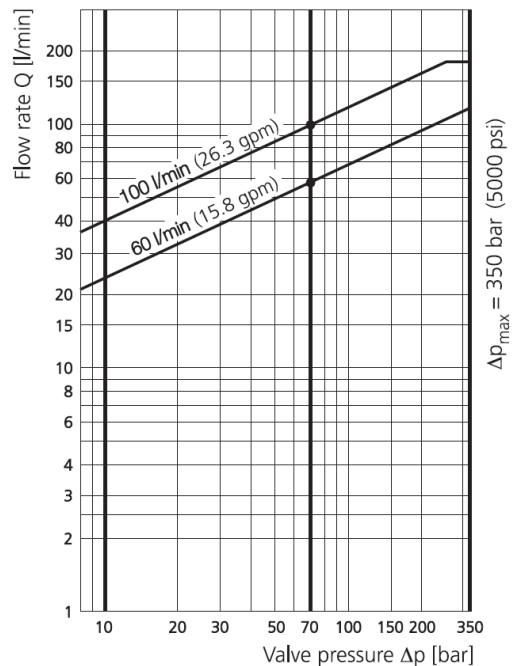


Figure A.20: Flow diagram for MOOG D634.

A.2.2 Accumulator Dimensioning

In previous work by the authors (Pedersen and Jørgensen, 2016) problems in maintaining a constant supply pressure were experienced since the mounted accumulator was not pre-charged to the desired pressure level. For this system the accumulator volume should be large enough with an appropriate pre-charging to assure a steady supply pressure to increase control performance. The accumulator for maintaining a steady supply pressure for the hydraulic system should be designed to fulfil the following requirements.

- Secure a steady supply pressure at a flow of $91 \frac{\text{L}}{\text{min}}$.
- Maintain a supply pressure of 250 ± 10 bar to ensure a reasonable accumulator size.

The pump's ability to supply the system with a constant pressure independently of the required flow is dependent on the dynamics of the pump control loop. It is assumed that the pump can maintain a constant pressure when the flow requirement is steady state. A problem may occur when it is desired to control the piston position as a sine wave. For low frequencies, below the pump's closed loop bandwidth, it should be possible to maintain a constant supply pressure, yet for trajectory frequencies higher than this bandwidth the supply pressure may start to fluctuate. The maximum flow required for a sine velocity trajectory is approximately $91 \frac{\text{L}}{\text{min}}$ in one direction and $86 \frac{\text{L}}{\text{min}}$ in the other direction which occurs at a sine velocity trajectory $\dot{x}_p = 0.25 \cdot \sin(2\pi t)$. As seen in Figure A.22 the accumulator should have a working volume of approximately $\Delta V_{\text{Akku}} = 0.2 \text{ L}$ using a safety factor of 2. The data in the plots is based on that the pump should deliver a constant flow during the sine trajectory and that the accumulator should account for the changes in the flow.

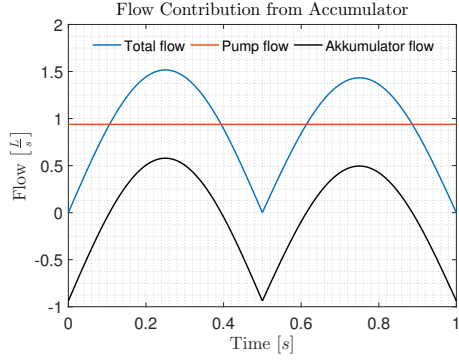


Figure A.21: The necessary accumulator flow contribution during one cycle of a velocity trajectory of $\dot{x}_p = 0.25 \cdot \sin(2\pi t)$ when it is assumed that the pump supplies a constant flow.

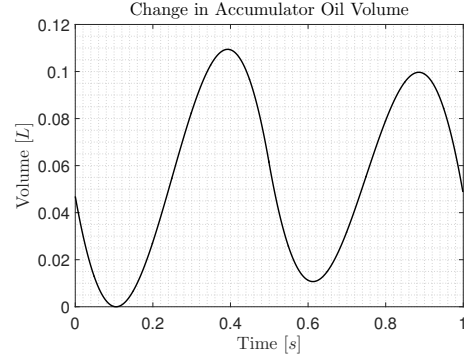


Figure A.22: Change in accumulator oil volume during one cycle of a velocity trajectory of $\dot{x}_p = 0.25 \cdot \sin(2\pi t)$.

In the case of this system the trajectories will be run such the accumulator will be loaded and unloaded within few seconds why an adiabatic process can be assumed. Furthermore it is preferred that the supply pressure stay within the desired region with a tolerance of ± 10 bar. The desired supply pressure should always be above 240 bar such the mean desired supply pressure is 250 bar. Following (Rasmussen, 1996) the precharge pressure of the accumulator should be 90 % of the minimum pressure, $p_{\text{precharge}} = 0.9p_{\text{min}} = 216\text{bar}$. The necessary accumulator volume, V_{Accu} , is calculated as (Rasmussen, 1996):

$$V_{\text{Accu}} = \frac{\Delta V_{\text{Akku}}}{\left(\frac{p_{\text{precharge}}}{p_{\text{min}}}\right)^{\frac{1}{\kappa}} - \left(\frac{p_{\text{precharge}}}{p_{\text{max}}}\right)^{\frac{1}{\kappa}}} C_a \approx 3.9\text{L} \quad (\text{A.20})$$

Where $C_a = 1.43$ is a correction factor for ideal gasses at adiabatic conditions to compensate for the different properties of nitrogen at high pressures compared to an ideal gas and $\kappa = 1.4$ is the adiabatic exponent (Rasmussen, 1996). p_{min} is the minimum pressure of 240 bar and p_{max} is the maximum pressure of 260 bar.

An accumulator of at least 4L is desired to assure a steady supply pressure. Yet a larger accumulator of 6L will be implemented since this is available at the institute.

A.2.3 Hoses

In this section requirements for the dimensions of the hoses are made. These requirements are based on the pressure loss between the accumulator and the manifold. Hoses with an internal diameter of $1/2''$ is available, why the pressure loss using this hose is investigated. The maximum flow in the hose from the accumulator to the manifold is at a piston velocity of -0.25 m/s where the flow is 91 L/min. For a hose with a diameter of $D = 1/2''$ the velocity in the hose is:

$$\dot{x}_{\text{flow,max}} = \frac{91}{\frac{60 \cdot 1000}{\left(\frac{0.5 \cdot 0.0254}{2}\right)^2 \pi}} = 2.99 \frac{\text{m}}{\text{s}} \quad (\text{A.21})$$

Reynolds number for this flow is:

$$\text{Re} = \frac{\rho \cdot \dot{x}_{\text{flow,max}} \cdot D}{\mu} = 1628 \quad (\text{A.22})$$

The density of the fluid is $\rho = 910 \frac{\text{kg}}{\text{m}^3}$ and the absolute viscosity is $0.0425 \frac{\text{kg}}{\text{s} \cdot \text{m}}$. The Reynolds number is used to determine if the flow is laminar or turbulent. From (Andersen and Hansen, 2007) the transition between laminar and turbulent flow is approximately at a Reynolds number of 2300, why the flow is laminar.

The pressure loss in this hose is calculated as:

$$\Delta P_{\text{hose}} = \lambda \cdot \frac{L}{D} \cdot \rho \cdot \frac{\dot{x}_{\text{flow,max}}^2}{2} = 0.13 \text{bar} \quad (\text{A.23})$$

Where $\lambda = \frac{64}{\text{Re}} = 0.028$ and the hose is assumed to be $L = 2\text{m}$ long. Since the pressure drop only is 0.13 bar, hoses with a diameter of 1/2" is utilised.

A.3 Sensor Setup

In this section the sensor system will be elaborated. The system consists of the following sensors for friction measurement, control and monitoring.

- Pressure transducers on the main cylinder for high accuracy pressure measurements and control feedback.
- Position/Velocity/Acceleration sensor for high accuracy measurements and control feedback.
- Load cell for high accuracy force measurement on the main cylinder.
- Pressure transducers on load cylinder for control feedback.
- Pressure transducers on supply and tank pressure line for control feedback and monitoring.
- Temperature sensor on supply pressure line for monitoring of temperature.

Measurements of the velocity and load force are made directly on the rod end of the main cylinder, to be able to measure the friction force accurately without undesired disturbances. Data acquisition is made through a NI Compact Rio and the wiring of this is described in Supplement F.2.

A.3.1 Position/Velocity/Acceleration Measurement

The position, velocity and acceleration is to be measured. The position is only for feedback control why high resolution is not a necessity. High accuracy in the velocity and acceleration measurement are desired since these are used for friction force measurements.

The position is measured in a range of 0.7m and digital measurements are desired to avoid noise. It is desired to have a resolution as high as possible. This is convenient in the pre-sliding domain during a direction change where a high resolution is necessary to detect the direction change in the velocity. If the velocity measurement are too inaccurate for acceleration estimates, an additional accelerometer can be mounted. For this purpose different sensors are considered. A cable pull encoder, a laser, an inductive position transducer and a linear encoder.

The most accurate of the considered sensors are the linear encoder why this is chosen. A

linear encoder reads the magnetic pulses on a magnetic band placed under the encoder. The linear encoder has, as a cable pull encoder, the advantage of being digital, thus avoiding noise. The linear encoder has, as the laser sensor, the advantage of being a non contact sensor, why it does not interfere with the system.

The most accurate found is the Baumer MIL10 which have an accuracy of $60\mu\text{m}$ per meter and $\epsilon_{\text{pulse}} = \pm 0.15$ nm accuracy between the pulses, which is placed with a distance of $\Delta x_{\text{pulse}} = 5\mu\text{m}$ between every edge, this is assumed to be a sufficient resolution to detect pre-sliding behavior.

With an accuracy of $\epsilon_{\text{pulse}} = \pm 0.15$ nm between the pulses, the fastest velocity desired, $\dot{x}_{p,\text{max}} = 0.25$ m/s, results in a velocity accuracy of $\epsilon_{\text{vel}} = 15\mu\text{m/s}$ as:

$$\epsilon_{\text{vel}} = \frac{2 \cdot \epsilon_{\text{pulse}}}{\frac{\Delta x_{\text{pulse}}}{\dot{x}_{p,\text{max}}}} = 15 \frac{\mu\text{m}}{\text{s}} \quad (\text{A.24})$$

At the lowest desired velocity, of 0.001 m/s, the update rate is 200 Hz which is much higher than the bandwidth of the closed loop control system.

A.3.2 Force Measurement

The force sensor is placed directly on the cylinder rod through a coupling from m22 to m20. This way all disturbance forces to the main cylinder are accounted for by the force sensor. Different types of load cells are used for different applications, though the most accurate load cell is a S beam cell which is seen in Figure A.23. Several dealers have been contacted, but the most accurate load cell is the TCTN-9110 from NTT (-50kN - 50kN), with an accuracy of 0.04% FS.



Figure A.23: TCTN-911 S beam load cell from NTT.

The load cell is directly mounted on the rod of the main cylinder. Couplings with a jam nut are used on both sides of the load cell.

A.3.3 Pressure Transducer

Two high precision transducers are desired for the main cylinder. Four transducers are required for control and monitoring, two on the load cylinder and one on the supply and tank pressure line. These four transducers should not meet specific requirements why Danfoss

MBS32 is chosen since these are available at the institute.

For the case of high accuracy measurements of the main cylinder pressures, two TPlab14 (0-250bar) transducers are implemented with an accuracy of 0.05 %Fs.

During practical measurements it is seen that the TPlab14 is very sensitive to noise why two Danfoss MBS32 also will be connected to the main cylinder for control purposes.

A.3.4 Temperature Sensor

It is desired to monitor the fluid temperature since the viscosity dependency in the friction force is neglected, thus assuming a constant temperature. The temperature measurement is made at the supply line with a Parker SCT-150-14-07.

A.3.5 Summary

A Baumer MIL10 linear encoder is chosen since this provides a high accuracy and a digital signal. From this solution it is possible to obtain position, velocity and acceleration with high accuracy from the same sensor. The MIL10 is an incremental encoder, why a reference point is necessary to locate its position.

A TCTN-9110 s-beam load cell is chosen as the most accurate load cell to measure the load force acting on the main cylinder.

Two TPlab14 pressure transducers are mounted to measure accurate pressures in the main cylinder, and Danfoss MBS32 transducers are mounted to measure the pressures in the load cylinder and the supply and tank pressure. Furthermore a temperature sensor is mounted in the supply line to monitor the oil temperature.

B | System Modelling and Analysis

B.1 System Model

In this section the system will be modelled. The inputs to the model is the three valve references and the outputs are the chamber pressures in the main cylinder and the velocity of the system. The following assumptions is made in the modelling:

- **Pressure Loss:** The pressure loss in the hoses are neglected since these are very low and will only affect the control performance very little.
- **Pressure Wave Dynamics:** The pressure wave dynamics in the hoses and the cylinders are neglected and the hydraulic system is regarded as a lumped system with four control volumes.
- **Temperature Dependency:** The temperature are assumed constant why it is omitted in the fluid model. This is reasonable since a temperature controller is implemented in the tank of the pump.

The system is seen in Figure B.1.

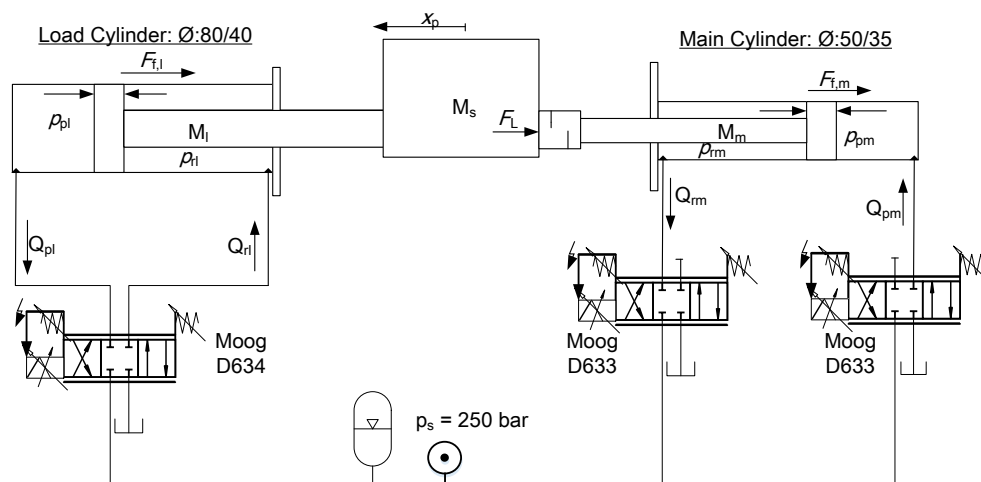


Figure B.1: Mechanical and hydraulic system.

The model consists of the following parts:

- Mechanical Model
- Valve Model
- Pressure Dynamics
- Bulk Modulus Model

A table containing model parameters are found in F.3

B.1.1 Mechanical Model

The mechanical motion is modelled with Newtons 2. law for the load side and the main side as:

$$\ddot{x}_p = \underbrace{\frac{p_{pm}A_{pm} - p_{rm}A_{rm} - F_{f,m} - F_L}{M_m}}_{\text{Main Side}} = \underbrace{\frac{p_{rl}A_{rl} - p_{pl}A_{pl} - F_{f,l} + F_L}{M_l + M_s}}_{\text{Load Side}} \quad (\text{B.1})$$

Where M_m , M_l and M_s is the mass of the main piston and rod, the load piston and rod and the slider system respectively. $F_{f,m}$ and $F_{f,l}$ is the friction force for the main cylinder and the combined friction force of the load cylinder and slider system respectively. This can be rewritten as:

$$\ddot{x}_p(M_m + M_l + M_s) = p_{pm}A_{pm} - p_{rm}A_{rm} - F_{f,m} + p_{rl}A_{rl} - p_{pl}A_{pl} - F_{f,l} \quad (\text{B.2})$$

B.1.2 Valves

In this section the valves will be modelled, the flow through the valves is dependent on the valve spool position and the pressures which changes dynamically. In Figure B.1 a diagram of the pressures and flows are shown.

Valve Flow

The flow through the valves are described by the following orifice equation as (Moog, 2009):

$$Q_i = x_j Q_{N,j} \sqrt{\frac{|\Delta p_i|}{\Delta p_N}} \text{sgn}(\Delta p_i) \quad \text{for } \begin{array}{l} i = [pm, rm, rl, pl] \\ j = [vp, vr, vl, vl] \end{array} \quad (\text{B.3})$$

Where Q_N is the nominal valve flow and p_N is the nominal pressure drop across the valve. Q_N is different for the Moog-D633 and the Moog-D634 valve.

The following pressure drops are used to calculate the flow:

$$\begin{aligned} \Delta p_{pm} &= \begin{cases} PS - p_{pm} & , & x_{vp} \geq 0 \\ PT - p_{pm} & , & x_{vp} < 0 \end{cases} \\ \Delta p_{rm} &= \begin{cases} p_{rm} - PT & , & x_{vr} \geq 0 \\ p_{rm} - PS & , & x_{vr} < 0 \end{cases} \\ \Delta p_{rl} &= \begin{cases} PS - p_{rl} & , & x_{vl} \geq 0 \\ PT - p_{rl} & , & x_{vl} < 0 \end{cases} \\ \Delta p_{pl} &= \begin{cases} p_{pl} - PT & , & x_{vl} \geq 0 \\ p_{pl} - PS & , & x_{vl} < 0 \end{cases} \end{aligned} \quad (\text{B.4})$$

Valve Dynamics

The valve dynamics is seen in Figure A.17 and A.18 for respectively the main side valves and the load side valve. The valve dynamics is described by a second order system as:

$$\frac{X_v}{X_{v,ref}} = \frac{\omega_{n,i}^2}{s^2 + 2\omega_{n,i}\zeta_i s + \omega_{n,i}^2} \quad \text{for } i = [m, l] \quad (\text{B.5})$$

Where $\omega_{n,i}$ is the natural frequency for the valves at a 10 % step and ζ is the damping ratio of the valve, where $i=m$ denotes the main side valve and $i=l$ denotes the load side valve. The valve dynamics are limited by a slew rate of 8500 %/s.

B.1.3 Pressure Dynamics

The pressure dynamics are calculated utilising the continuity equation as:

$$Q_{in} - Q_{out} = \dot{V} + \frac{V}{\beta} \dot{p} \quad (B.6)$$

\dot{V} is the change in the chamber volume caused by the piston movement. It is assumed that potential leakage in the cylinders are negligible, why the only flow in the chambers is the flow through the valves. The volume V is calculated from the piston position and the dead volume in the piston and hoses. The pressure dynamics can thus be described as:

$$\dot{p}_{pm} = \frac{\beta_{pm}}{V_{pm0} + A_{pm}x_p} (Q_{pm} - A_{pm}\dot{x}_p) \quad (B.7)$$

$$\dot{p}_{rm} = \frac{\beta_{rm}}{V_{rm0} - A_{rm}x_p} (-Q_{rm} + A_{rm}\dot{x}_p) \quad (B.8)$$

$$\dot{p}_{pl} = \frac{\beta_{pl}}{V_{pl0} - A_{pl}x_p} (-Q_{pl} + A_{pl}\dot{x}_p) \quad (B.9)$$

$$\dot{p}_{rl} = \frac{\beta_{rl}}{V_{rl0} + A_{rl}x_p} (Q_{rl} - A_{rl}\dot{x}_p) \quad (B.10)$$

Bulk Modulus Model

The Bulk modulus of the oil in the cylinder chambers is modelled to be pressure dependent (Andersen, 2003). The oil contains air which makes the fluid compressible, such the effective Bulk modulus for this fluid/air mixture is calculated as:

$$\beta = \frac{1}{\frac{1}{\beta_F} + \epsilon_A \left(\frac{1}{\beta_A} - \frac{1}{\beta_F} \right)} \quad (B.11)$$

Where β_A and β_f are the bulk modulus for respectively air and fluid, and ϵ_A is the volumetric ratio of air in the fluid, which is calculated as:

$$\epsilon_A = \frac{1}{\frac{1-\epsilon_{A0}}{\epsilon_{A0}} \left(\frac{p_{atm}}{p} \right)^{\frac{-1}{c_{ad}}} + 1} \quad (B.12)$$

Where ϵ_{A0} is the volumetric ratio of air in the fluid under atmospheric pressure, p_{atm} . The bulk modulus of the air is calculated by assuming adiabatic conditions, with the adiabatic constant, c_{ad} , as:

$$\beta_A = c_{ad} p \quad (B.13)$$

B.1.4 Model Validation

In Figure B.2 a comparison of the modelled system and measurements from the test facility is shown. From the figure it is seen that the general dynamics are correct, though the modelled

steady state values does not correspond to the measured in all operating point. This is especially seen in the velocity, from 5s to 9s, where the the residual of the steady state velocity is approximately 0.015 m/s. Furthermore the amplitude of the modelled pressures are wrong in many cases. These steady state errors are probably due to a wrong or too simple valve model. Furthermore an offset in the valves are observed in the physical system. The dynamics of the velocity is seen to be well modelled, though prior to the step from positive to negative velocity at approximately 10 second, the modelled velocity is seen to be less damped than the measured. This might be due to a wrong friction model. The dynamics of the pressures are seen to be modelled correctly in most operating areas, though some error in the dynamical behavior of the pressures are seen. This might be due to a wrong modelled valve, wrong dead volume in the hoses or a wrong model of the bulk modulus.

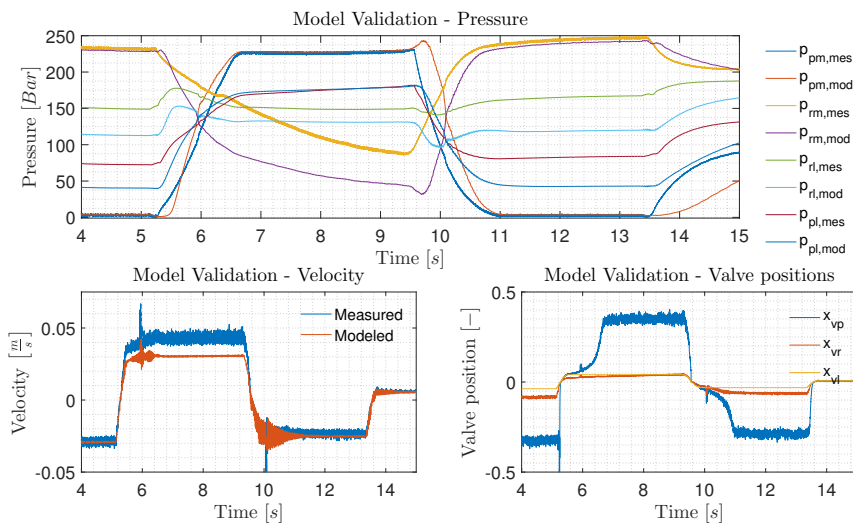


Figure B.2: Comparison of modelled and measured states, modelled with the measured valve input, supply pressure and tank pressure.

This concludes the modelling of the system. In the next section the model will be linearised and analysed before the design of the control scheme will be made.

B.2 Analysis and Control

In this section a control strategy will be made for the hydraulic system such the system is able to fulfil the requirements made in Section 3.1.3. This control strategy is based on an analysis of a linearised representation of the non-linear model and a RGA analysis which reveals couplings in the different input / output combinations.

This chapter contains the following sections:

- Linearisation of complete non-linear model
- Analysis of linear model
- Control design

B.2.1 Linear Model

The plant model with the valve positions as input and the valve model with the valve position reference as input will be modelled separately for simplicity and combined in the end. The linear model is illustrated in the diagram in Figure B.3.

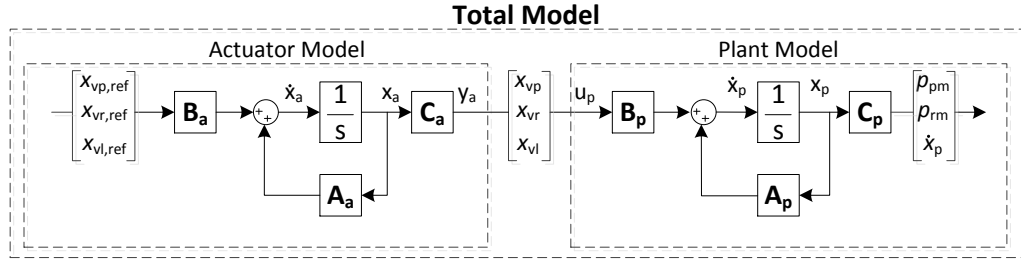


Figure B.3: Complete linear model, consisting of plant model and actuator model.

Linear Representation of the Plant

The motion of the system is described by Newton's 2. law, where the friction force is simplified to the viscous friction such Newton's 2. law simplifies to:

$$m\ddot{x}_p = p_{pm}A_{pm} - p_{rm}A_{rm} + p_{rl}A_{rl} - p_{pl}A_{pl} - \sigma_2\dot{x}_p \quad (B.14)$$

Where m is the total moving mass of the system. The pressure dynamics is represented on linear form by assuming constant control volume, $V|_0$ and constant Bulk modulus, $\beta|_0$ as:

$$\begin{aligned} \dot{p}_{pm} &= \frac{\beta_{pm}|_0}{V_{pm} + A_{pm}x_p|_0} (Q_{pm} - A_{pm}\dot{x}_p) \\ \dot{p}_{rm} &= \frac{\beta_{rm}|_0}{V_{rm} - A_{rm}x_p|_0} (-Q_{rm} + A_{rm}\dot{x}_p) \\ \dot{p}_{rl} &= \frac{\beta_{rl}|_0}{V_{rl} + A_{rl}x_p|_0} (Q_{rl} - A_{rl}\dot{x}_p) \\ \dot{p}_{pl} &= \frac{\beta_{pl}|_0}{V_{pl} - A_{pl}x_p|_0} (-Q_{pl} + A_{pm}\dot{x}_p) \end{aligned} \quad (B.15)$$

The orifice equations describing the flow through the valves is linearised by first order Taylor approximations as:

$$\Delta Q_{pm} = \underbrace{\frac{\partial Q_{pm}}{\partial x_{vp}} \Big|_{x=x_0}}_{k_{q,pm}} \Delta x_{vp} + \underbrace{\frac{\partial Q_{pm}}{\partial p_{pm}} \Big|_{x=x_0}}_{k_{qp,pm}} \Delta p_{pm} \quad (B.16)$$

$$\Delta Q_{rm} = \underbrace{\frac{\partial Q_{rm}}{\partial x_{vr}} \Big|_{x=x_0}}_{k_{q,rm}} \Delta x_{vr} - \underbrace{\frac{\partial Q_{rm}}{\partial p_{rm}} \Big|_{x=x_0}}_{k_{qp,rm}} \Delta p_{rm} \quad (B.17)$$

$$\Delta Q_{rl} = \underbrace{\frac{\partial Q_{rl}}{\partial x_{vl}} \Big|_{x=x_0}}_{k_{q,rl}} \Delta x_{vl} + \underbrace{\frac{\partial Q_{rl}}{\partial p_{rl}} \Big|_{x=x_0}}_{k_{qp,rl}} \Delta p_{rl} \quad (B.18)$$

$$\Delta Q_{pl} = \underbrace{\frac{\partial Q_{pl}}{\partial x_{vl}} \Big|_{x=x_0}}_{k_{q,pl}} \Delta x_{vl} - \underbrace{\frac{\partial Q_{pl}}{\partial p_{pl}} \Big|_{x=x_0}}_{k_{qp,pl}} \Delta p_{pl} \quad (B.19)$$

Where x is the state vector.

State Space Representation

$$\dot{\mathbf{x}}_p = \mathbf{A}_p \mathbf{x}_p + \mathbf{B}_p \mathbf{u}_p, \quad \mathbf{y}_p = \mathbf{x}_p \mathbf{C}_p + \mathbf{D}_p \mathbf{u}_p \quad (B.20)$$

Where the input vector, \mathbf{u}_p , is the valve positions such $\mathbf{u}_p = [x_{vp}, x_{vr}, x_{vl}]^T$ and the state vector, \mathbf{x}_p is the pressures and the velocity such $\mathbf{x}_p = [p_{pm}, p_{rm}, p_{rl}, p_{pl}, \dot{x}_p]^T$. The following system matrices can then describe the plant dynamics with the feedforward matrix $\mathbf{D}_p = 0$:

$$\mathbf{B}_p = \begin{bmatrix} \frac{\beta_{pm}|_0}{V_{pm}|_0} k_{q,pm} & 0 & 0 \\ 0 & -\frac{\beta_{rm}|_0}{V_{rm}|_0} k_{q,rm} & 0 \\ 0 & 0 & \frac{\beta_{rl}|_0}{V_{rl}|_0} k_{q,rl} \\ 0 & 0 & -\frac{\beta_{pl}|_0}{V_{pl}|_0} k_{q,pl} \\ 0 & 0 & 0 \end{bmatrix} \quad \mathbf{C}_p = \begin{bmatrix} 1 & 0 & 0 \\ 0 & 1 & 0 \\ 0 & 0 & 0 \\ 0 & 0 & 0 \\ 0 & 0 & 1 \end{bmatrix}^T \quad (B.21)$$

$$\mathbf{A}_p = \begin{bmatrix} -\frac{\beta_{pm}|_0}{V_{pm}|_0} k_{qp,pm} & 0 & 0 & 0 & -A_{pm} \frac{\beta_{pm}|_0}{V_{pm}|_0} \\ 0 & \frac{\beta_{rm}|_0}{V_{rm}|_0} k_{qp,rm} & 0 & 0 & A_{rm} \frac{\beta_{rm}|_0}{V_{rm}|_0} \\ 0 & 0 & -\frac{\beta_{rl}|_0}{V_{rl}|_0} k_{qp,rl} & 0 & -A_{rl} \frac{\beta_{rl}|_0}{V_{rl}|_0} \\ 0 & 0 & 0 & \frac{\beta_{pl}|_0}{V_{pl}|_0} k_{qp,pl} & A_{pl} \frac{\beta_{pl}|_0}{V_{pl}|_0} \\ \frac{A_{pm}}{m} & -\frac{A_{rm}}{m} & \frac{A_{rl}}{m} & -\frac{A_{pl}}{m} & -\frac{B}{m} \end{bmatrix} \quad (B.22)$$

The input to the plant model is the valve position, though this position changes dynamically. This is described by the valve model in the next subsection.

Valve Dynamics Model

The valve dynamics is described by the following 2. order system:

$$\frac{X_v}{X_{v,ref}} = \frac{\omega_{n,i}^2}{s^2 + 2\omega_{n,i}\zeta_i s + \omega_{n,i}^2} \quad \text{for } i = [m, l] \quad (\text{B.23})$$

Where $i=m$ denotes the main side valves and $i=l$ denotes the load side valve. This can be transformed to the time domain as:

$$\ddot{x}_v = x_{v,ref}\omega_{n,i} - 2\zeta_i\omega_{n,i}\dot{x}_v - x_v\omega_{n,i}^2 \quad (\text{B.24})$$

State Space Representation

$$\dot{\mathbf{x}}_a = \mathbf{A}_a\mathbf{x}_a + \mathbf{B}_a\mathbf{u}_a, \quad \mathbf{y}_a = \mathbf{x}_a\mathbf{C}_a + \mathbf{D}_a\mathbf{u}_a \quad (\text{B.25})$$

Where the following matrices describes the dynamics with the feedforward matrix as $\mathbf{D}_a = 0$:

$$\mathbf{u}_a = \begin{bmatrix} X_{vp,ref} \\ X_{vr,ref} \\ X_{vl,ref} \end{bmatrix}, \quad \mathbf{x}_a = \begin{bmatrix} X_{vp} \\ \dot{X}_{vp} \\ X_{vr} \\ \dot{X}_{vr} \\ X_{vl} \\ \dot{X}_{vl} \end{bmatrix}, \quad \mathbf{B}_a = \begin{bmatrix} 0 & 0 & 0 \\ \omega_{n,m}^2 & 0 & 0 \\ 0 & 0 & 0 \\ 0 & \omega_{n,m}^2 & 0 \\ 0 & 0 & 0 \\ 0 & 0 & \omega_{n,l}^2 \end{bmatrix}, \quad \mathbf{C}_a = \begin{bmatrix} 1 & 0 & 0 \\ 0 & 0 & 0 \\ 0 & 1 & 0 \\ 0 & 0 & 0 \\ 0 & 0 & 1 \\ 0 & 0 & 0 \end{bmatrix}^T \quad (\text{B.26})$$

$$\mathbf{A}_a = \begin{bmatrix} 0 & 1 & 0 & 0 & 0 & 0 \\ -\omega_{n,m}^2 & -2\zeta_m\omega_{n,m} & 0 & 0 & 0 & 0 \\ 0 & 0 & 0 & 1 & 0 & 0 \\ 0 & 0 & -\omega_{n,m}^2 & -2\zeta_m\omega_{n,m} & 0 & 0 \\ 0 & 0 & 0 & 0 & 0 & 1 \\ 0 & 0 & 0 & 0 & -\omega_{n,l}^2 & -2\zeta_l\omega_{n,l} \end{bmatrix} \quad (\text{B.27})$$

Combined Model

The state space model describing the plant and the valve dynamics is combined in a complete model by the following matrices:

$$\mathbf{A}_{tot} = \begin{bmatrix} \mathbf{A}_a & 0 \\ \mathbf{B}_p\mathbf{C}_a & \mathbf{A}_p \end{bmatrix}, \quad \mathbf{B}_{tot} = \begin{bmatrix} \mathbf{B}_a \\ \mathbf{B}_p\mathbf{D}_a \end{bmatrix}, \quad \mathbf{C}_{tot} = [\mathbf{D}_p\mathbf{C}_a, \mathbf{C}_p] \quad (\text{B.28})$$

The output vector, \mathbf{y}_{tot} , is equal to the plant output, \mathbf{y}_p and the input vector, \mathbf{u}_{tot} , is equal to the valve input vector, \mathbf{u}_a . The states are described as $\mathbf{x}_{tot} = [\mathbf{x}_a^T, \mathbf{x}_p^T]^T$.

From the combined state space model the transfer function matrix \mathbf{G}_{tot} is found as:

$$\mathbf{G}_{tot} = \mathbf{C}_{tot}(s\mathbf{I} - \mathbf{A}_{tot})^{-1}\mathbf{B}_{tot} + \mathbf{D}_{tot} \quad (\text{B.29})$$

Such the system can be described in the following form:

$$\begin{bmatrix} p_{pm} \\ p_{rm} \\ \dot{x}_p \end{bmatrix} = \mathbf{G}_{tot} \begin{bmatrix} X_{vp,ref} \\ X_{vr,ref} \\ X_{vl,ref} \end{bmatrix} \quad (\text{B.30})$$

Linear Model Validation

In this subsection a validation is made of the linear model representation made in the previous section. The linearisation point used is:

$$\mathbf{x}_0 = \begin{bmatrix} \dot{x}_p,0 & p_{pm,0} & p_{rm,0} & x_p \\ 0.1 & 100e5 & 100e5 & 0 \end{bmatrix} \quad (\text{B.31})$$

In Figure B.4 a comparison of the non-linear model and linear model representation is shown with a step on the load valve of 0.05 at 0.1s, a step on the rod side main valve of 0.02 at 0.4s and a step on the piston side main valve of 0.02 at 0.8s. From the figure a good compliance is seen between the non-linear model and the linear model representation which indicates that the linear model is representative in a large range away from the linearisation point.

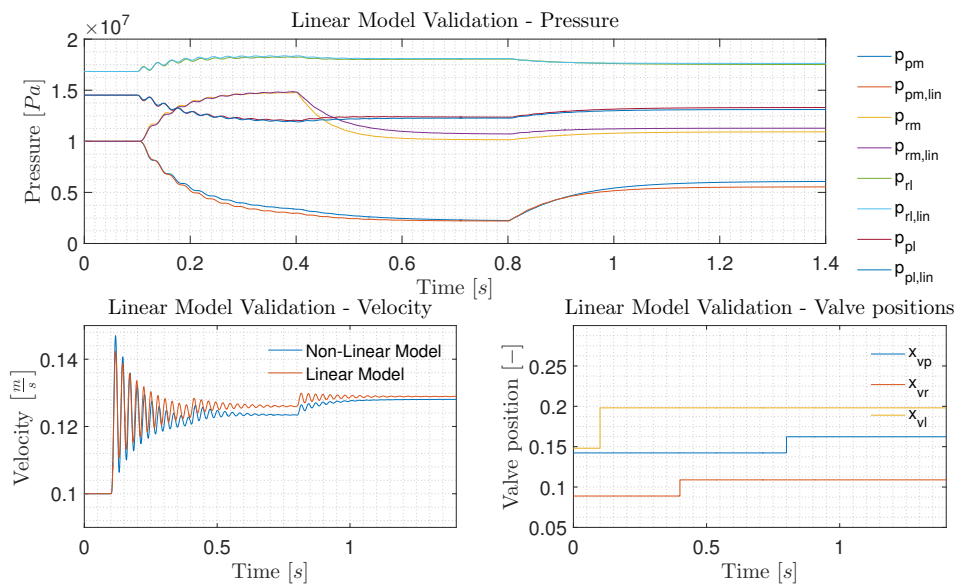


Figure B.4: Linear model validation utilising a linearisation point of $\dot{x}_p,0 = 0.1\text{m/s}$, $p_{pm,0} = 100e5$, $p_{rm,0} = 100e5$ and $x_p = 0$.

B.2.2 Analysis of Linear Model

In this section the linear model will be analysed and a linearisation point with the slowest dynamics will be found. The reason for this, is that if a controller is designed to perform very good at higher system frequencies with small gain margin and phase margin, the system may become unstable at lower natural frequencies. Yet the controller to be designed is analysed at higher system frequencies to ensure stability. Subsequently a coupling analysis will be performed to investigate the desired input/output combinations and to investigate how coupled the system is.

Linearisation Point

It is desired to investigate where the system frequency is lowest. In Figure S10, it is seen that the slowest system response is at low pressures such $p_{pm,0} = p_{rm,0} = 20\text{bar}$. From Figure S11 and S12 it is seen that the lowest natural frequency occurs at $\dot{x}_p = -0.25$ and

$x_p \approx 0$ resulting in the following linearisation point:

$$\mathbf{x}_0 = \begin{bmatrix} x_{vp,0} & x_{vr,0} & x_{vl,0} & P_{pm,0} & P_{rm,0} & P_{rl,0} & P_{pl,0} & x_{p,0} & \dot{x}_{p,0} \\ -0.9740 & -0.1465 & -0.3393 & 20\text{bar} & 20\text{bar} & 97.19\text{bar} & 77.22\text{bar} & 0\text{m} & -0.25\text{m/s} \end{bmatrix} \quad (\text{B.32})$$

Coupling Analysis

It is desired to make a cross coupling analysis of the linear system. Since the system is a MIMO system with three inputs and three outputs, there may exist couplings between the different possible input / output combinations. If the system is very coupled it may be necessary to decouple the system, and decentralised SISO control strategies may be inadequate to control the system. A method to analyse the system couplings is known as the Relative Gain Array (RGA). Furthermore the RGA analysis can imply which input / output pairings is the most advantageous. The RGA of the total linear system defined in Section B.2.1, \mathbf{G}_{tot} , is defined in Equation (B.33) (Sigurd Skogestad, 2001) where ' \times ' denotes element-by-element multiplication.

$$\text{RGA}(\mathbf{G}_{\text{tot}}) = \Lambda(\mathbf{G}_{\text{tot}}) = \mathbf{G}_{\text{tot}} \times (\mathbf{G}_{\text{tot}}^{-1})^T \quad (\text{B.33})$$

The magnitude of the RGA elements as function of frequency is shown in Figure B.5. To have an ideally decoupled system the RGA elements of the diagonal should equal one no matter the frequency, such $\text{RGA}(\mathbf{G}_{\text{tot}}) = \mathbf{I}$.

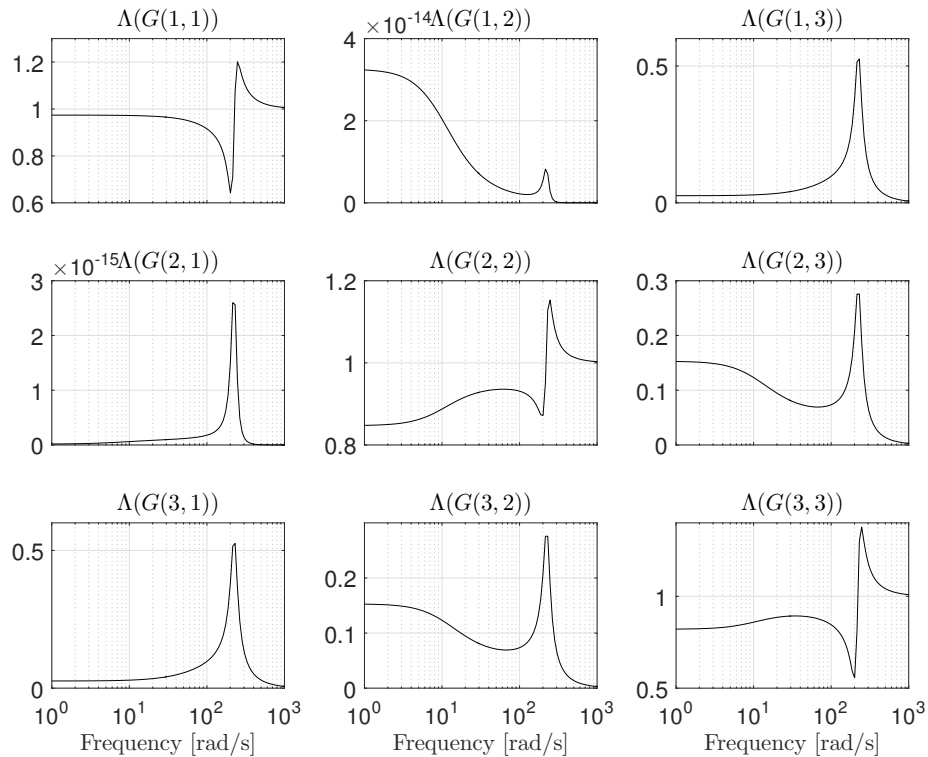


Figure B.5: RGA analysis of the transfer function matrix \mathbf{G}_{tot} .

From the RGA elements plotted in Figure B.5 it is seen that the diagonal, $\Lambda(G(1,1))$,

$\Lambda(G(2, 2))$ and $\Lambda(G(3, 3))$ is dominating and have values closest to 1 compared to the other input / output combinations. Therefore these input / output combinations are chosen for further control design such:

- x_{vp} controls p_{pm}
- x_{vr} controls p_{rm}
- x_{vl} controls \dot{x}_p

Though some couplings are acting between other input / output combinations, it will be investigated in the next section if a decentralised control strategy is adequate to fulfil the requirements in Section 3.1.3.

The controlled closed loop bandwidth of each input / output combination should be placed before the sudden changes in the RGA elements from Figure B.5 seen at approximately 100 rad/s, such great couplings are avoided. Since all the outputs are coupled it is chosen to design the closed loop bandwidths of the chosen input/output combinations at different frequencies. For the purpose of the control design for this system, the closed loop bandwidths are chosen such the input/output with highest to lowest bandwidth are: p_{rm} , \dot{x}_p and p_{pm} . This method will be tested in the next section.

B.2.3 Control Design

In this section the control scheme for the system is designed. It is desired to test a decentralised SISO control strategy. A PI controller with active damping is designed for the piston velocity control loop, and two PID controllers are designed for the two pressure control loops. Flow feedforward is utilised for all the control loops.

In Figure B.6 the frequency response for the chosen input output combinations are shown. As seen, the sub plants, $G_{tot}(1, 1)$, $G_{tot}(2, 2)$ and $G_{tot}(3, 3)$, are of type 0. To avoid steady state errors, the controllers for each sub plant should contain an integral part (Phillips and Parr, 2011). To increase the bandwidth and improve stability of the pressure control loops a derivative part is added to the controllers for $G_{tot}(1, 1)$ and $G_{tot}(2, 2)$. To damp the velocity response, high pass leakage is introduced to the load pressure for the load side cylinder.

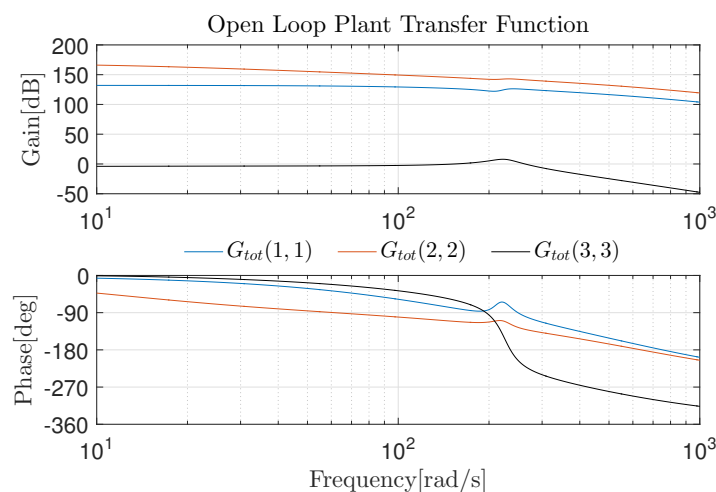


Figure B.6: Open loop frequency of the chosen input/output combinations.

In Figure B.7 the complete control scheme is illustrated for the three control loops.

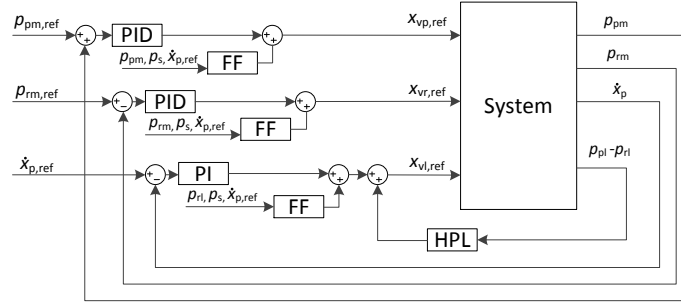


Figure B.7: Complete control scheme. FF denotes flow feed forward and hpl denotes high pass leakage.

Flow Feed Forward

Active flow feed forward is added to the control output, this way the controller should only compensate for the difference between transient and static flow, along with disturbances and inaccurate modelling. Flow feed forward is calculated from the orifice equation during steady state conditions such:

$$\dot{x}_{p,ref} A_i = Q_i = x_{j,ff} Q_{N,j} \sqrt{\frac{|\Delta p_i|}{\Delta p_N}} \text{sgn}(\Delta p_i) \quad \text{for } \begin{matrix} i = [pm, rm, rl, rp] \\ j = [vp, vr, vl, vl] \end{matrix} \quad (\text{B.34})$$

Isolating the orifice equation for the flow feed forward control output, $x_{j,ff}$, and utilising the pressure drops described in Section B.1.2 the flow feed forward is implemented as function of the measured pressures and the velocity reference.

High Pass Leakage

To damp the system, high pass leakage (hpl) is introduced on the load valve in the following manner:

$$\mathbf{G} = \mathbf{G}_{tot} \mathbf{u}_{hpl} \quad (\text{B.35})$$

Where \mathbf{u}_{hpl} is the control input from the high pass leakage which is calculated as:

$$\dot{\mathbf{u}}_{hpl} = \begin{bmatrix} 0 \\ 0 \\ (\dot{p}_{pl} - \dot{p}_{rl}) C_{hpl} \end{bmatrix} - \omega_{hpl} \mathbf{u}_{hpl} \quad (\text{B.36})$$

Where C_{hpl} is the leakage coefficient. The high pass leakage is introduced with a cut off frequency below the frequency of the under damped pole pair in $G_{tot}(3, 3)$ with the following parameters:

$$\omega_{hpl} = 100 \text{ rad/s} \quad C_{hpl,3} = 2 \cdot 10^{-8} \quad (\text{B.37})$$

The leakage coefficient is determined ad hoc. Since the sub plants are coupled as shown in Section B.2.2, the high pass leakage on the load valve affects the remaining system. The

frequency response for the sub plants are seen in Figure B.8, B.9 and B.10, where the original open loop response is seen along with the damped response.

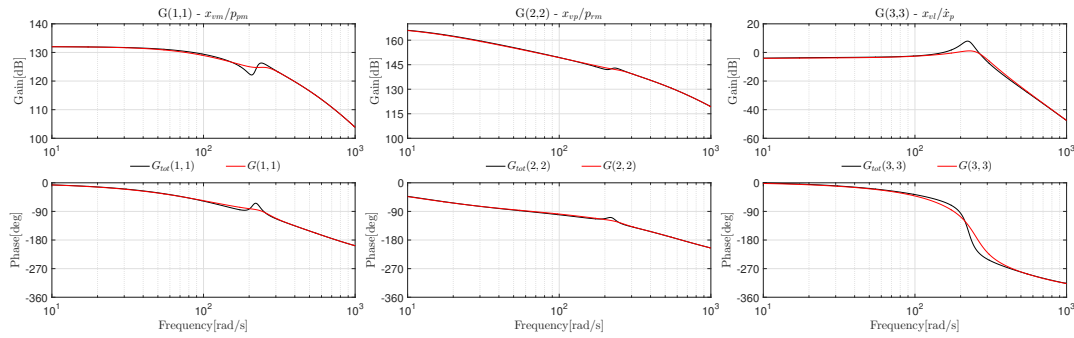


Figure B.8: Frequency response for $G(1,1)$ with and without high pass leakage.

Figure B.9: Frequency response for $G(2,2)$ with and without high pass leakage.

Figure B.10: Frequency response for $G(3,3)$ with and without high pass leakage.

The leakage output is added to the control output. The system with high pass leakage will be used in the remaining control design.

SISO Control

In this subsection a linear decentralised control strategy will be designed for the purpose of controlling the two chamber pressures of the main cylinder and the velocity of the system. The input/output combinations used to control the system is based on the RGA analysis made in Section B.2.2.

First the bode plots will be analysed to determine which control strategy may be adequate to control each input output combination. Subsequently a test of the controllers will be made in the non-linear model, based on the requirements in Section 3.1.3.

In Figure B.8 to B.10 the bode plots of the sub plants are shown with the implementation of high pass leakage. It is chosen to implement PID controllers on the two pressures $G(1,1)$ and $G(2,2)$. The PID controllers can be described for the piston side valve, p , and the rod side valve, r , for the sub plants $G(1,1)$ and $G(2,2)$ respectively as:

$$G_{c,i} = + \frac{K_{D,i}s^2 + K_{P,i}s + K_{I,i}}{s} \quad \text{for } i = [p, r] \quad (\text{B.38})$$

It is chosen to implement a PI to control the velocity for $G(3,3)$ such $K_D=0$.

The controllers are tuned in the model to obtain good closed loop performance. The controller gains are listed below:

$$K_P = \begin{Bmatrix} 5 \cdot 10^{-8} \\ 0.5 \cdot 10^{-7} \\ 0.1 \end{Bmatrix} \quad K_I = \begin{Bmatrix} 2 \cdot 10^{-6} \\ 2 \cdot 10^{-7} \\ 20 \end{Bmatrix} \quad K_D = \begin{Bmatrix} 2 \cdot 10^{-10} \\ 1 \cdot 10^{-10} \\ 0 \end{Bmatrix} \quad (\text{B.39})$$

These gains results in the following cut off frequency for the integral part $\omega_{0,I} = [40 \ 4 \ 200]\text{rad/s}$ and a cut off frequency of the derivative part of $\omega_{0,D} = [250 \ 500 \ -]\text{rad/s}$.

Implementing this control strategy results in the open loop response for the three sub plants

as seen in Figure B.11. The resulting gain margin, GM, and phase margin, PM, for the three compensated sub plants are:

$$\text{PM} = \begin{cases} 98.8^\circ \\ 87.1^\circ \\ 84.7^\circ \end{cases} \quad \text{GM} = \begin{cases} \text{inf} \\ \text{inf} \\ 13\text{dB} \end{cases} \quad (\text{B.40})$$

These gain margins and phase margins are satisfying to ensure stability of the system (Phillips and Parr, 2011).

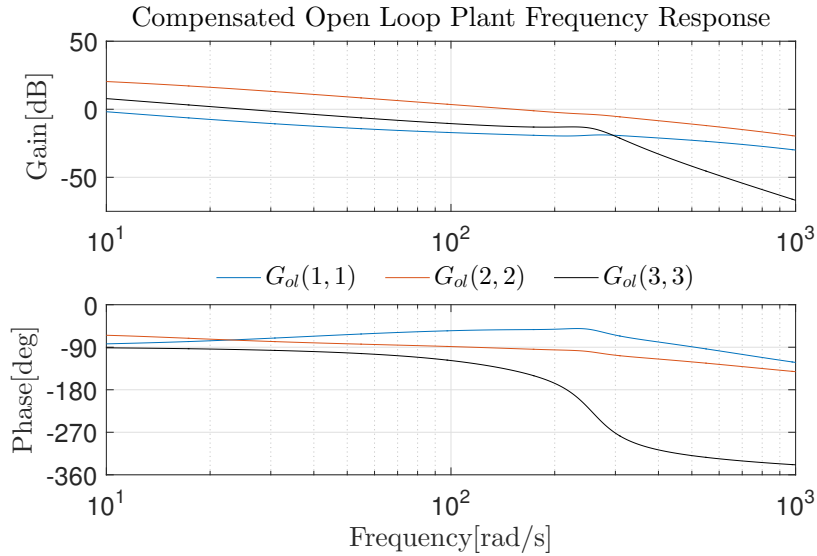


Figure B.11: Compensated open loop response of the three sub plants.

The controllers are evaluated in the lowest system frequency, though as seen in Figure S10 to S12, the dynamics of the system changes with the linearisation point. In Figure B.12 the compensated open loop frequency response is seen in the linearisation point yielding the highest system frequency, i.e. $p_{rm,0} = 200\text{bar}$, $p_{pm,0} = 200\text{bar}$, $\dot{x}_0 = 0.05\text{m/s}$ and $x_0 = 0.25\text{m}$. In this linearisation point, the gain margin and phase margin are:

$$\text{PM} = \begin{cases} 94.9^\circ \\ 66.6^\circ \\ 91.8^\circ \end{cases} \quad \text{GM} = \begin{cases} \text{inf} \\ \text{inf} \\ 2.4\text{dB} \end{cases} \quad (\text{B.41})$$

The phase margin is in every case still satisfying, though the gain margin for the velocity control loop is much smaller, though the system is still stable.

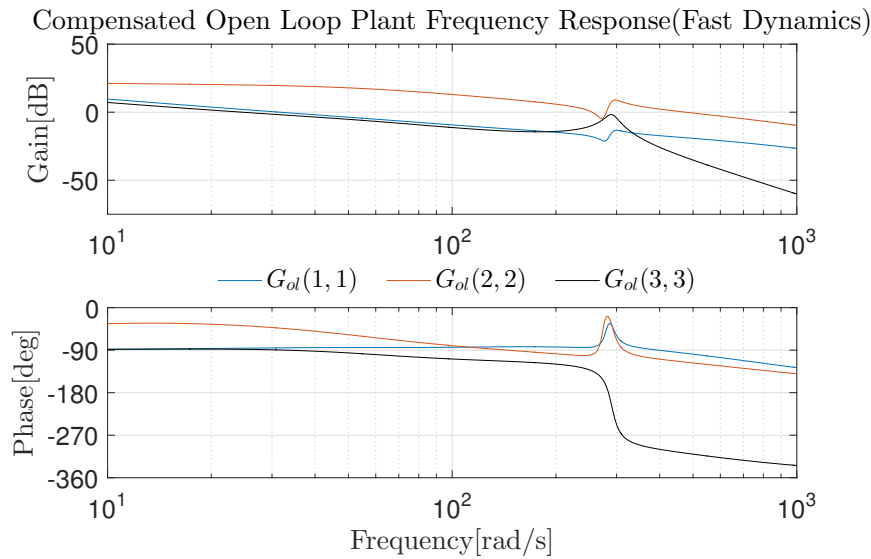


Figure B.12: Compensated open loop response for the highest frequency of the under damped pole pair.

The compensated closed loop response for the three sub plants are seen in Figure B.13. The control is seen to be well damped. The controllers will be tested in the non-linear model to verify the performance of these control structures.

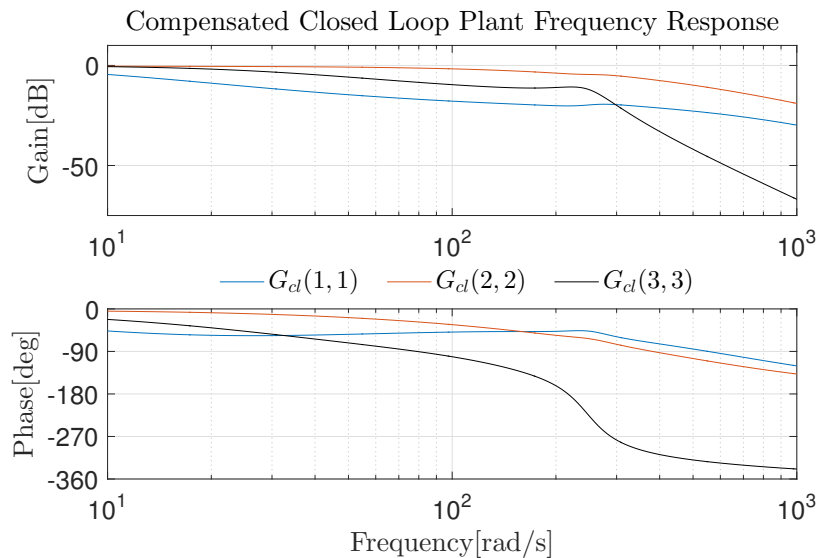


Figure B.13: Compensated closed loop response of the three sub plants.

In Figure B.14 the controlled states is plotted for a sinus velocity trajectory of 1Hz where the cylinder starts at $x_p = 0\text{m}$, and the pressures are set to 20bar. In Figure B.15 the velocity trajectory is also a sinus with a frequency of 1Hz where the cylinder starts at $x_p = 0.25\text{m}$, and the pressures are set to 200bar. In both cases the designed controllers can fulfil the requirements from Section 3.1.3. In Figure B.16 and B.17 the system performance are shown for a negative velocity step where the piston position starts in respectively $x_p = 0\text{m}$ and $x_p = 0.25\text{m}$. It is seen that the system can follow the references, yet the pressures oscillates more than the requirements allow when a velocity step is utilised. Though the

trajectories used to estimate the friction parameters will not contain steps, why the control strategy elaborated in this section is adequate. The control structures will furthermore be tested on the test bench later in the thesis.

Other methods to control the system may result in better system performance, yet the control method proposed here is adequate for the purpose of this thesis.

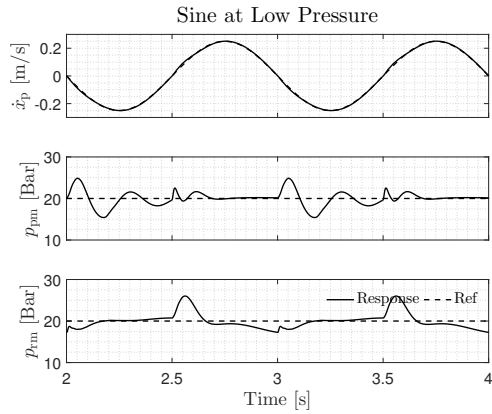


Figure B.14: Sine velocity trajectory and constant pressure references of 20 bar. The piston starts in $x_p = 0\text{m}$.

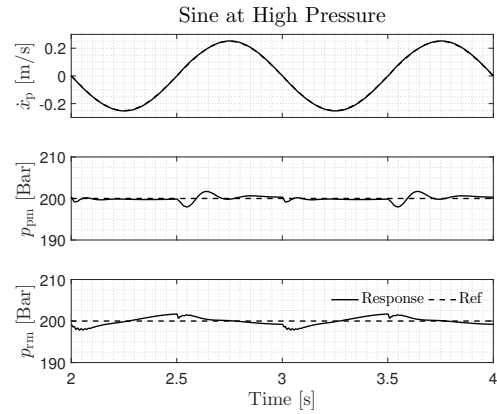


Figure B.15: Sine velocity trajectory and constant pressure references of 200 bar. The piston starts in $x_p = 0.25\text{m}$.

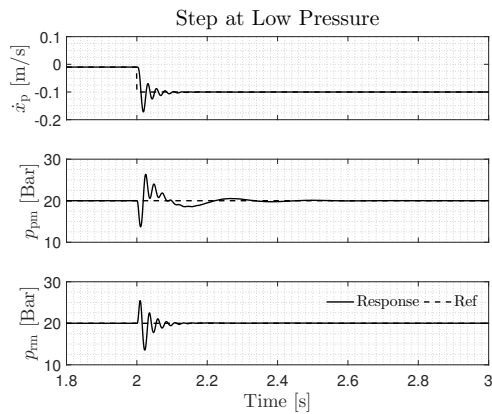


Figure B.16: Step velocity trajectory and constant pressure references of 20 bar. The piston starts in $x_p = 0\text{m}$.

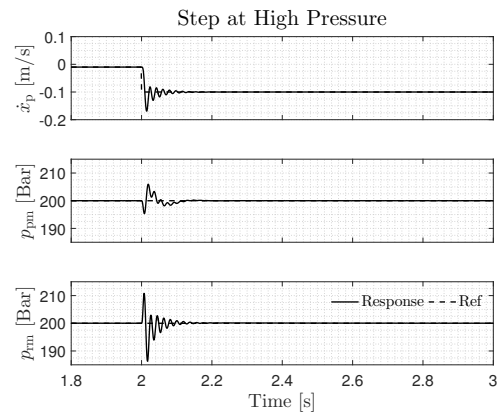


Figure B.17: Step velocity trajectory and constant pressure references of 200 bar. The piston starts in $x_p = 0.25\text{m}$.

C | Appendix for Part I

C.1 Method to Place Sampling Points

A method to assure that more friction force samples are made in the start of the negative resistance regime than the fluid film lubrication regime, is to choose the friction sample velocities as function of the derivative of the steady state friction curve. The higher derivative value, the more frequent the friction should be sampled. In this thesis the eight previous friction models shown in Table 4.1 is used to determine the maximum derivative for all the eight cases as shown in Figure C.1. In this project no further analysis is made of the optimal method to distribute the samples, yet in this project the maximum derivative is utilised as a standardised method. This maximum derivative is fitted with an exponential function with an offset to ensure that the fitted curve is always greater than the derivative curve of the eight parameter sets from Table 4.1, such samples are made in the fluid lubrication regime as well. This is necessary since the viscous friction coefficient, σ_2 , is most sensitive at higher velocities. This fit is shown as the red line in Figure C.1. The maximum derivative is described by the equation: $F(\dot{x}_p) = 192900 \cdot \exp(-91.1\dot{x}_p) + 6000$. Using this method more samples will be made in the sensitive negative resistance regime as desired, yet a better method for individual mechanical systems may exist.

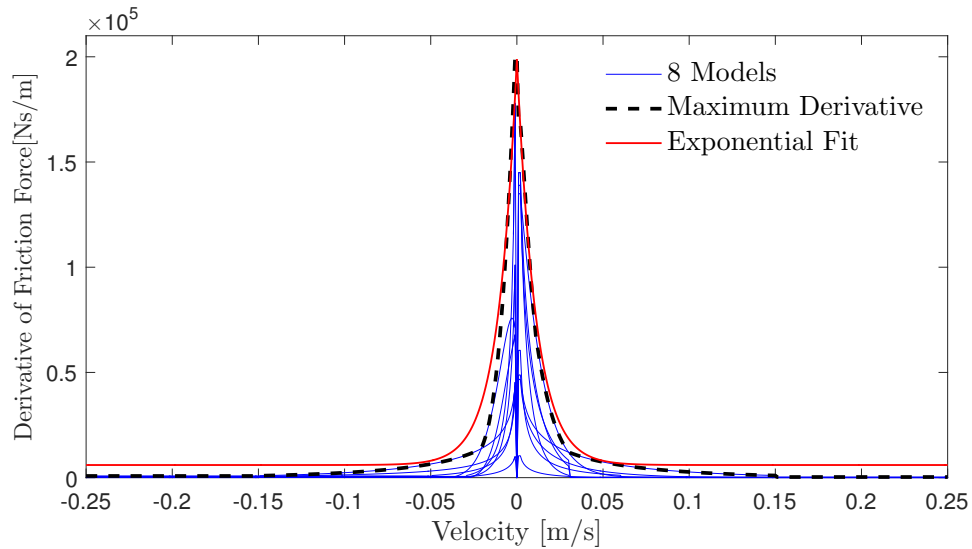


Figure C.1: The derivative curves of the eight found parameter sets from Table 4.1 are plotted together with the maximum derivative and its fit.

The method developed for this purpose is to place the samples such the area under the curve between each sample is equal. This is described by the following equation:

$$\int_{0.001}^{\dot{x}_s} F(\dot{x}) \, d\dot{x} = \int_{0.001}^{0.25} F(\dot{x}) \, d\dot{x} \frac{1}{n_s - 1} \cdot i_s \quad \text{for } i_s = [1 : n_s - 1] \quad (\text{C.1})$$

Where n_s is the number of samples and $\dot{x}_s(i_s)$ is the sample velocity for $i_s = [1 : n_s - 1]$. The first sample velocity is chosen to be at 0.001 m/s since this is the lowest velocity required of the system as stated in Section 3.1.3. Solving the above equation for $\dot{x}_s(i)$ results in the

following equation to calculate the samples velocities:

$$\dot{x}_s(i) = 0.256 - 0.011 \ln \left(\frac{2.29 \cdot 10^8 i_s + 1.69 \cdot 10^8 (1 - n_s)}{n_s - 1} \right) \quad \text{for } i_s = [1 : n_s - 1] \quad (\text{C.2})$$

In Figure C.2 an example is given to illustrate how the friction samples are placed for $n_s = 5$ and $n_s = 20$. It should be noted that this method to determine the distribution of the friction force measurements is just one way to do it. This method makes it possible to evaluate how many steady state friction force samples it is necessary to have to obtain an accurate steady state parameter estimation. Other methods to distribute the friction force samples may be more adequate.

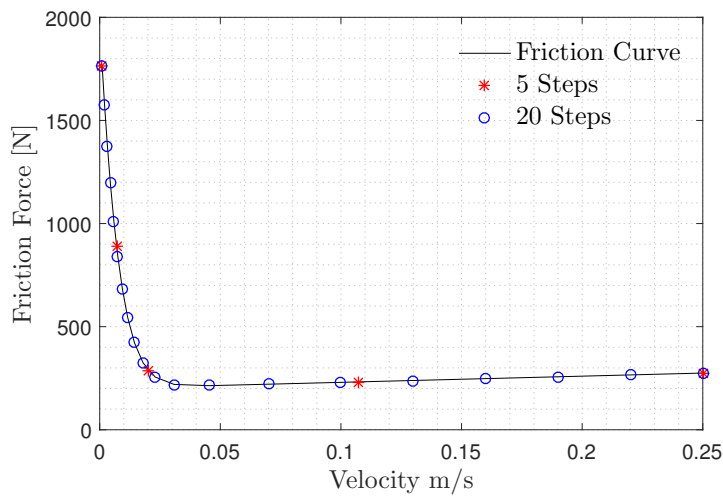


Figure C.2: Example showing the sample points utilising the sample distribution method proposed in this section.

D | Experimental Measurements

D.1 Break in

In this chapter the break in trajectory will be designed to break in the cylinder as fast as possible. During the break in period a trajectory containing steady state velocity steps, sine velocities and a step velocity will be run on the practical setup to investigate how the friction force changes during the break in period. This trajectory is like the one used for the measurements of the pressure dependency of friction in this thesis. The friction model parameters have been estimated during break in, but no tendency is seen why it can not be concluded from these if the cylinder is broken in.

D.1.1 Trajectory Planning

The velocity trajectory used during the break in period is based on assumptions on which patterns of the velocity and pressure states may result in a fast break in period. The Archard wear equation says that the wear is proportional to the sliding distance and the normal load (Zmitrowicz, 2006). Furthermore it is assumed that the sealings inside the cylinder will deform differently for different pressures, and that velocity reversals will speed up the break in period. Based on these assumptions, a slow sine wave with a low velocity amplitude combined with a faster sine wave with a high velocity amplitude is realised, such many velocity reversals is realised over the full stroke length. The two main chamber pressure trajectories will also be sinusoidal such the sealings are exposed to different deformations during break in. These are chosen to vary between high pressures of 75bar to 175bar since a high pressures is assumed to increase the normal load between the sealings and the cylinder, which according to Archard results in accelerated wear. The resulting break in trajectory is shown in Figure D.1.

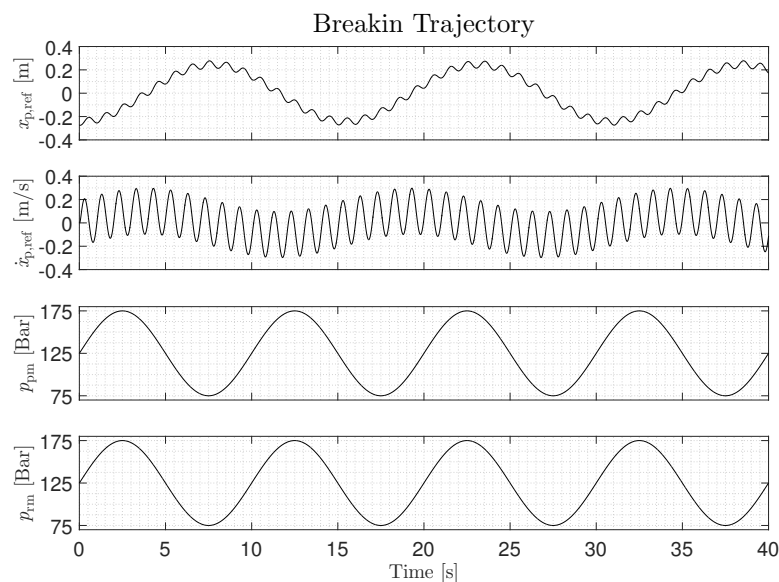


Figure D.1: Trajectory designed to be used during break in.

D.1.2 Change in Friction During Break in Period

The break in is investigated by analysing the friction force at different instances of the break in. It is assumed that the break in period is completed when the friction force is constant for the same velocity and pressure cycle. The results are shown in Figure D.2 where the measured friction force is plotted for different stages of the break in period and the total distance travelled by the cylinder is stated for each friction force curve in the figure. From the figure it is seen that the friction force mostly increases during break in and it can not be concluded that the cylinder has reached break in. The first four steps are made in the middle of the stroke and the remaining are made at approximately -0.25m. As seen from the figure the changes in the friction force during break in is different depending on the piston position.

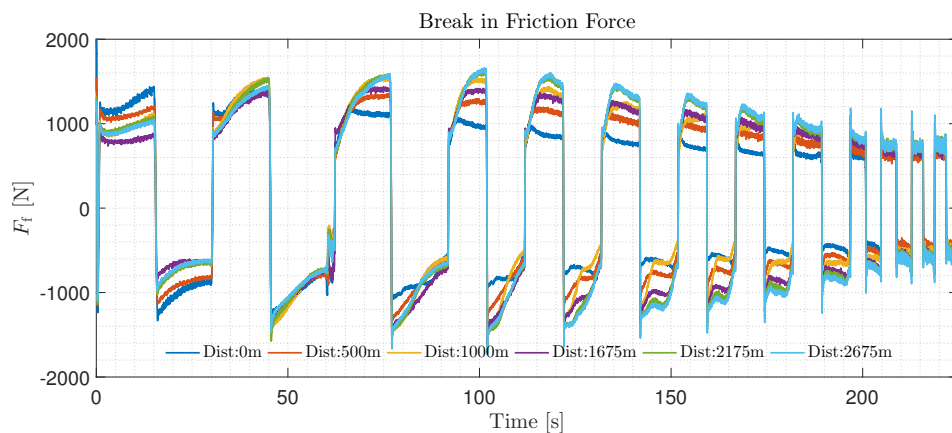


Figure D.2: Measurements made during break in.

D.2 Evaluation of Velocity Step Duration for Steady State Measurements

To validate the steady state model, a trajectory with 30 velocity steps in each direction, following the method in Section 6.1.1 with a velocity step duration of 4s for each step, is tested on the practical test bench. The results are shown in Figure D.3 in the form of measured friction and velocity where the pressures are controlled to 50 bar. From the figure it is seen that the velocity is constant for a long period of each velocity step and the pressures are approximately 50 bar at the end of each step, yet the friction force is not seen to be constant.

It is preferred that the velocity step duration is longer such the pressures and friction will be at steady state some time before the friction samples are made at the last 0.1s of each velocity step.

A trajectory with velocity steps of 15s is seen in Figure D.2 for different instances in the break in period. The same problem is seen here, why it is assessed to be necessary to have a longer velocity step duration to reach a constant friction force at the sampling instance. Based on the observations from the measurements in Figure D.2 and D.3 the final trajectory is chosen to have a velocity step duration of 30s when possible. Due to stroke limitations this is not possible for higher velocities, why these will be run for as long as possible.

The resulting trajectory used to estimate the parameters as function of pressure is shown in

Figure 7.2.

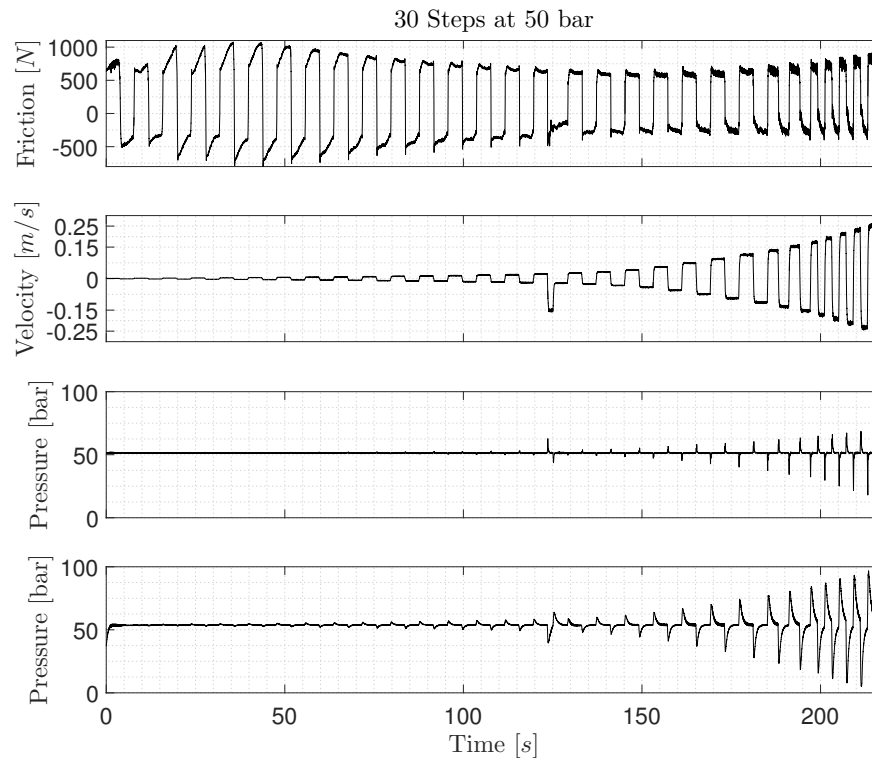


Figure D.3: Measurements of the friction force and velocity from the test bench at main chamber pressures of 50bar. The measurements is filtered with a 2nd order Savitzky-Golay filter with 51 frames, due to noise on the measurements.

D.3 Steady State Friction Sampling Instance

During the validation of the steady state friction model in Section 7.1 it was observed that the friction force in negative velocity direction at first were sampled at instances where the friction force was very different from the rest of the sampling points. This problem is investigated in this section. Figure D.4 shows the measurement data from the experiment with 30 velocity steps in each direction and a pressure reference of 100 bar used in the validation of the steady state friction model. Figure D.5 is a zoom from this figure. At first the friction samples are calculated as the mean during the last 0.1s before a direction change and these are illustrated by the blue crosses in the figures.

From the figures it is seen that the friction force measured at positive velocities is not constant before the sampling instance in many cases even though the velocity steady state conditions are met at all sampling instances. Furthermore the pressures are constant for small velocity steps, but for higher velocity steps it is seen, in Figure D.5, that steady state is only obtained just before the sampling instance. Yet the friction force is seen to be at steady state in these cases.

The friction force measured from negative velocities are also varying before the sampling instance, in fact the problem is worse. The first 10 friction samples are not made during a constant friction, the next approximately 15 sample points are made at an instance where

the friction force suddenly increases more than 200 N and the last 5 sample points are approximately made during a constant friction force. For negative velocities the velocity is at steady state at all sample instances and the pressures are almost always at the desired value at the sampling instance, yet a problem also occurs at high velocity steps which is also the case for positive velocity steps.

The reason for the non-steady behaviour of the friction force may be due to a position dependency. The first 4 samplings of the friction measurements for negative velocities are sampled in the middle of the main cylinder. The subsequent friction measurements for negative velocity are sampled at a position of approximately -0.25m. The first steps are sampled in the middle since model simulations indicates control issues for low velocities conducted in the end of the cylinder, and the higher velocities are sampled in the end of the cylinder such a long stroke can be utilised. It is observed that the friction behaves differently when the piston position reaches this position.

From Figure D.4 it is seen that the characteristics of the friction force have the same tendencies for positive velocity steps and the subsequent negative velocity step. This indicates a position dependent friction force since each pair of positive and negative velocity are travelling at the same piston position. Furthermore a little perturbation is seen in the friction force for positive velocities, illustrated in Figure D.4 by the red box. Subsequently a perturbation is seen in the friction force for negative velocity, which occur at the same piston position, $x_p \approx 0\text{m}$. This may indicate that the friction force is position dependent, which could be caused by a lag of complete break in of the cylinder. This assumption is confirmed in Appendix D.4.

Since it is assessed that the friction samples for negative velocities are made at a position with different friction characteristics than the rest of the stroke, it is desired to conduct the friction force samples at the time instance before the friction force suddenly changes a lot from the fifth negative velocity step. This problem is not seen for the friction samples at positive velocities since these are made at another cylinder position.

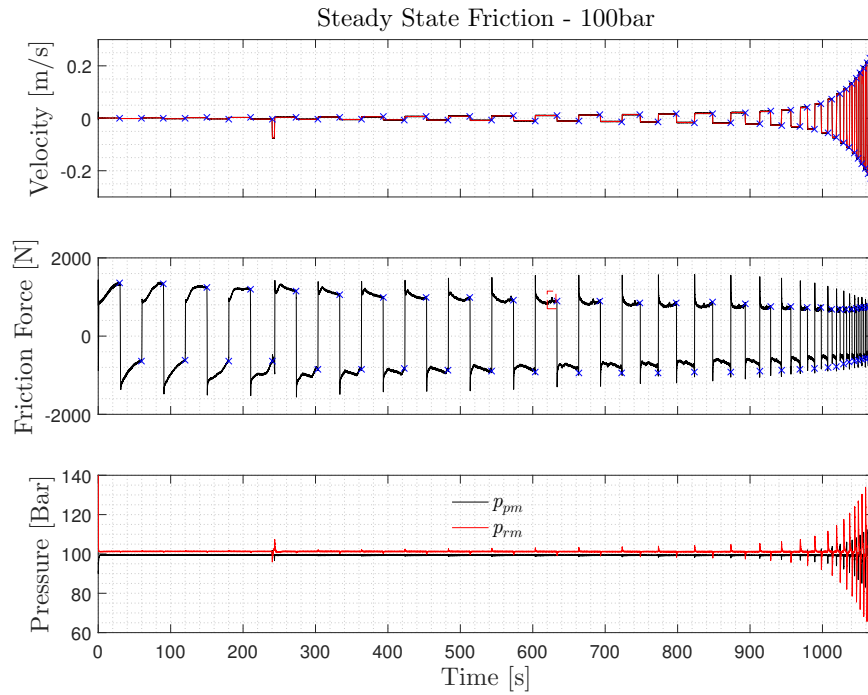


Figure D.4: Measured velocity, friction force and pressures during a steady state trajectory with 30 friction sample points in each velocity direction. The blue crosses illustrates the sample time.

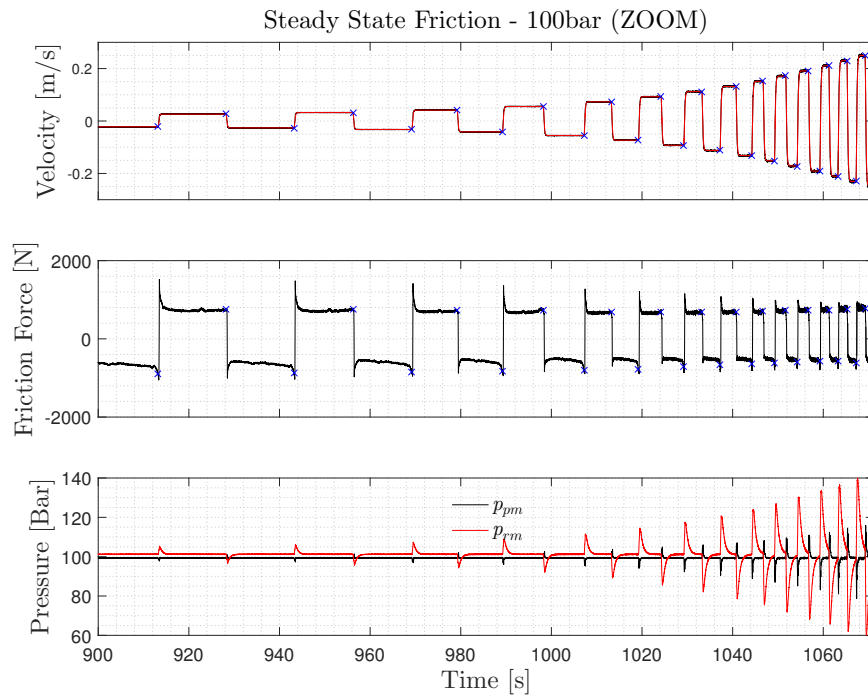


Figure D.5: Zoom from Figure D.4.

Further problems regarding the sampling of the friction force were observed during the re-

sulting measurements to determine the pressure dependency of the friction force. It was observed that the system control is unable to maintain pressures of 20 bar for high velocity steps of 0.16m/s to 0.25m/s, such the pressure attains 1 bar. Due to this it is not possible to obtain steady state conditions for these velocities. This have subsequent to measurements shown to be caused by an error in the control algorithm, which resulted in the flow feed forward for the main cylinder was unused.

During an examination of measurement data it is determined that the last three velocity steps in negative direction should be disregarded for the measurements where p_{rm} is controlled to 20 bar together with the last two velocity steps for negative velocity where p_{pm} is controlled to 20 bar. An example of one of the measurements with p_{rm} controlled at 20 bar and p_{pm} controlled at 200 bar is shown in Figure D.6. It is clearly seen that the pressure equals 1 bar for the three last velocity steps in negative direction.

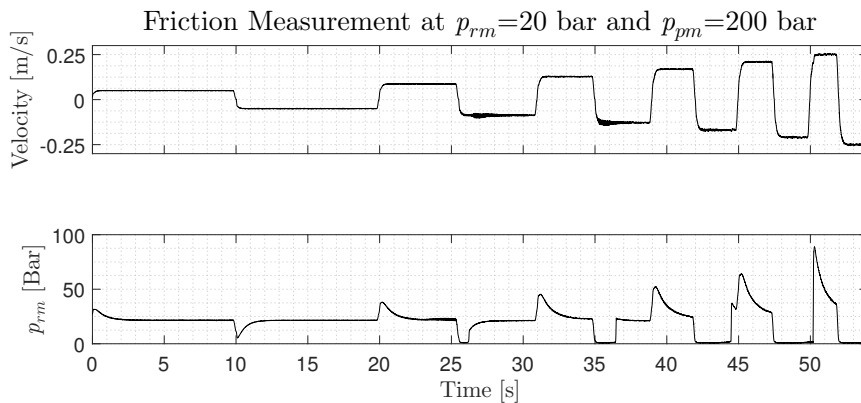


Figure D.6: Velocity and rod side pressure during a trajectory where the rod side and piston side pressure respectively are controlled at 20 bar and 200 bar.

D.4 Position Dependency

An investigation of a potential position dependency in the friction force is investigated. The piston velocity is controlled to a constant velocity from -0.275m to 0.275m of the stroke and the pressures are controlled at 100 bar. The results are shown in Figure D.7. As seen from the figure the friction changes greatly over the stroke during velocities of 0.005 m/s and 0.025 m/s. It is seen that a large position dependency is seen around -0.25m which is where the steady state friction samples for negative velocity are made why this influences the measurements. For positive velocity the samples are made in different positions which also influences the measurements. Furthermore a lump is seen in the middle of the stroke, this lump is also seen in the steady state measurements in Figure D.4.

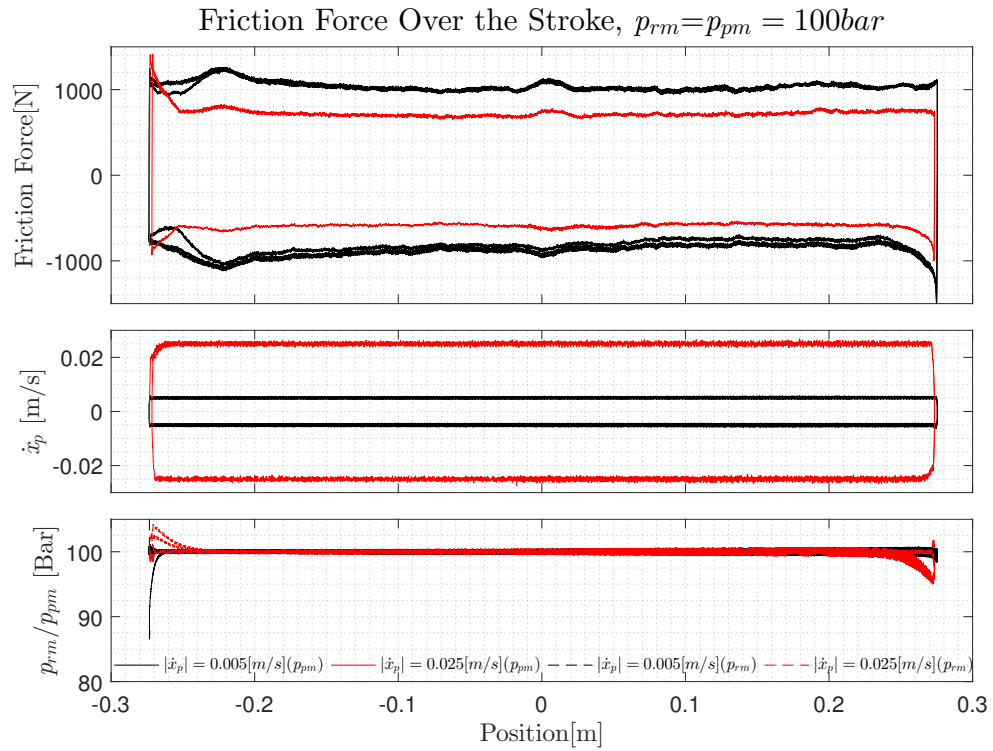


Figure D.7: Position Dependency seen at constant velocities for extending an retracting stroke at 100 bar chamber pressures.

Part IV

Supplement

Supplement E System Topology	137
E.1 Variable Mass as Load	137
E.1.1 Fulfilment of Requirements	138
E.1.2 Topologies	139
E.1.3 Comparison	140
E.2 Dynamic Load	141
E.2.1 Fulfilment of Requirements	141
E.2.2 Topologies	141
E.2.3 Comparison	143
E.2.4 Choise of Topology	143
E.3 Further Analysis of Hydraulic Load Solution	144
E.3.1 Choise of Mass	145
E.3.2 Performance of System with Hydraulic Load	146
Supplement F Further Design Considerations	149
F.1 Friction Joints and Pre tensioning	149
F.1.1 Pre Tensioning of Strut Joint	149
F.1.2 Pre Tensioning of Alignment Coupler	149
F.1.3 From Construction To Bench	149
F.1.4 From Bench to Floor	150
F.2 Electrical Network	150
F.3 Model Parameters	151

E | System Topology

In the following chapter different topologies will be described and analysed. In Figure S1 the general system is seen. For the system to full fill the requirements regarding the operating area it is necessary to vary the load on the cylinder. For the system being able to fulfil the requirements of decoupling the pressure and velocity dependent friction, it is necessary to separately control each main cylinder chamber pressure and the velocity. This can be done by implementing a valve setup which allows each chamber pressure to be controlled individually as well as having a load force, F_l , which can be varied.

Two different general topologies will be investigated. A mass system where a gravitational force is used to load the system, and a topology with a dynamic load force, either from an electrical machine or a hydraulic cylinder. As mentioned in Section 3.1.3 it is desired that the test facility should be able to test cylinders up to $\varnothing 80$. In the case of this thesis a $\varnothing 80$ cylinder is also interesting for the dynamical load topologies due to the accuracy requirement. The following topologies is discussed regarding a $\varnothing 80$ and $\varnothing 50$ hydraulic main cylinder.

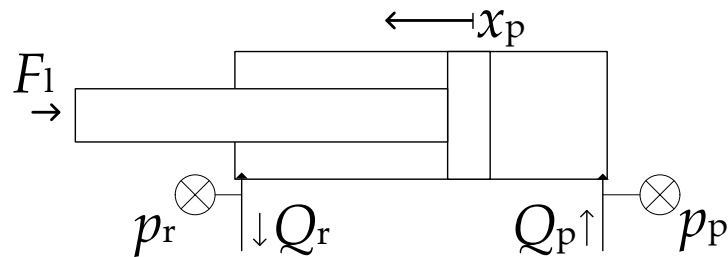


Figure S1: Diagram of main cylinder.

The force equilibrium for the system is described by Newtons 2. law as when disregarding the friction force:

$$\ddot{x}_p m = p_p A_p - p_r A_r - F_l \quad (\text{E.1})$$

Where F_l is the load force on the cylinder.

E.1 Variable Mass as Load

In this section, topologies where a varying mass acts as a load force on the cylinder will be investigated. The advantage of using a mass as load is that the load force is constant and accurate measurements of the friction force can be obtained since it is not necessary to measure the load force. The disadvantage is that it is only possible to load the system in one direction depending on the topology.

The fulfilment of the requirements in Section 3.1.3 is investigated and the pros and cons of the systems are stated.

E.1.1 Fulfilment of Requirements

An investigation of the fulfilment of the requirements are made in this section. This investigation covers all of the topologies with a mass as load.

When using gravitational force as load force it is only possible to obtain a load in one direction, either compressive or tensile force, depending on the topology. In Figure S2 and S3 a map of the load force necessary to obtain different pressure combinations as seen for cylinders with \varnothing : 80mm and \varnothing : 50mm respectively. As seen, the operational area is limited due to the unidirectional load force. When using gravitation as load force it is thus not possible to obtain all the desired pressure combinations, though a mass as load yield an advantage since it is not necessary to measure the load force, thus increasing the accuracy. Furthermore the load side will have no dynamic behaviour making it easier to control the system, though this also means that it is not possible to maintain constant pressures during transient response.

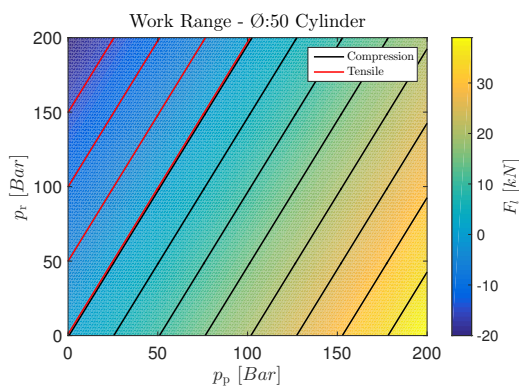


Figure S2: Work Range for \varnothing :50 cylinder, assuming ideal pressure control and steady state.

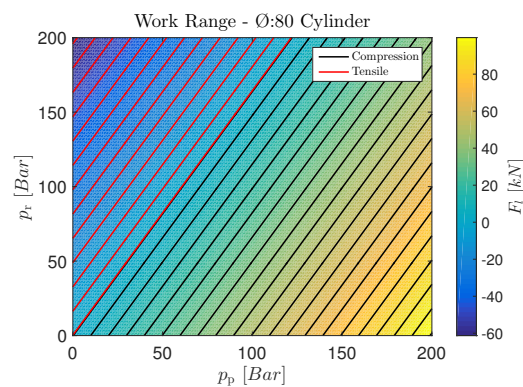


Figure S3: Work Range for \varnothing :80 cylinder, assuming ideal pressure control and steady state.

E.1.2 Topologies

In this section different topologies are proposed and their pros and cons are discussed.

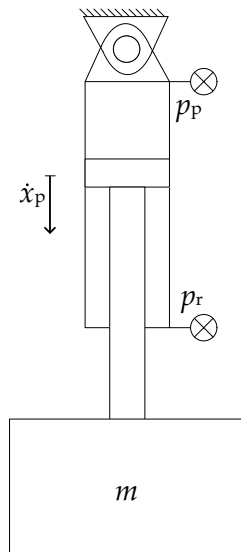


Figure S4: System topology with a downside mounted cylinder and a hanging variable mass.

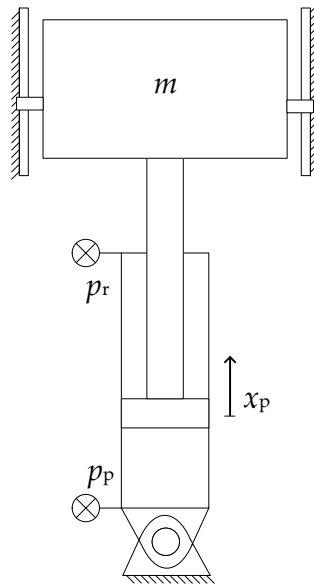


Figure S5: System topology with an upside mounted cylinder supporting a variable mass.

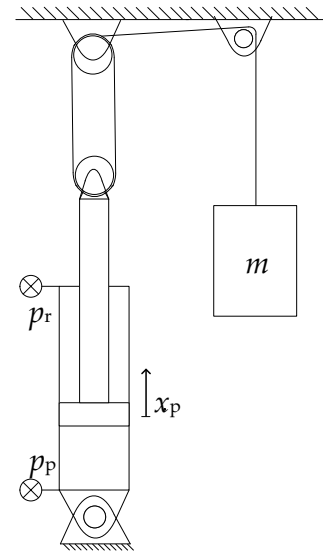


Figure S6: System topology with cylinder mounted to a pulley system.

Downright Cylinder - Hanging Load

One way to construct a system with a mass as load is to have a top mounted cylinder with a variable hanging mass as seen in Figure S4. This way, gravitational force creates a tension in the cylinder. This design is simple and would require minimal guidance of the load. When utilising this design, it may be possible to create an easy weight changing mechanism.

Pros:

- Minimal Guidance
- Simple Design
- High accuracy since no force measurement is required
- Lower mass necessary compared to upright
- Easy load changing system
- Simple control due to a static load

Cons:

- Limited working area
- Manual load for change
- Impossible to maintain constant pressures during transient response

For this system a mass of 2040 kg and 6200 kg for respectively a $\varnothing 50\text{mm}$ and $\varnothing 80\text{mm}$ cylinder are needed to obtain a pressure of 200 bar in one chamber.

Upright Cylinder - Holding Load

Another way is to have an upright cylinder with a variable load on top as seen in Figure S5. This design will result in a larger obtainable pressure working range as seen in Figure S2 and

S3. Due to the gravitational compression it might be necessary to enhance the guidance system compared to the downright hanging cylinder. Furthermore the design of the bench is more complex since the masses are placed above the cylinder, thus also making a load changing mechanism more complex.

Pros:

- Simple design
- High accuracy since no force measurement is required
- Larger working area than downright hanging cylinder

Cons:

- More external friction due to more guidance than downright
- More mass necessary than downright hanging cylinder
- Difficult load changing system
- Limited working area
- Manuel load change
- Impossible to maintain constant pressures during transient response

For this system a mass of 4000 kg and 10200 kg for respectively a Ø50mm and Ø80mm cylinder are needed to obtain a pressure of 200 bar in one pressure.

Load Through a Pulley

A design where the necessity for a large mass is omitted is by having a tensile load through a pulley system as seen in Figure S6. When utilising a pulley system, the amount of mass can be lowered to obtain the same load forces. When using a pulley, the external friction from the pulley results in a lower accuracy and further guidance of the mass is also necessary.

A reasonable pulley exchange might be 1:3, causing the mass requirement to be lowered by a factor of 3 compared to the downright hanging topology.

Pros:

- Lower mass needed than upright and downright cylinder
- Simple design
- High accuracy since no force measurement is required

Cons:

- More external friction from bearing and guidance than downright and upright system
- Limited working area
- Manuel load change
- Impossible to maintain constant pressures during transient response
- Mass is not mechanically secured to the cylinder → If the cylinder accelerates faster than the mass, there will be no load.

For this system a mass of 680 kg and 2060 kg for respectively a Ø50mm and Ø80mm cylinder is needed to obtain a pressure of 200 bar in one chamber.

E.1.3 Comparison

When considering a mass as load, two general problems evolve. It is not possible to operate at all desired pressure combinations and the load should be changed manually. When considering the three topologies where a mass acts as a load, the two most plausible solutions is if the load acts as a tensile load i.e. the downright hanging cylinder and the pulley system, since this makes the changing of mass easier and the necessary mass is more reasonable. In both cases the loss in accuracy from the acceleration is the same, though a large uncertainty is

seen in the pulley system due to the error from the external friction forces in the pulley. When utilising mass as a load, the mass should be very large to be able to operate in the desired areas, though the pulley system has the advantage of a lower mass compared to the downright hanging cylinder. Alternatively it would require less mass if a smaller cylinder was utilised.

E.2 Dynamic Load

Instead of a constant mass as load it may be preferable to vary the load dynamically. By doing this, it is possible to obtain different load situations continuously in one measurement series instead of changing the mass load manually in discrete steps. Furthermore it is possible to obtain both compressive loads and tensile loads continuously, opposite to the mass load solution. Yet the dynamical load solution will require additional control of the load and additional sensors to measure the load force. In the next section the requirements from Chapter 3.1 is discussed for this kind of system.

E.2.1 Fulfilment of Requirements

A hydraulic cylinder with a dynamic varying load can assure both compressive loads and tensile loads. This kind of load makes it possible to achieve pressures in the main cylinder in the required region of 0-200 bar in both rod chamber and piston chamber independent of each other if the load can be accurately controlled. Figure S2 and S3 shows the required pressure region and the required load force.

When a dynamical load is used it is required to have some guidance of the coupling between the main cylinder and the load actuator to have a controlled force direction. Furthermore it is required that the force between the main cylinder and the guidance, F_L , is measured such the friction force from the guidance can be disregarded. By this the friction force can be estimated using Newtons 2. law.

As shown in Figure S2 and S3 it is seen that the required load force is respectively 40 kN and 100 kN, why a load sensor in this range is required. A load sensor in the range of 0-100 kN is found with an accuracy of 0.05 % of full range and 0.04% F_s . for a 0-50 kN sensor. This gives an additional lack of accuracy of 20N and 50N respectively for the ranges 0-50 kN and 0-100 kN.

E.2.2 Topologies

Three topologies are discussed in the following subsections. One with an electric motor as load where the torque is transferred to a linear motion by a screw drive, one where the torque is transferred to a linear force by a rack and pinion and a last topology where a hydraulic cylinder is used as load. For all of these three topologies additional mass can be added to obtain the preferred system dynamics.

Motor with Spindel

The two topologies using an electric motor is interesting since the dynamic performance of an electrical motor is very good, indeed for torque control since the torque can directly be

controlled by the current in the motor. One way to convert the motor torque to a linear force is by a spindle drive. Yet there may be some degree of axial play in the ball screw which may degrade the system performance. One way to construct the test system with this topology is shown in Figure S7. The spindle is inside the bar, connected to the motor.

The dynamic performance of this system is assumed to be very good since torque control of the motor can obtain a high bandwidth.

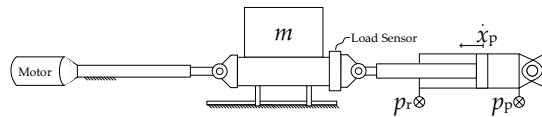


Figure S7: One way to construct the topology using a motor and a ball screw.

Pros:

- Can vary the load force dynamical
- Can be bought as plug and play
- High performance ensures good control of the load force

Cons:

- Axial play might be seen
- Expensive solution
- Loss of accuracy due to the load cell
- Complex setup and control design compared to mass as load

Motor with toothed rack

A rack and pinion is another way to convert the motor torque to a linear force. One method in which this topology can be manufactured is shown in Figure S8. The motor should be able to deliver at least 40 kN for the $\varnothing 50$ cylinder and 100 kN for the $\varnothing 80$ cylinder at linear velocities of up to 0.25 m/s. One problem with this topology is that a rack and pinion may result in axial play which acts as a disturbance to the system.

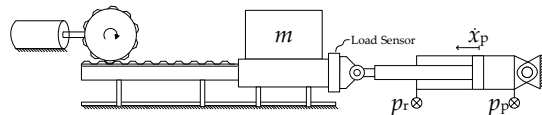


Figure S8: Topology using an electric motor and a rack and pinion.

Pros:

- Can vary the load force dynamical
- Cheap solution compared to spindle solution
- High performance ensures good control of the load force

Cons:

- Axial play might be seen in the toothed rack
- Loss of accuracy due to the load cell
- Complex setup and control design compared to mass as load

Hydraulic Cylinder

The last dynamical load topology covered is a hydraulic cylinder acting as load. The size of this load cylinder can be dimensioned to obtain the preferred dynamic performance of the load force. One way to design this topology is shown in Figure S9.

The dynamic performance of the hydraulic load solution is not as fast as the motor actuator solution. Though the dynamic performance is for now assumed to be adequate to control

the system within the desired performance requirements.

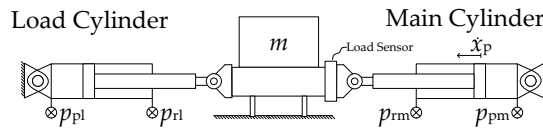


Figure S9: Topology where a hydraulic cylinder is used as load.

Pros:

- Can vary the load force dynamical
- Cheap solution compared to motor actuator solution

Cons:

- Slower system response than the motor actuator system
- Loss of accuracy due to the load cell
- Complex setup and control design compared to mass as load

E.2.3 Comparison

Three different topologies regarding a dynamical load have been discussed. The two topologies utilising an electrical motor as load actuator will have a good dynamical performance compared to the topology utilising a hydraulic cylinder as load actuator due to a possibility of fast closed loop response. Yet the two motor topologies are much more expensive than the hydraulic topology due to the price of the motor and the inverter in the desired torque range. Furthermore a large gearing is necessary in the two topologies utilising an electrical motor which may result in axial play which will compromise the dynamical performance of these topologies. The topology utilising an electrical motor and a spindle can be bought as a plug and play solution which is preferable. Yet the cheaper hydraulic topology may be adequate to control the system.

E.2.4 Choise of Topology

In this section one of the previous discussed topologies will be chosen as the method to load the hydraulic main cylinder. This choice is based on a comparison of the price for the total system together with the ability to fulfil the requirements in Section 3.1.3. An Ø50 main cylinder is chosen as main cylinder for the dynamic load topologies since this results in a higher accuracy of the measurements.

The following price estimates for each topology are obtained from different companies, neglecting the price for the hydraulic equipment, guidance and physical stand.

Topology	Pressure Sensor[dkr]	Pos/Vel [dkr]	Load Cell [dkr]	Load [dkr]	Total [dkr]
Mass-Downright Ø50	10000	2300	0	33320	45620
Mass-Pulley Ø50	10000	2300	0	11107	23407
Mass-Upright Ø50	10000	2300	0	65333	77633
Mass-Downright Ø80	10000	2300	0	101270	113570
Mass-Pulley Ø80	10000	2300	0	33647	45947
Mass-Upright Ø80	10000	2300	0	166600	178900
Cylinder Load	10000	2300	4500	16817	33617
Spindle drive Load	10000	2300	4500	123933	140733
Motor/rack and pinion load	10000	2300	4500	64433	81233

Table S1: Price Estimates for different solutions.

In all the cases the two pressure transducers are of the type TP14Lab sold by NTT for 5000Dkk each. The position sensor used for all the topologies is a MIL10 sold by Baumer A/S for a price of 2300Dkk. The price for the mass used for the topologies is 16.4Dkk/kg sold by www.getbig.dk. For all the dynamical load topologies a mass of 700kg is used. The cylinder used for the topology utilising a cylinder as load is sold by LJM for 5384Dkk and the spindle drive is sold by Bosch Rexroth for 112500Dkk. The load cell used for all the dynamical load topologies is a TCTN-9110 sold by NTT for 4500Dkk. The topology with a motor and rack and pinion consist of a motor and inverter sold by Bosch Rexroth for 50000Dkk and a rack and pinion sold by Brd. Klee for 3000Dkk.

From the price estimates in Table S1 it is clearly seen that the dynamical load topologies utilising a motor as load is expensive. Furthermore it is seen that the dynamical load topology utilising a hydraulic cylinder is one of the cheapest topologies. By using a hydraulic load it is possible to operate in the entire area defined in the requirements in Section 3.1.3, why this topology is preferable compared to the gravitational load topologies. Yet there may be an issue in controlling the system as desired. If the topology utilising a hydraulic load can not be controlled as desired, the only solution to achieve all the main cylinder pressures in the desired pressure range is one of the expensive topologies utilising an electrical motor.

In the next section, the dynamical load topology utilising a hydraulic cylinder will be further investigated to indicate if this topology can be controlled to fulfil the requirements made in Section 3.1.3.

E.3 Further Analysis of Hydraulic Load Solution

In this section the dynamical load topology utilising a hydraulic cylinder will be analysed to determine if this system can be controlled such the requirements in Section 3.1.3 is fulfilled. First the desired mass of the system is determined based on an analysis of a linear representation of the hydraulic system consisting of the Ø50 main cylinder, a mass and a Ø80 load cylinder. The mass is chosen such the maximum natural frequency is in the range of the valves to increase the control performance. When the desired system mass is chosen, a control strategy is used in a simulation model of the system to investigate if the dynamic performance fulfils the requirements. Furthermore it is investigated how axial play in the couplings will affect the control performance.

E.3.1 Choise of Mass

This analysis will be used to chose a mass for the system which results in a frequency of the least damped pole pair which enables the possibility of implementing active damping using the valves. In Figure S10 the frequency of the least damped pole pair is seen in the entire pressure range at $\dot{x}_p = 0.1\text{m/s}$, $m=500\text{ kg}$ and $x_p = 0$. To investigate the system under conditions where the least damped pole pair have the highest frequency, the system is investigated at pressures of $p_{pm} = 200\text{ bar}$ and $p_{rm} = 200\text{ bar}$.

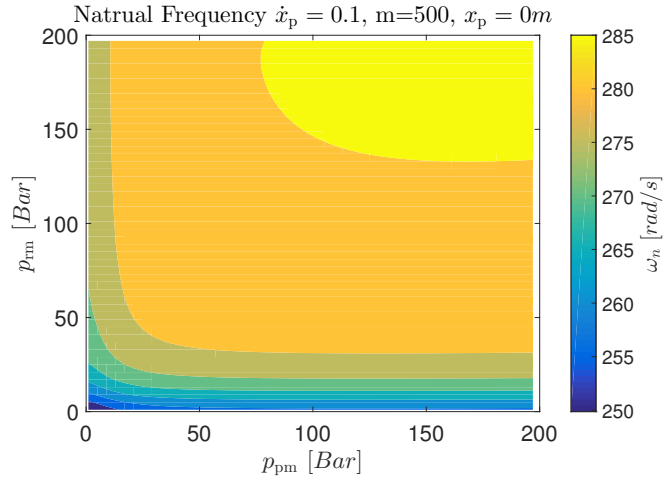


Figure S10: Natural frequency in the pressure range, with $\dot{x}_p = 0.1$, $x_p = 0$ and $m=500\text{ kg}$.

The frequency of the under damped pole pair is investigated in the velocity and position range as well. In Figure S11 the frequency is seen in the velocity range for different masses, with $p_{pm} = 200\text{ bar}$, $p_{rm} = 200\text{ bar}$ and $x_p = 0\text{ m/s}$. As seen, the highest frequency occurs at 0.05 m/s . In Figure S12 the frequency of the under damped pole pair is seen in the position range for different masses with $p_{pm} = 200\text{ bar}$ and $p_{rm} = 200\text{ bar}$ and $\dot{x}_p = 0.05\text{ m/s}$.

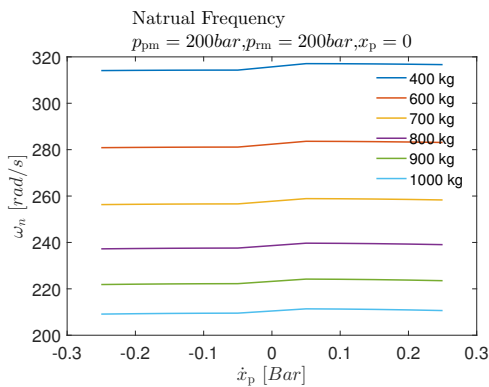


Figure S11: Natural frequency in the velocity range, with $p_{pm} = 200\text{ bar}$, $p_{rm} = 200\text{ bar}$ and $x_p = 0\text{ m/s}$.

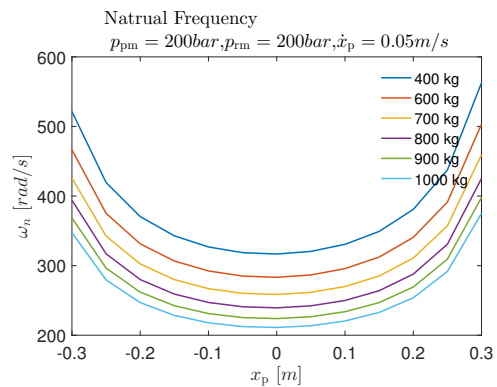


Figure S12: Natural frequency in the position range, with $p_{pm} = 200\text{ bar}$, $p_{rm} = 200\text{ bar}$ and $\dot{x}_p = 0\text{ m/s}$.

To keep the desired mass at a reasonable level it is assumed that a mass of 700kg is adequate. In section A.2.1 the bandwidth of the valve for the load cylinder is found to 30Hz and the

valves used for the main cylinder have a bandwidth of 60 Hz. With a desired mass of 700 kg, the maximum frequency of the under damped pole pair is between 41-71Hz.

In the next section the dynamical performance of the hydraulic system is investigated with a mass of 700 kg to determine if the dynamical load topology utilising a hydraulic cylinder is adequate to fulfil the requirements from Section 3.1.3.

E.3.2 Performance of System with Hydraulic Load

The system consists of a 50/35x700 main cylinder and a 80/40x680 load cylinder with two Moog D633 valves used to control each flow into the main cylinder and a Moog D634 to control the flow of the load cylinder. A mass of 700kg is applied and the supply pressure is set to 250 bar.

The control of this system is made as follows:

- Velocity
 - Utilising the valve on the load cylinder using a PI controller, flow feed-forward and high pass leakage.
- p_{pm}
 - Utilising the piston-side valve on the main cylinder using a PID controller with flow feed-forward.
- p_{rm}
 - Utilising the rod-side valve on the main cylinder using a PID controller with flow feed-forward.

The performance of the system is both evaluated at pressures of 20bar and 200bar. The simulations is made for a sinus trajectory with an amplitude of 0.25 m/s and a frequency of 1 Hz where the piston position starts in $x_p = 0.25$. The results is shown in Figure S13 and S14.

As seen from the figure the system can be well controlled to follow the references. It is seen that the pressures fluctuates less than ± 5 bar which complies with the requirements and is therefore accepted.

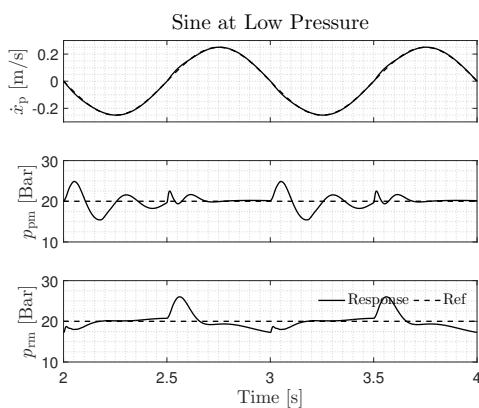


Figure S13: Simulated and reference velocity and pressures of a system with a 50/35x700 main cylinder and a 80/50x680 load cylinder. Noise is added to the signals used in control.

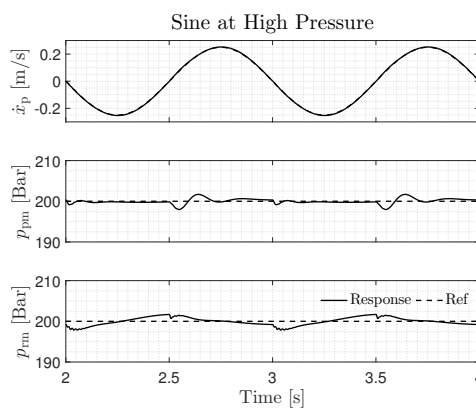


Figure S14: Simulated and reference velocity and pressures of a system with a 50/35x700 main cylinder and a 80/50x680 load cylinder. Noise is added to the signals used in control.

Performance Degradation Due to Axial Play in Coupling

Some axial play in the cylinder mount is expected. In this subsection it will be investigated what impact axial play will have on the system performance. The system may be exposed to axial play in some cases where the pressures in the main cylinder results in a load force around 0 N due to the direction dependent friction and acceleration forces. Figure S15 is showing the main cylinder pressure combinations at which the resulting force from the main cylinder equals 0N.

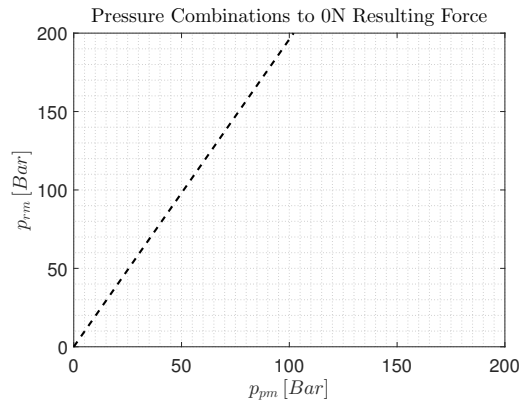


Figure S15: The dashed line illustrates the pressure combinations for the main cylinder ($\text{\O}50\times35$) which results in a resulting cylinder force of 0N.

Since it is preferred that the system can be controlled regardless of axial play, a simulation of the system is performed tracking a sine wave with an amplitude of 0.25 m/s and a frequency of 1 Hz. Before the first change from positive to negative velocity, where the load cylinder force changes direction, the load side is modelled not to be in contact with the rest of the system until the relative displacement between the load cylinder and the rest of the system is 0.25 mm, since this is the maximum axial play stated by the supplier of an alignment coupler. The simulation is made for a main cylinder pressure combination on the line of Figure S15, which results in zero force from the main cylinder. The simulation for the main cylinder pressure combinations of 100 and 51 bar of respectively p_{rm} and p_{pm} is shown in Figure S16. The simulations show that the axial play in this region does not have any remarkable impact on the system performance. This might be due to the small amount of axial play in the coupling together with a small load force. The investigation indicates that a system with a hydraulic cylinder as a load can fulfil the requirements of Section 3.1.3.

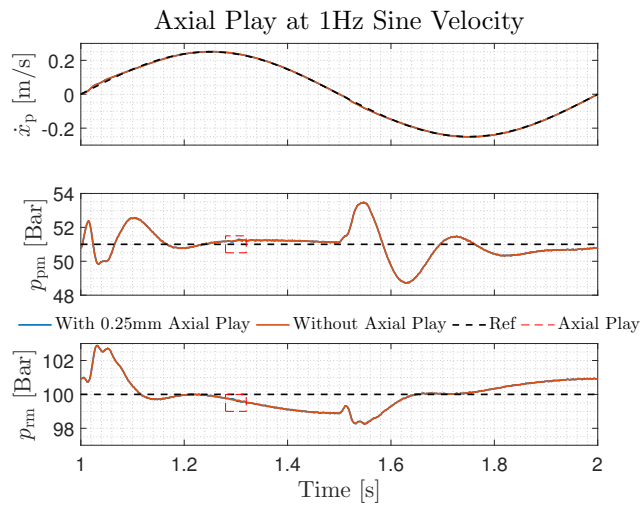


Figure S16: Illustration of axial play from positive to negative velocity for a sine velocity of 1Hz.

F | Further Design Considerations

F.1 Friction Joints and Pre tensioning

F.1.1 Pre Tensioning of Strut Joint

The pretension of the bolted friction joints from the struts to the end plate is calculated to 247 kN. To pre tension this in practice one way is to convert it to a tightening torque. This can be calculated in the following way (Norton, 2000):

$$T = 0.21F_{p,c}d = 1140Nm \quad (F.1)$$

where $F_{p,c}$ is the pre tensioning, 150.8 kN, and d is the diameter, 36 mm.

F.1.2 Pre Tensioning of Alignment Coupler

The pre tensioning for the alignment coupler are converted to a tightening torque as (Norton, 2000):

$$T = 0.21F_{p,c}d = 1245Nm \quad (F.2)$$

where $F_{p,c}$ is the pre tensioning, 247 kN, and d is the diameter, 24 mm.

F.1.3 From Construction To Bench

The construction is mounted to the bench with four m12 bolts. The friction force, $F_{s,Rd}$ in the joint, is directly proportional to the pre tension of the bolt, though the bolt should only be pre tensioned up to 70% of the ultimate tensile strength. 10.9 class bolts have a ultimate tensile strength of $\sigma_{ub} = 1000N/mm^2$, thus calculating the maximum pretension allowed, $F_{p,c}$, as:

$$F_{p,c} = 0.7\sigma_{ub}A_b = 59kN \quad (F.3)$$

Where A_b is the tensile stress area, 84.3 mm² for m12 (Fastenal, 1993).

The friction acting in the joint can be calculated as:

$$F_{s,rd} = \frac{k_s n \mu_s}{\gamma_{m3}} F_{p,c} = 12kN \quad (F.4)$$

With the hole factor, $k_s = 0.85$, for oversized holes, number of surfaces $n=1$, safety factor $\gamma_{m3} = 1.25$ and the friction factor $\mu_s = 0.3$ for steel/steel surfaces.

With the four bolts, $n_b = 4$, a mass of 700 kg, $m=700$, and a safety factor of two, $S_f = 2$, the maximum allowed acceleration is calculated as:

$$\ddot{x} = \frac{n_b F_{s,rd}}{S_f m} = 34m/s^2 \quad (F.5)$$

According to (Norton, 2000), the tightening torque, T , of the bolts can be calculated with the following relationship assuming the thread is lubricated and a bolt diameter of $d=12mm$:

$$T = 0.21F_{p,c}d = 148Nm \quad (F.6)$$

F.1.4 From Bench to Floor

The bench stands on rubber feet on an epoxy floor. According to (Y.M El-Sherbiny, 2012) this combination yields a friction coefficient, μ of minimum 0.5. Approximating the moving mass, m , to be 700 kg and the stationary mass, m_{bench} , to be 600 kg, the maximum allowed acceleration is calculated with a safety factor of two, $S_f = 2$:

$$\ddot{x} = \frac{g(m + m_{\text{bench}})\mu}{S_f m} \approx 4.6\text{m/s}^2 \quad (\text{F.7})$$

F.2 Electrical Network

The electric setup via the Compact Rio is shown in Figure S1. The Compact Rio and all the sensors are supplied via the same 24 VDC power supply.

The encoder is connected through a digital module for the compact rio, a NI-9401 and the data sampling is done on the Compact Rio FPGA at 40MHz. The encoder is supplied externally with 5V

The load cell is supplied with 5 V and have a sensitivity of 3 mV/V with an input resistance of 385 Ω . The load cell is connected through a NI 9237 bridge module which have an internal power maximum of 150 mW, why the load cell should be excited with 5V.

The setup of the Danfoss MBS32 transducer has in earlier work (Pedersen and Jørgensen, 2016) proven to be best if a differential measurement between signal and ground from the sensor is used and the shield is grounded at both the bench and supply. The measurement is thus a differential voltage measurement through a NI9205 module.

The TPLab14 pressure transducers have a current output between 4-20mA which is measured as a voltage from 2-10 V across a 500 Ω resistance.

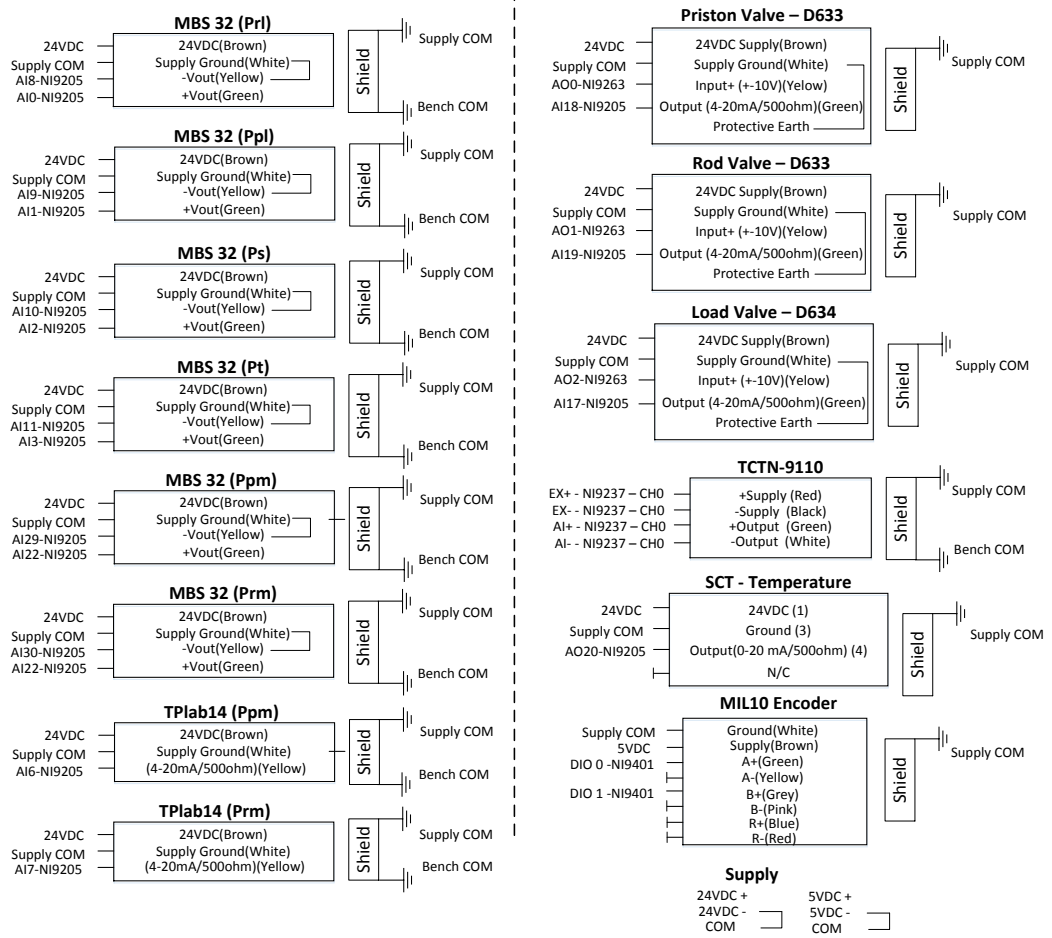


Figure S1: Complete electrical circuit for data acquisition and control.

F.3 Model Parameters

Parameter	Value	Unit	Parameter	Value	Unit	Parameter	Value	Unit
D_{pm}	50	[mm]	M_m	10	[kg]	$Q_{n,m}$	40	[l/min]
D_{rm}	35	[mm]	M_l	20	[kg]	$Q_{n,l}$	100	[l/min]
D_{pl}	80	[mm]	M_s	700	[kg]	$p_{n,m}$	35	[Bar]
D_{rl}	40	[mm]	p_s	250	[Bar]	$p_{n,l}$	35	[Bar]
V_{pm0}	0.79	[l]	p_T	1	[Bar]	$\omega_{n,m}$	200π	[rad/s]
V_{rm0}	0.45	[l]				$\omega_{n,l}$	120π	[rad/s]
V_{pl0}	1.81	[l]				ζ_m	0.707	[-]
V_{rl0}	1.38	[l]				ζ_l	1	[-]

Table S1: Model parameters used in simulations

